4

ORNL-2648
Particle Accelerators and
High-Voltage Machines

Cy. 4

THE OAK RIDGE RELATIVISTIC ISOCHRONOUS CYCLOTRON

OAK RIDGE NATIONAL LABORATORY · U.S. ATOMIC ENERGY COMMISSION

OAK RIDGE NATIONAL LABORATORY
operated by
UNION CARBIDE CORPORATION
for the
U.S. ATOMIC ENERGY COMMISSION

Printed in USA. Price $2.75 Available from the

Office of Technical Services
U. S. Department of Commerce
Washington 25, D. C.

ORNL-2648

Contract No. W-7405-eng-26

THE OAK RIDGE RELATIVISTIC ISOCHRONOUS CYCLOTRON

Compiled and Edited by

R. S. Livingston

and

F. T. Howard

Electronuclear Research Division

September 1958

OAK RIDGE NATIONAL LABORATORY
Operated by
UNION CARBIDE CORPORATION
for the
U.S. ATOMIC ENERGY COMMISSION
Post Office Box X
Oak Ridge, Tennessee

Contributors

This document was originally organized by B. L. Cohen. It represents a summary of the combined efforts of many individuals. Those who were responsible for the large amount of experimental, theoretical, and design work reported here and for the preparation of the various sections are:

Cyclotron Development: B. L. Cohen, J. A. Martin, R. E. Worsham, and A. Zucker.

Scientific Motivation: R. S. Bender, B. L. Cohen, and A. Zucker.

Magnetic Field Design: H. G. Blosser, B. L. Cohen, E. D. Hudson, R. S. Lord, and B. D. Williams.

Radial Stability: M. M. Gordon and T. A. Welton.

Beam Deflection: M. M. Gordon and T. A. Welton.

Radio-Frequency System: R. E. Worsham and T. A. Welton.

Engineering Studies: R. J. Jones, W. R. Smith, and E. G. Richardson, Jr.

Experimental Facilities: R. S. Bender and A. Zucker.

Added Note

This document was originally submitted in support of the proposal to AEC for the construction of the cyclotron. Construction of the Oak Ridge Relativistic Isochronous Cyclotron has since been approved. The proposal document, with corrections and minor changes in title and terminology, is now being issued for general distribution.

Table of Contents

I. INTRODUCTION AND SUMMARY

During the first decade after Lawrence's introduction of the cyclotron, this nuclear research instrument underwent rapid development to the stage best represented by the classic 60-inch cyclotron. This latter design has been adapted over the years to the needs of many research institutions throughout the world. In the drive toward ever higher energies, attention was for a time centered on the development of frequency-modulated cyclotrons and, more recently, on proton synchrotrons. For precision work in the region of lower energies the Van de Graaff machine has been developed to a high state of perfection.

Most recently there has been an increasing interest in more precise work in the intermediate energy field. Attention has been focused on the improvement of the fixed-frequency cyclotron. Efforts have been directed especially toward overcoming the limitations of energy imposed by the relativity effect, on providing greater flexibility both in the choice of energy and the choice of the particle to be accelerated, on improving the energy definition, and on increasing the beam current and stability.

A number of novel accelerator features have been developed, and in some cases applied individually to cyclotrons, to increase their level of performance, their reliability, and their versatility. Many of these new features have been incorporated in the Oak Ridge Relativistic Isochronous Cyclotron (ORIC) to provide the greatly enlarged research potential which now appears practical for a fixed-frequency cyclotron in the intermediate energy field. Among these novel features are: (1) the use of an azimuthally varying magnetic field (AVF) to provide axial focusing, (2) the use of an average magnetic field increasing with radius in a manner to keep the accelerated particle approximately synchronous, thus to minimize the threshold voltage required, (3) the use of an oscillator adjustable through an extended range, 3:1, of fixed frequencies, (4) the use of harmonic acceleration to provide additional bands of frequencies, (5) the use of auxiliary coils of various types to control the magnetic field configurations within a wide range of average field strengths, (6) the use of defining grids near the center to eliminate components of the beam with radial oscillations of large amplitude, and (7) the use of r-f amplitude control to reduce the energy spread in the beam.

The purpose of this brochure is to describe the ORIC and to review recent studies which have led to the choice of certain design features.

A cyclotron can be described in terms of its performance, or in terms of its design characteristics; in the following two tables information is provided in each category.

Design Performance

The ORIC is a variable-energy, azimuthally-varying-field, 76-inch, fixed-frequency cyclotron designed to accelerate various particles with e/m ratios from 1 to 0.125 over a wide range of energies, up to 145 Mev. The machine is designed to accomodate large ion currents, with a total beam power up to 75 kw (one milliampere of protons at 75 Mev). The conditions associated with the acceleration of various particles to their maximum respective energies are tabulated below and presented graphically in Figs. 1 and 2.

	Charge State	Max Energy (Mev)	Energy Per Nucleon (Mev)	Orbital Frequency (Mc/sec)	Central Magnetic Field (kilogauss)
Proton	+1	75	75	22.5	14.8
Deuteron	+1	39	19.5	12.3	14.5
Helium 3	+2	100	34	15	14.7
Alpha	+2	78	19.5	12.3	14.5
$Carbon^{12}$	+4	115	9.5	8.6	17
$Nitrogen^{14}$	+4	100	7.3	7.5	17
$Oxygen^{16}$	+4	88	5.7	6.5	17
$Neon^{20}$	+5	108	5.7	6.5	17
$Argon^{40}$	+7	103	2.8	4.6	17
$Krypton^{84}$	+12	145	1.8	3.7	17

UNCLASSIFIED
2-02-015-491

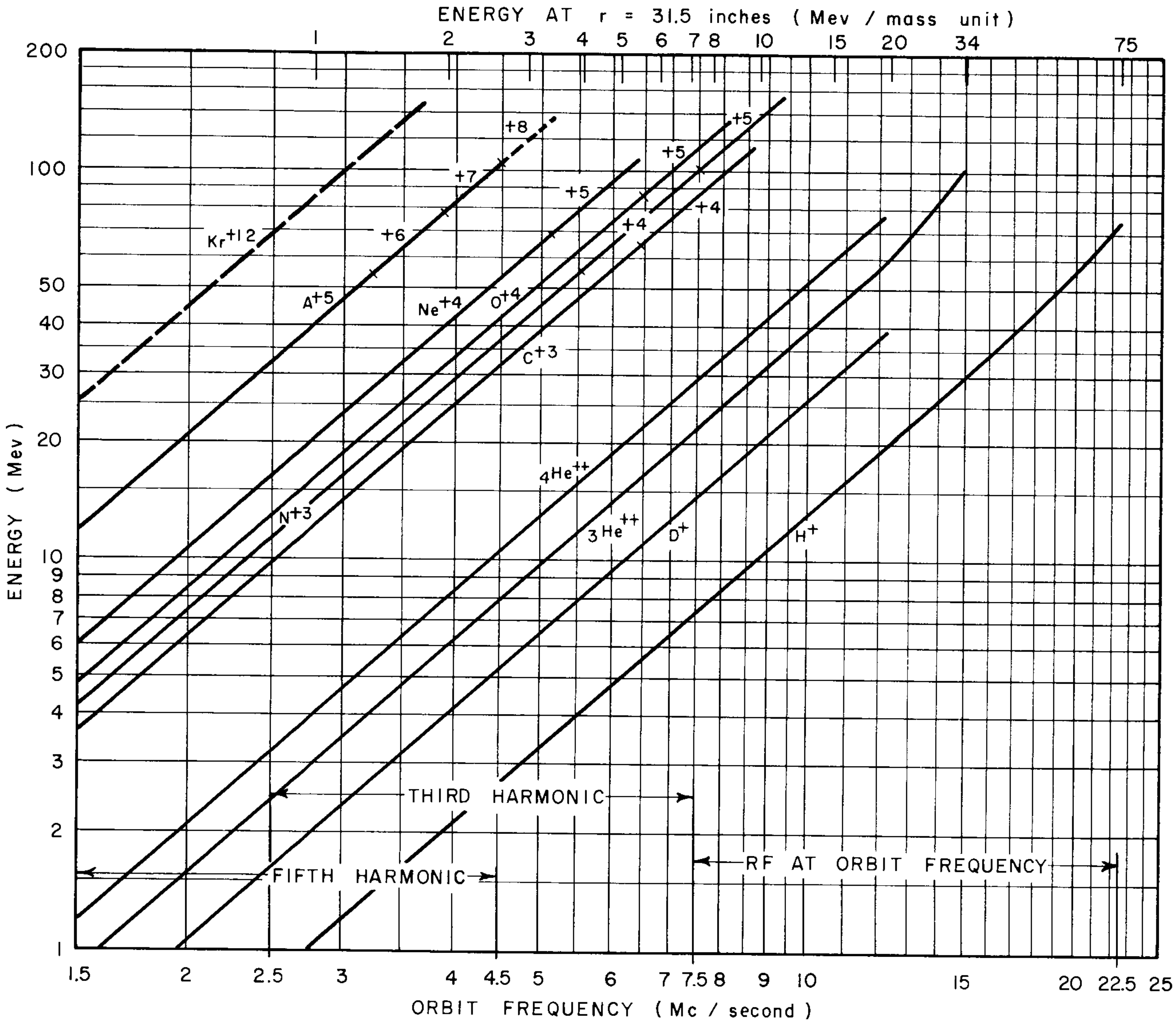

Fig. 1. Accelerated Particles and Energies Available in the Oak Ridge Relativistic Isochronous Cyclotron.

UNCLASSIFIED
ORNL-LR-DWG. 30819

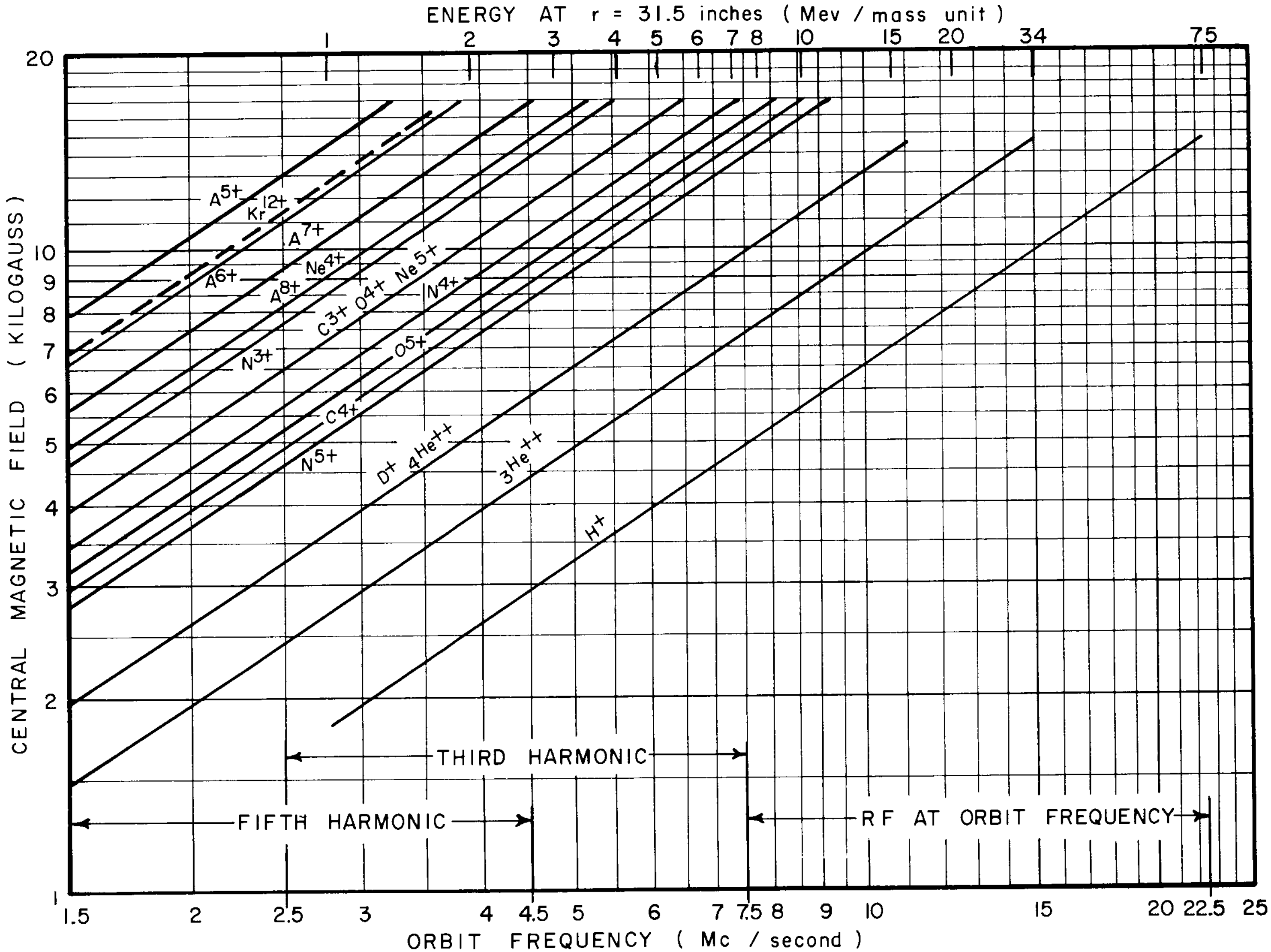

Fig. 2. Resonance Conditions for Acceleration of Various Ions.

Design Characteristics

The most conspicuous features of the ORIC are shown in a photograph of the model, Fig. 3. The three-sector magnet pole, with slight spiral, is shown at the left. One concept for the wide-range, variable, radio-frequency system is at the right. The more important design characteristics may be summarized as follows:

Magnet Data

Magnet field configuration	3 sector
Magnet core dia	76 in.
Magnet pole tip dia	76 in.
Beam radius, average max	31.5 in.
Magnet gap, hill	7.5 in.
valley	28.5 in.
Central magnetic field, max ave	17 kgauss
Magnet field rise with radius (max)	8%
Magnet excitation	1.23×10^6 amp-turns
Magnet weight	208 tons
Magnet cooling	water

R-F System

Dee diameter	71 in.
Dee aperture	1.87 in.
Dee-to-dee gap	2 in.
Oscillator tube	RCA 6949
Oscillator input power	650 kw max
Oscillator output power	500 kw max
Frequency	22.5 to 7.5 Mc/sec
As 3rd and 5th harmonics	7.5 to 1.5 Mc/sec

Miscellaneous

Beam extraction type	Regenerative
Ion source	Hot cathode
Shielding	7 ft ordinary concrete

Beam Power

Protons	75 kw (1 ma protons at 75 Mev other ions comparable)

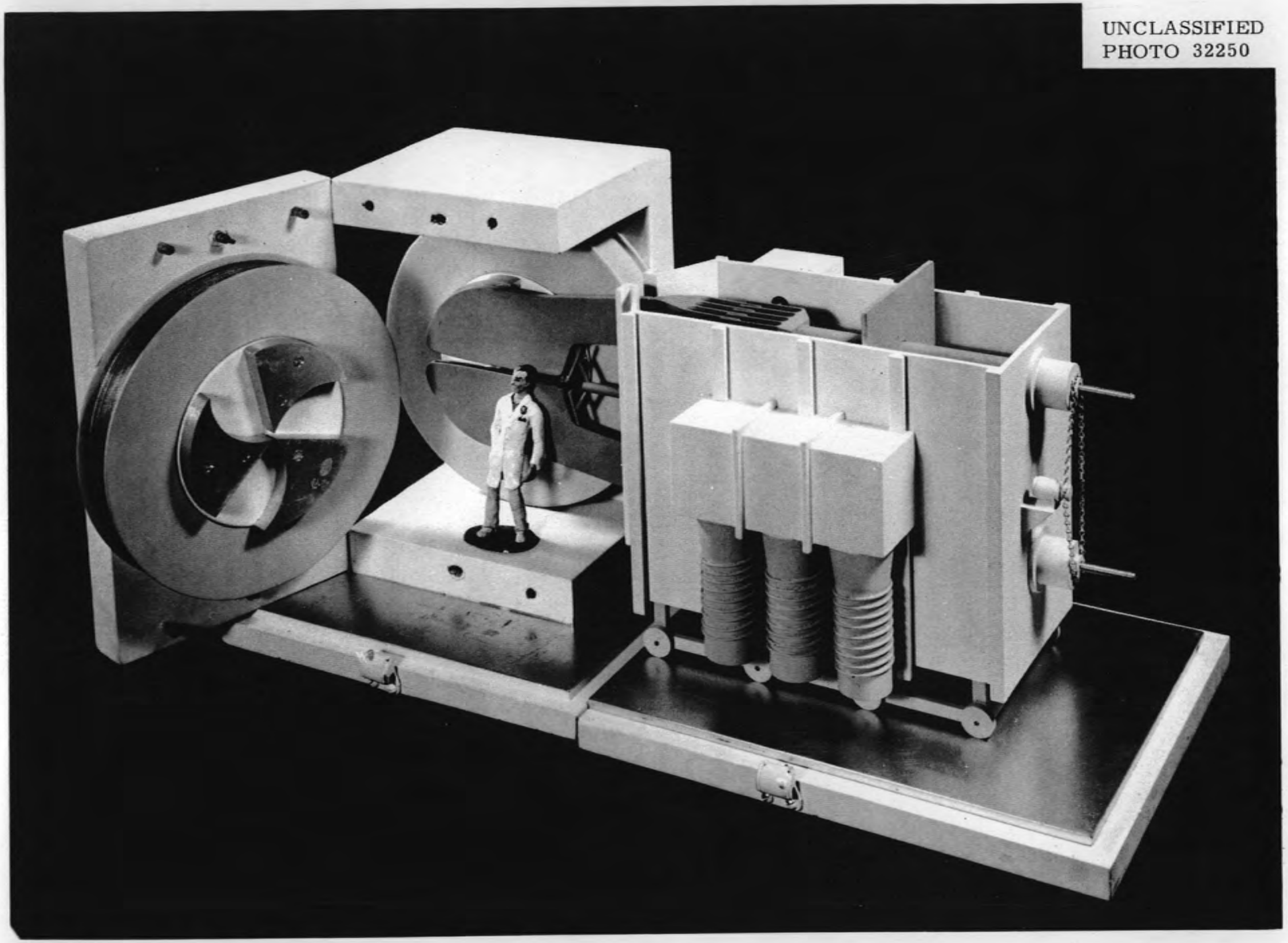

Fig. 3. Model of the Oak Ridge Relativistic Isochronous Cyclotron Showing the Three-Sector Magnet Pole Tips and the Dees with One of the Resonant Circuits Studied.

In subsequent sections of this report, the work on the preliminary design of the magnetic field and of the radio-frequency system is described. Some work on a study of the stability regions of the machine is included,as is a preliminary study of beam deflection. The report also includes background material on the genesis of the ORIC design, on the intended research applications, and on other design features.

II. CYCLOTRON DEVELOPMENT

The Oak Ridge Relativistic Isochronous Cyclotron is an outgrowth of the successful research programs with two unusual cyclotrons built at Oak Ridge, the ORNL 86-Inch and the ORNL 63-Inch cyclotrons. In subsequent paragraphs the origin, characteristics, and accomplishments of these two ORNL cyclotrons are reviewed.

Construction of a new cyclotron was proposed by the Laboratory to free the heavy-particle experimental program from the handicaps of the physical environment of the 63-inch cyclotron and, by increasing the particle energy, to open up the upper two-thirds of the periodical table as possible experimental territory. In 1955 the Laboratory proposed that a replacement cyclotron, designated the 48-inch, be constructed to permit heavy-ion physics to continue under improved (but still limited) circumstances in an adjunct to Building 9201-2 at Y-12. In 1957 the Commission approved this project to the amount of $459,000.

Meanwhile advances in technology were being made at a remarkable rate. Studies of properties of ion orbits (for high-energy particles) have shown the superior performance possible with alternating strong and weak sections in the magnetic field. Accelerating protons to 75 Mev in a fixed-frequency cyclotron, previously impossible, thus becomes straightforward. New systems for varying the radio frequency offer the possibility for continuous variation of the energy. New ideas for control of radial oscillations and r-f amplitude indicate beams of much finer definition are possible.

In the face of these technological developments it was decided that a truly modern and versatile cyclotron should be sought. The concept of the ORIC was advanced as a replacement for both the 86-inch and the 63-inch cyclotrons and as an alternate to the 48-inch.

A. The ORNL 86-Inch Cyclotron

The 86-inch cyclotron produced its first proton beam on November 11, 1950 after a construction period lasting only a little more than a year. This machine, which provides both internal and external 23-Mev proton beams, has been an extremely effective tool both for basic nuclear physics research and for applied uses such as isotope production and neutron production for biological research. The versatility of the machine was greatly enhanced in 1956 by the additon of a deflector system and beam room facilities.

The 86-inch cyclotron is at present the best machine in the world for isotope production. Production rates for most isotopes are orders of magnitude greater than were obtained in other machines previous to 1950. At least one isotope of medical importance, As^{74}, is being produced on a semiroutine basis.

The machine incorporates several innovations in cyclotron design. The median plane is vertical rather than horizontal; the magnet yoke is U-shaped with the top open to permit the easy transfer of large cyclotron components with an overhead crane. The high dee-to-dee potential needed to accelerate protons to an energy of over 20 Mev is provided by a self-excited, grounded-grid, single-tube oscillator. Ion loading, which often impedes oscillation in self-excited oscillator systems, is eliminated by maintaining the whole dee structure at a negative potential of one kilovolt.

The deflector is unique in several ways: electrostatic deflection is produced wholly by the r-f dee potential -- no d-c potential is used. The septum, or beam-splitter, is a grid of water-cooled aluminum tubes and is mounted in a fixed position on the dees; the beam is positioned by introducing a controlled first harmonic in the magnetic field. (The same result is obtained in conventional machines by a complicated mechanical arrangement which moves the septum.) The beam passes from the electrostatic deflector through a magnetic channel which sharply reduces the magnetic field and permits the beam to cross the fringing magnetic field easily. Focusing of the deflected beam is accomplished by a set of 2-in. aperture quadrupole magnets. For nuclear physics experiments the beam is piped a distance of 40 ft to a reaction room.

At present the 86-inch cyclotron is operated 16 hours a day, five days a week. A brief list of the characteristics of the machine follows.

Diameter of pole piece (in.)	86
Proton energy (Mev)	23
Proton current	
Routine internal beam (μa)	2000-3000
Maximum internal beam (μa)	4000
Deflected and focused (0.6 in.^{2}) (μa)	80
Dee-to-dee potential (kv)	300 to 500
Magnetic field (gauss)	8790
Resonance frequency (Mc/sec)	13.4

Published research papers describing the work done by the 86-inch cyclotron group are listed in Appendix I.

B. The ORNL 63-Inch Cyclotron

The 63-inch cyclotron was the first such machine expressly designed to accelerate heavy ions, i.e., ions with masses greater than helium. The use of obsolete electromagnetic plant equipment made this cyclotron probably the cheapest machine of its size built; the total construction cost was $150,000. It was originally built as a test machine to determine the feasibility of accelerating heavy ions and to explore in a preliminary way the possibilities for nuclear research. The heavy-particle nuclear physics field is now well established; heavy ions are now being accelerated by seven machines in the world, and at least four other accelerators are in various stages of development or construction.

The 63-inch cyclotron was built largely of existing components formerly used in the electromagnetic separation of uranium isotopes. An existing magnetic gap was reduced to six-inch clearance and shimmed to operate at a field of 15,000 gauss. An ion source was developed which produces copious quantities of N^{3+} and N^{4+} ions. A new dee system and oscillator were designed and built to operate at the prescribed frequency of 5 Mc/sec. Existing power supplies were modified to provide high voltage for the oscillator tube and the deflector. The time schedule was approximately as follows: The idea was conceived in October, 1950. By January, 1951, a working ion source was developed, and construction of the machine was authorized in April, 1951. An internal beam was obtained in May, 1952. Experiments were carried out with the internal beam until the spring of 1953. Then, the magnetic field was reshimmed and a beam deflector system was installed. A satisfactory deflected beam was obtained in November, 1953, and has been used for atomic and nuclear physics experiments ever since.

At present the cyclotron operates twelve hours a day, five days a week. The circulating beam of N^{3+} ions is about 100 μa; the deflected beam is about 2 μa at an energy of about 28 Mev.

Published papers describing the physics research done in connection with the 63-inch heavy-particle cyclotron are listed in Appendix II.

C. The Azimuthally-Varying-Field (AVF) Cyclotron Concept

The basic dilemma of the cyclotron mechanism lies in the contradictory demands which the focusing and resonance requirements place on the typical circularly symmetric magnetic field of the cyclotron. In 1938, L. H. Thomas pointed out a solution to this dilemma based on the introduction of azimuthal variations into the magnetic field in a fashion so as to provide both focusing and synchronous acceleration. The technology of this type of machine was explored in theoretical and model studies at the University of California and at ORNL in the years 1950-52 on a "classified" basis. The principles involved were independently rediscovered in "unclassified" work by the MURA group; this group also called attention to the important effect of spiral, and they applied these principles to their concept of a spiral-ridge synchrotron. The generalization to cyclotrons was straightforward from their work, and detailed design studies for conversion of existing cyclotrons to AVF were also undertaken at the University of Illinois and at AERE, Harwell.

Various studies have conclusively established the feasibility of the azimuthally-varying-field, fixed-frequency cyclotron as an instrument for obtaining relativistic particles. At the same time, new and powerful methods have been worked out for straightforwardly obtaining the complex magnetic field shapes required. These methods, in conjunction with presently available techniques for the use of pole-face windings as current shims, now make it possible to design a magnet which will give the proper field shape over a considerable range of field strengths, thereby allowing the acceleration of various ions to a wide range of energies.

Active interest in the construction of an azimuthally-varying-field cyclotron was renewed at the Oak Ridge National Laboratory in late 1954, and an extensive theoretical study of the properties of machines of this type was begun. Analytical studies of these devices lead rather quickly to severe difficulties, and so, at an early stage, numerical integration procedures were devised and coded for the digital computer so that orbit behavior in complex fields could be studied in precise detail. These integration routines and their subsequent refinements have since been the major tool in both theoretical explorations and detailed design of devices. It can, indeed, be said with considerable emphasis that the rather remarkable progress achieved in the development of the AVF cyclotron in the past half decade is due in large measure to the coming of age of the digital computer.

Theoretical studies have included studies of the fundamental acceleration process, the focusing properties of the fields, the effects of nonlinearities and resonance difficulties, the effects of factors which determine beam quality, and details of deflection systems appropriate for such devices.

In addition to these theoretical studies, an operating relativistic AVF cyclotron has been constructed for the purpose of experimentally verifying the various computational results. This device, known as the Cyclotron Analogue I, accelerates electrons to a velocity of 0.7 c (in units of velocity of light) and to a radial focusing frequency of 2 (in units of the orbital frequency). The magnetic field in the Analogue is of a four-sector radial configuration; the field is obtained from a precisely fabricated set of air-cored coils, the detailed performance of which was completely and accurately precalculated. In operation, the Analogue has strikingly verified the design calculations, particularly those on the crucial question of resonance behavior, and thus demonstrates the complete feasibility, from an orbit dynamics standpoint, of the AVF cyclotron.

A second analogue having a spiral magnetic field configuration is presently under construction for studying in more detail the performance of a proposed 850-Mev f-f cyclotron.

D. Variable Frequency Cyclotrons

Because of the relationship between the maximum energy, the magnetic field strength, and the frequency of rotation of the particle being accelerated, any variation of energy means that the accelerating system of the cyclotron must tune over some range of frequencies. The high dee voltage required in cyclotrons can be achieved for practical driving power only by using a high-Q resonant circuit; high Q means that the energy storage is large relative to the power loss per cycle.

The frequencies at which cyclotrons operate make possible the use of transmission line elements as components of the circuit. Thus, the resonant system, the dees and their stems, are a $\lambda/4$ resonant circuit foreshortened by the dee capacity. To tune such a system, three variables are available:

(1) C, the dee capacity

(2) l, the length of the dee stems

(3) Z_0, the characteristic impedance of the dee stems.

On most cyclotrons, the dee capacitance can be changed but a small amount and is used only for fine tuning of the accelerating frequency. The resonant frequency varies nearly inversely with the square root of the capacity. Therefore, a change in the frequency of 2:1 would require a maximum to minimum capacity ratio of 4. The large capacity of the dees is nearly fixed, however, by the area of the dee surfaces parallel to the magnet pole face. Normally it is the capacity along the edge of the dee which can be varied, and this quantity is relatively small. The spacing between the dees and the dee liner next to the magnet poles is set to the minimum required for voltage breakdown between the dees and liner. The designers of the 90-Inch Cyclotron at Livermore[1] made use of the fact that the threshold voltage varied with the energy of the particle such that the highest voltage is required at the highest

[1] UCRL-2620

frequency. Therefore, they have designed a movable liner which allows the voltage to be greater than threshold at each frequency, but which allows tuning over the range from 4 to 6.2 or 6.2 to 9.5 Mc/s; the two ranges correspond to two shorting-bar positions.

The second method, variation of the length of the dee stems by moving the shorting bar along the stems, allows a wide variation of frequency. It also requires long stems and movement at the joint through which the current is highest in the machine. The cyclotrons at Rochester(1) and Los Alamos, and the planned machine at Illinois, all use this method. The 90-inch cyclotron uses only two fixed positions of the shorting bar, as mentioned above. The connection to the shorting bar requires great pressure obtained by means of bolts. This leads to long time intervals required to reset the frequency. The connection can also be remotely-controlled with hydraulic pistions, a much faster method. It should be pointed out that the 90-inch cyclotrons is the largest of the variable-energy machines. It is the only one using high r-f power, such as will be required in the ORIC.

The dee stems must present an inductive reactance equal to the dee capacitive reactance for resonance. In addition to, or instead of, tuning this inductive reactance by varying the length of the dee stems, the characteristic impedance of the stems may be varied. The properties of lines with non-uniform characteristics impedance has been studied by Donaldson.[2] Cyclotron tuning schemes using this method, or some modification, have been considered at Colorado, Berkeley, and UCLA. A "barn door" method considered at Colorado involved movement of the dee-stem liner surface; because of quite low Q at low frequecies the system was abandoned. A variation which consists of making the stem and lines like long enmeshed capacitor plates has been considered at UCLA and Berkeley. Since the surface area of the lines can be large this system shows promise for a low-loss, wide-range tuning scheme.

---

1. NYO-7816
2. M. R. Donaldson, <u>An Investigation of Resonant Properties of Short Exponentially and Linearly Tapered Lines</u>, ORNL-2260 (May, 1958).

III. SCIENTIFIC MOTIVATION

The study of the atomic nucleus is still a growing field; the energy region between 20 and 100 Mev is largely unexplored. Even in the energy region up to 5 Mev, where many experimental groups have been working during the past twenty years, much remains to be done. In what follows we enumerate specific fields which at this juncture seem manifestly worth investigating. It can be seen that a flexible program of research will profit extensively from the availability of different bombarding particles, from a continuously variable energy, from intense beams, and from the use of beams which are continuous rather than pulsed.

Nuclear Spectroscopy - The location of nuclear energy levels and the determinations of their properties, such as spin, parity width, and electric and magnetic moments is perhaps the most important source of information on nuclear structure. Many new techniques for these studies are made available by the use of medium-energy nuclear reactions. The utility of deuteron stripping is a well-known example. Experimental evidence recently obtained at the Laboratory indicates that inelastic scattering excites principally collective states while deuteron stripping excites essentially only particle states. Recent experimental and theoretical investigations of angular distributions of inelastic scattering at this and other laboratories give reason to hope that this will develop into a useful tool for spectroscopy. As other nuclear reactions are studied and become understood, there is every reason to believe that new spectroscopy techniques will evolve from them. Precision spectroscopy requires large, high quality beams of variable energy. The availability of various bombarding particles is also of great advantage.

Nuclear Reactions - A most important source of information on nuclear interactions is the study of mechanisms for nuclear reactions and scattering. The work on heavy-particle transfer reactions at this laboratory provides an excellent example of this. Nuclear reaction studies become most interesting in the energy region between 10 and 100 Mev, which is just the region covered by the ORIC. The availability of a large variety of energetic ions is a most important asset in this work. Since coincidence techniques will be necessary in most of these studies, a cyclotron with its essentially continuous beam possesses great advantages over linear accelerators and other machines which provide only pulsed beams.

Coulomb Excitation - Since the electric interaction is well known and understood, Coulomb excitation provides a unique opportunity for studies of nuclear structure. While extensive work in this field has been done with protons and alpha particles, work with heavy ions is still in its infancy. The variable energy feature of the ORIC would be of great advantage in these studies because experience with heavy-ion linear accelerators has shown that energy reduction with absorbers introduces very serious background difficulties.

Polarized Particles - Investigations with polarized particles are gaining in importance. The primary requirement for the production of such particles is a high intensity beam. It is interesting to note here that polarized protons may be produced in two ways: from p-He^4 scattering and from the equivalent α-H scattering. The latter is preferable in many cases because it gives higher yields. For example, the production of 20-Mev polarized protons gives about fifty times higher yields from the α-H scattering than from the p-He^4 scattering. This case represents the highest energy proton for which polarization calculations have been made. Of course the investigation of polarization of, say, p-He^4 scattering at higher energies is a promising field in intself. Here again, variable energy is of great importance.

Neutron Physics - Neutron physics continues to be a most important field, for its own sake as well as because information obtained in this way is frequently directly applicable to reactor design. From estimates of neutrons produced by protons on uranium one would expect of the order of 10^{15} n/sec for a one-milliampere beam. Neutrons from a cyclotron are naturally bunched by the rf, and time-of-flight techniques can be used to measure neutron cross sections or the spectra of product neutrons. Provision has been made in the building layout for a long flight path. Large beams and high energy protons are necessary for the copious production of neutrons.

Nuclear Chemistry - In this field perhaps the most fruitful research lies in the production of transcalifornium elements with heavy-ion bombardment. High beam intensity is of great importance here. Also, variable energy is important in this connection because it is desirable that the incident ions have just enough energy to penetrate the Coulomb barrier of the target; any excess only increases the already large ratio of fission to spallation, and makes the production of the desired isotope less likely. The study of the fission process should be greatly aided by heavy-ion fission investigations. A number of new isotopes throughout the periodic table will undoubtedly be discovered with heavy-ion bombardments.

Production of Isotopes - The cyclotron will be employed chiefly as a research tool, but its excellent capabilities as a radioisotope producer will not be neglected. Very intense beams are an advantage in the production of isotopes. The variable energy is useful since it permits the bombardment of selected targets in such a manner that production of the desired isotope is optimized. The isotopes thus produced can be used for medical or industrial purposes, they can be used in other fields of research, and they can be studied in their own right as well. In general, these are positron-emitting isotopes that cannot be made in reactors. There is good reason to hope that new and useful isotopes can be produced that are not available in today's accelerators because of limitations in the energy, current, or range of ions that can be accelerated. Many of the isotopes can, of course, be prepared with high specific activity.

Solid State Physics - There should be many uses for such an accelerator in the field of solid state physics. The study of radiation damage is facilitated by the high power output of the beam. The 75 kw of beam available will, in general, be more than can be dissipated in the target. As a consequence, the time required for a given effect will not be determined by the accelerator but by the maximum temperature allowable in the target. The range of 75-Mev protons in aluminum is about 2 cm; this permits the use of relatively thick targets and a study of the effect of charged particles in the interior of the target material. With the acceleration of heavy ions to $\sim$ 100 Mev the surface effects of irradiation can be studied. Also, high-energy heavy ions can be used to simulate the effect of fission fragments without the high radiation background of a reactor. The use of protons or deuterons may be a major advantage over the use of reactor neutrons in that all the charged-particle energy is dissipated in the target.

Atomic Physics - The range-energy relations and the dependence of the ionic charge on the velocity have long been of interest to physicists. The field is still inadequately explored experimentally and theoretically. Different particles with variable energy provide an excellent tool for studies of this sort.

Obviously, research will not be performed at the same time in all the fields enumerated above. It is evident, however, that the great flexibility of the machine will make its use possible in any field which appears most interesting at the time. The flexibility also guarantees, as much as can be done for any accelerator, that it will not become obsolete. As long as there is interest in the structure and properties of the atomic nucleus, the ORIC will be a useful machine. Many of the fields mentioned above have, in fact, been fruitfully exploited by the two existing Oak Ridge cyclotrons. The experience which has been accumulated can be readily applied to the programs of the proposed cyclotron.

IV. MAGNETIC FIELD DESIGN

A. Design Requirements

In the early work on azimuthally-varying-field (AVF) cyclotrons, the desired magnetic field was determined from theory, and the principal construction problem was to determine the iron and current configurations to achieve this field. This is a most formidable task, and an unnecessarily restricted one, since all of the theoretical requirements on the field may be satisfied in an infinitely large variety of ways. The approach followed at this Laboratory was, therefore, to construct a model with simple iron and current configurations, make measurements and calculations to determine how it fails to satisfy the theoretical requirements, make changes in the model to correct these failures, make new measurements, etc. This turns out to be a rapidly converging process, with the errors decreasing by nearly an order of magnitude on each successive iteration. The theoretical requirements on the magnetic field are:

(1) Isochronism at all radii; that is, the time required for a particle to complete a revolution must be equal to a constant independent of radius, namely the period of the radio-frequency (r-f) voltage applied to the dees; at least that the phase shifting caused by differences between these periods must never allow the particle to get out of phase with the r-f voltage by as much as 90 degrees. The condition for isochronism is, to a good approximation, that at radius r the average magnetic field $\langle B \rangle$ (averaged around a complete turn) is

$$\langle B \rangle = \frac{B_o \left\{ 1 + \frac{F}{2N^2} \left(1 + \frac{r}{F} \frac{dF}{dr} \right) \right\}}{\sqrt{1 - (r/a)^2}} \qquad (1)$$

where F is the "flutter", defined as

$$F = \frac{\langle B^2 \rangle - \langle B \rangle^2}{\langle B \rangle^2} \qquad (2)$$

N is the number of sectors, and $\underline{a}$ is the cyclotron unit

$$a = \frac{m_o c^2}{e B_o} \tag{3}$$

where m_o and $\underline{e}$ are the rest mass and electric charge of the particle being accelerated, B_o is the field at the center of the cyclotron, and $\underline{c}$ is the velocity of light.

(2) Axial stability; that is, the excursions of the particle in the direction perpendicular to their normal plane of motion must not be so large that the particles will strike the dees. Since the available aperture in this direction is severely limited, this essentially requires that there be positive axial focusing at all radii. The axial focusing force, F_z, is

$$F_z = -4\pi^2 \nu_z^2 z \tag{4}$$

where the axial oscillation frequency, ν_z, is approximately

[illegible] change in field/unit radius

$$\nu_z^2 = -\frac{r}{\langle B \rangle} \frac{d\langle B \rangle}{dr} + \frac{N^2}{N^2 - 1} F(1 + 2\tan^2 \alpha) \tag{5}$$

where α is the spiral angle.

(3) Radial stability; that is, the radial oscillations must not become unduly large. In practice, when they become larger than some critical size, they begin to increase exponentially, so that the requirement is essentially that the radial oscillation amplitude must not reach this critical size.

As the principal requirement of simplicity of construction, it was decided that the iron configuration be achieved by bolting shims of uniform thickness (shims which can be cut from flat plates) on to the pole bases of the magnet. It was decided that the current configuration might include valley coils and circular trimming coils mounted on the pole faces in addition to the main exciting coils, although an arbitrary upper limit of 500 kw was set on the power consumption of these valley coils.

Since the effectiveness of valley coils increases rapidly with size, they are always designed to use all available space in the valleys. The design of the pole-face windings is determined by the fact that the cyclotron must be capable of accelerating both protons to 75 Mev and N^{4+} ions to at least 80 Mev, and that these energies must be easily adjustable to any lower values. (It turns out that the range of radio frequency and magnetic field adjustments necessary to fulfil these requirements include the adjustments necessary to obtain a large variety of other energetic particles including deuterons up to 40 Mev, alpha particles up to 80 Mev, etc.) The isochronism requirement demands a different average magnetic field at each radius for each final energy of each particle accelerated, and these variations must be achieved with the circular trimming coils. This determines their minimum design capabilities, and in fact, determines their actual design since the space occupied by these coils is very precious.

The parameters of the iron configuration that can be varied to satisfy the theoretical requirements on the magnetic field are: (a) number of sectors, (b) hill gap, (c) valley gap, (d) ratio of hill width to valley width as a function of radius, and (e) amount of spiral as a function of radius.

The axial focusing increases monotonically as the valley gap is increased, but when it becomes larger than the distance between neighboring hills, further increases are of little value. In view of this, and as a construction simplification, the valley gap was left as the gap between the pole bases.

A relatively large ratio of hill width to valley width must be used to obtain the necessary magnetic field strengths. Variations of this ratio with radius are used to keep the average field at each radius within a range such that isochronous fields for all particles can be obtained with minimum size circular trimming coils. Aside from these limitations, the valleys are made as wide as possible so as to allow the use of the largest possible valley coils (these contribute to flutter).

The remaining parameters, the number of sectors (N), the hill gap (g), and the spiral (α), must be chosen by relatively involved compromises. For both N and α the axial and radial stability requirements act in opposite directions, with low N and large α giving increased focusing, but reducing the radial stability. There was good reason to believe that N = 4 would give reasonable radial stability, and it was hoped that even N = 3 would be sufficiently stable in some cases, so that model investigations were made of both three-sector and four-sector magnets. For survey purposes, only two types of spiral were studied: A very weak spiral (actually negligible from the standpoint of radial stability), and the strongest spiral that is useful for axial focusing.(1) The flutter increases as g decreases, but as g is decreased, the aperture left for the beam is reduced very rapidly. Thus, g is made as large as is consistent with obtaining sufficient axial focusing.

It is clear from the above discussion that many of the design parameters can only be determined by model magnet tests. Some of these are:

(1) Size, current capacity, and number of circular trimming coils mounted on the pole faces.

(2) Effectiveness of valley coils in producing flutter.

(3) Ratio of hill width to valley width necessary to obtain necessary average field strengths, and the variation of this ratio with radius necessary to achieve isochronism.

(4) Maximum hill gap capable of producing the necessary axial focusing.

In addition, magnetic field configurations from model magnet tests were very useful in the radial stability calculations to be discussed in Section V and in axial stability calculations associated with deflection (Sec. VI). Thus, the model magnet test program played the central role in the design of the magnet.

---

(1) V. Bluemel, J. B. Carroll, and P. Stahelin, U. of Ill. Tech. Rept. No. 2, Navy Contract No. 1834 (05).

Section B, below, will describe the model magnet and some of the techniques used in gathering data with it. Section C will then describe the method of analyzing the model magnet data and determining the changes to be made in the subsequent model. The results and conclusions from this work will be given in Section D. Stability problems will be discussed in Sections V and VI. The former pertains to the problem of radial stability at small radii where, for heavy ions at least, the frequency of radial oscillations, ν_r, is nearly in resonance with the circulating frequency (that is usually expressed as $\nu_r = 1$). The latter pertains to a more complex instability which occurs when large radial oscillations are intentionally built up for purposes of beam deflection.

B. Model Magnet Measurements

Approximately 1/8-scale model magnets were energized with one and at times two 1750-kw generators. Most of the measurements were made with the model coils continuously energized; however some data was collected with intermittent excitation of all or part of the magnet coils.

Fig. 4 shows a model and the general arrangement for making model measurements. The intensity of the magnetic field is measured with a Rawson rotating coil fluxmeter connected to a Brown recorder. The fluxmeter probe is positioned by a milling machine table with an automatic stop. A cam operating a microswitch energizes a solenoid that releases the mechanical shift driving the table. A series of up to 44 points or positions 1/4 in. apart are measured along a line or chord of the magnet. Then the position of the table, and consequently the probe, is moved out 1/4 in. by hand, and a series of points along the next line are measured. A complete grid of points 1/4 in. apart is thus obtained over the entire model, or over any desired sector of the model. The position of the probe at each point is marked on the chart as the data is obtained, so that the field intensity at each

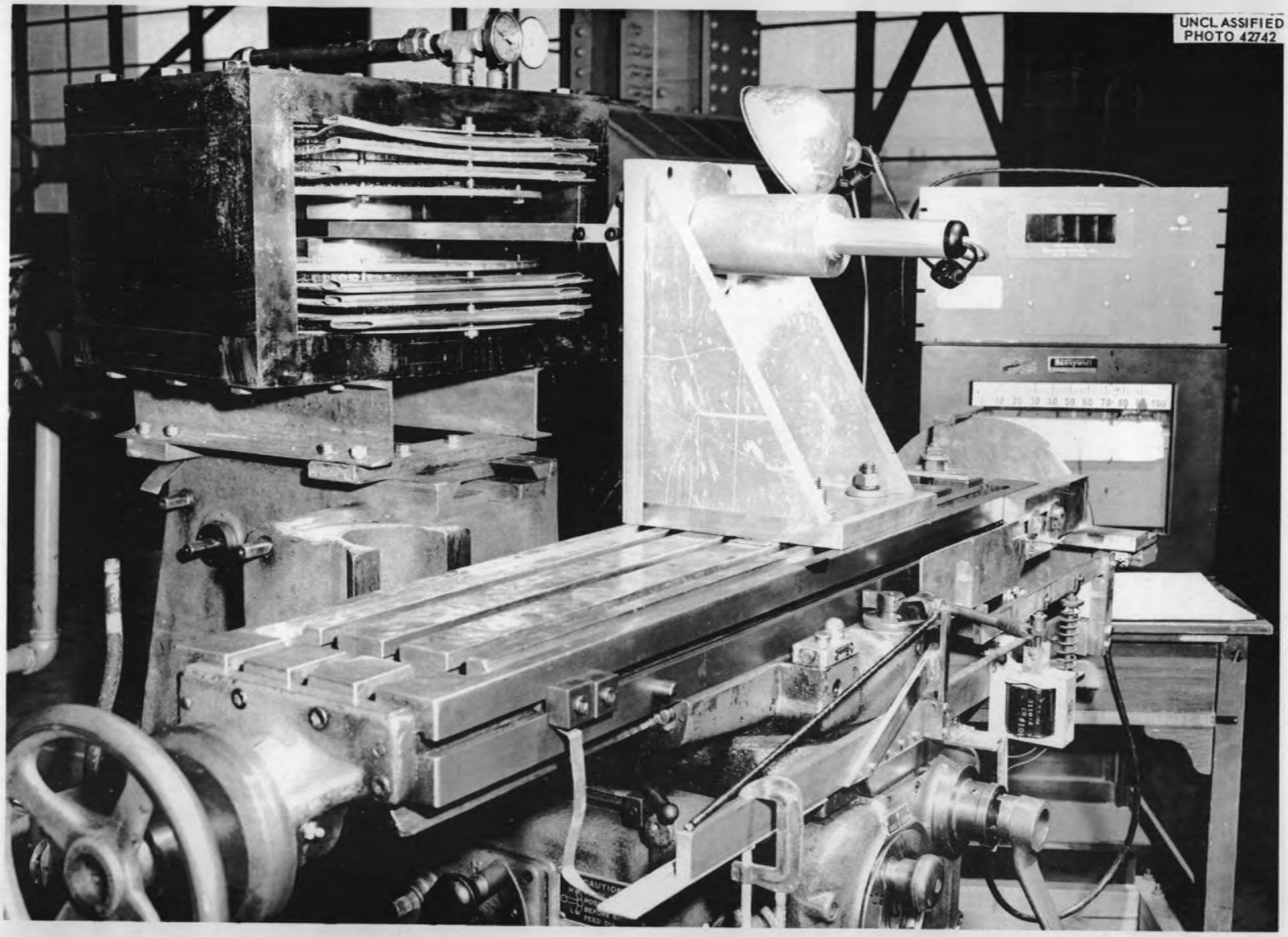

Fig. 4. Model Magnet and General Arrangement for Field Measurements.

point of the rectangular grid can be read and punched on paper tape for input to the computer. It should be pointed out that the data must be converted from rectangular to polar form before the properties of the magnet can be calculated.

A typical field contour obtained from a model is shown in Fig. 5. The field contours follow the shape of the iron reasonably well along most radii except for the central region and for the radii near the edge of the pole.

The accuracy of the data depends on several things:

Source of Error	% Error in Field
Recorder	0.2
Chart Reading	0.1
Probe Position	0.4
Fluxmeter	0.1
Current Regulation	0.3
Total RMS Error	0.6

The error due to probe position varies depending on the field gradient. The gradient varies from zero to 18 kilogauss per inch. When the errors in model construction are included, the error in field measurement will easily reach 1%. The errors listed, however, are for a given point. The errors for average B or for the flutter will be substantially lower. Some of the errors can be reduced by more accurate model construction and more accurate position of the fluxmeter probe; however techniques available to us at this time fall short of the desired 0.1% accuracy.

Most of the models tested have been exploratory in an effort to determine the general parameters for several types of machines. Fig. 6 shows a three-sector model with the upper half of the magnet moved up so that the tip geometry is visible. A similar view of a four-sector model is shown in Fig. 7.

UNCLASSIFIED
ORNL-LR-DWG 30107

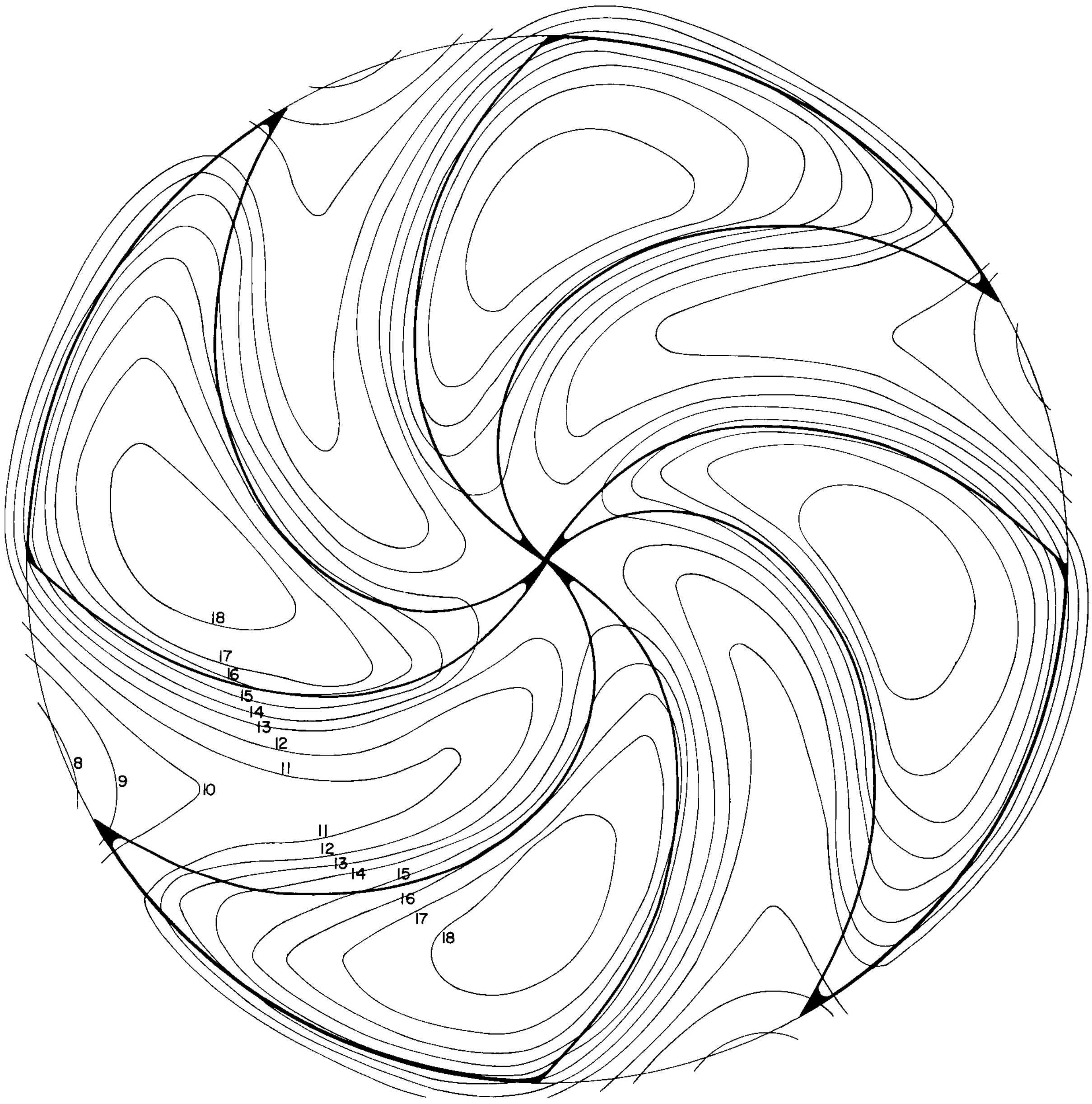

Fig. 5. Typical Field Contours Obtained for a Four-Sector Magnetic. No current in valley coils. (Magnetic field in kilogauss.)

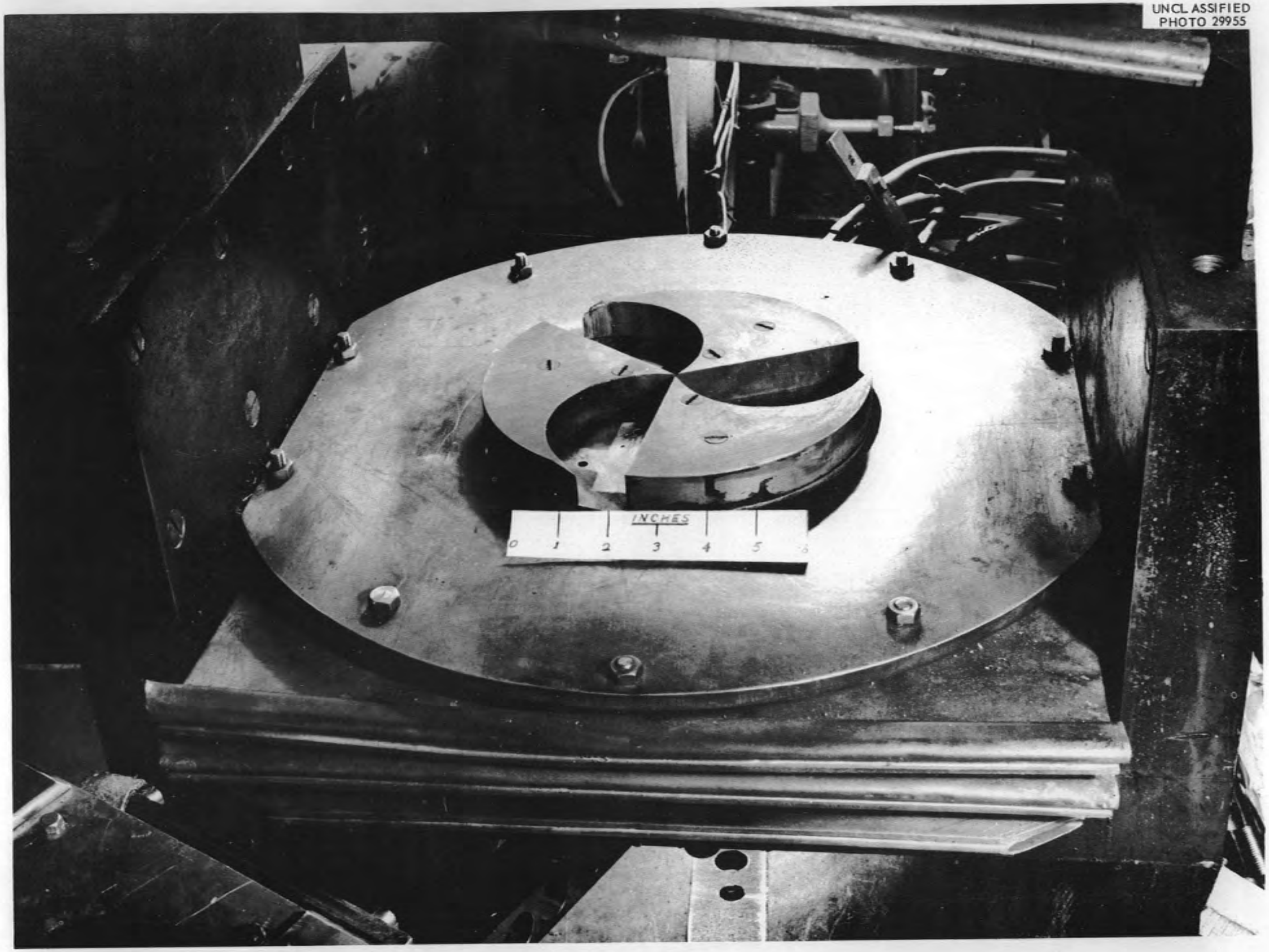

Fig. 6. Lower Half of Model Magnet with Three-Sector Pole Tip.

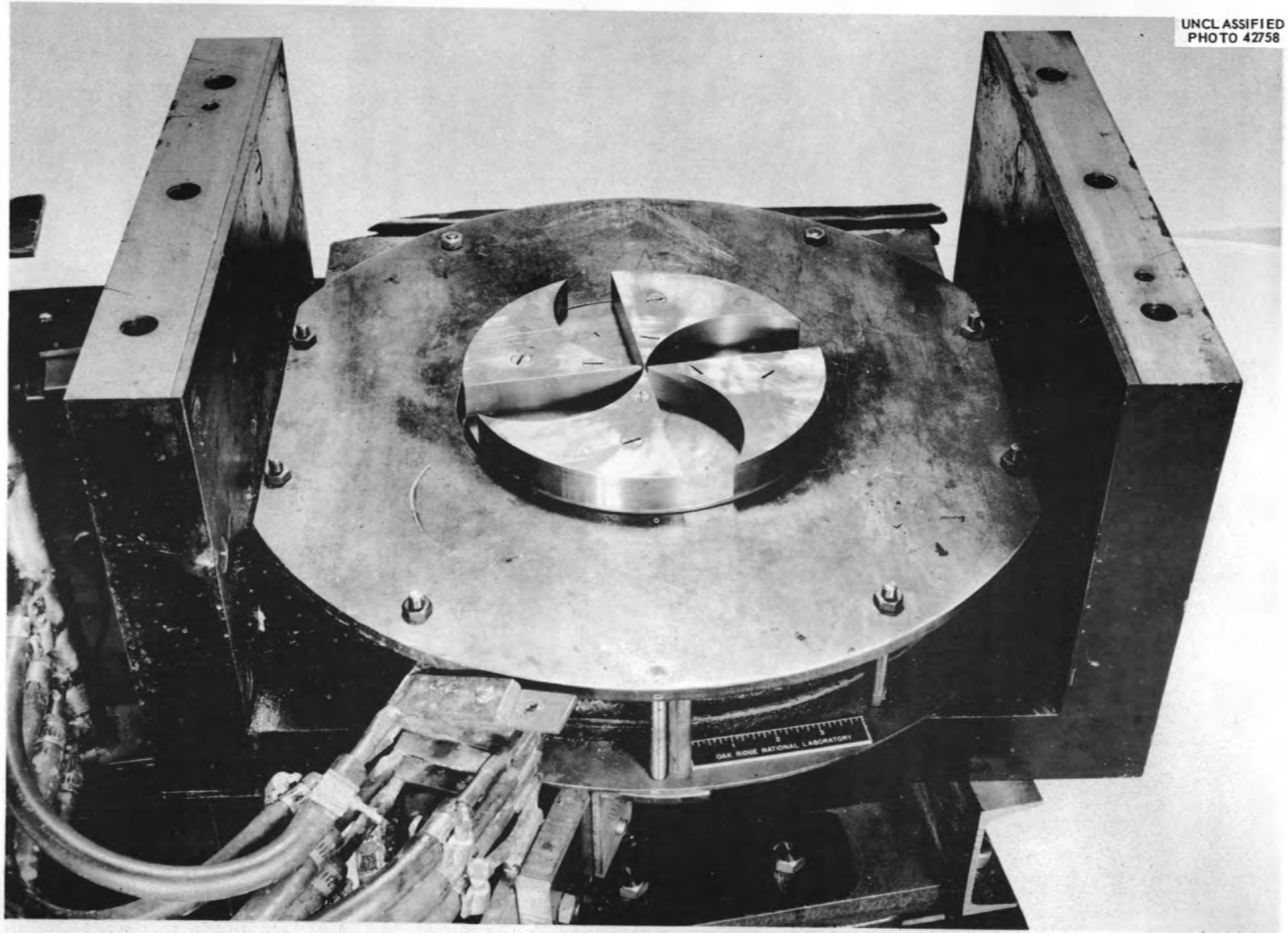

Fig. 7. Lower Half of Model Magnet with Four-Sector Pole Tip.

The auxiliary windings as well as valley coils of 1/2 x 1/16 in. are shown in Fig. 8. As the main coils are moved closer to the median plane or as a large percentage of the ampere turns are contributed by the auxiliary coils, the efficiency of the magnet increases. For example, when the hill field was 20 kilogauss the energizing current decreased 25% as the coils were moved one inch closer to the median plane.

The valley coils were pulsed at 1,000 to 2,000 amperes for 2 or 3 seconds; the data was recorded as shown in Fig. 9. The Brown chart runs continuously while the probe is moved from position to position and left at each position for about 10 seconds while the field at that position is recorded. When the valley coils are pulsed, the field contribution due to these coils appears as a negative pulse on the chart since their main function is to deepen the valley or lower the field in this region.

A set of coils shown in Fig. 10 was formed from 1/4 x 1/4 in. copper with 1/8 x 1/8 in. water passage. These coils were energized continuously at currents above 3,000 amperes for a current density of 70,000 amperes/in.^{2} The total power in the valley coils was 100 kw supplied by one generator while the 50 kw for the main magnet coils was supplied from a second generator . We are very fortunate to have available two 1,750-kw generators. Models seldom require over 200 kw; however at times the 350-volt rating of the generator has governed the test and in other tests the 5,000-ampere current rating has been the governing factor. When pulsed measurements are made, the currents are limited to approximately 2,000 amperes by the breaker used to interrupt the current.

Forces on the coils and the magnet cores are shown in Fig. 11. At low excitation currents the coil forces were away from the median plane, as is the usual case in iron-core magnets. The forces continued to be away from the gap with increasing magnitude until the excitation current reaches 1,500 amperes. The forces had started to decrease at 2,000 amperes which was the design operating point for this magnet; however the magnet was to be connected to a generator

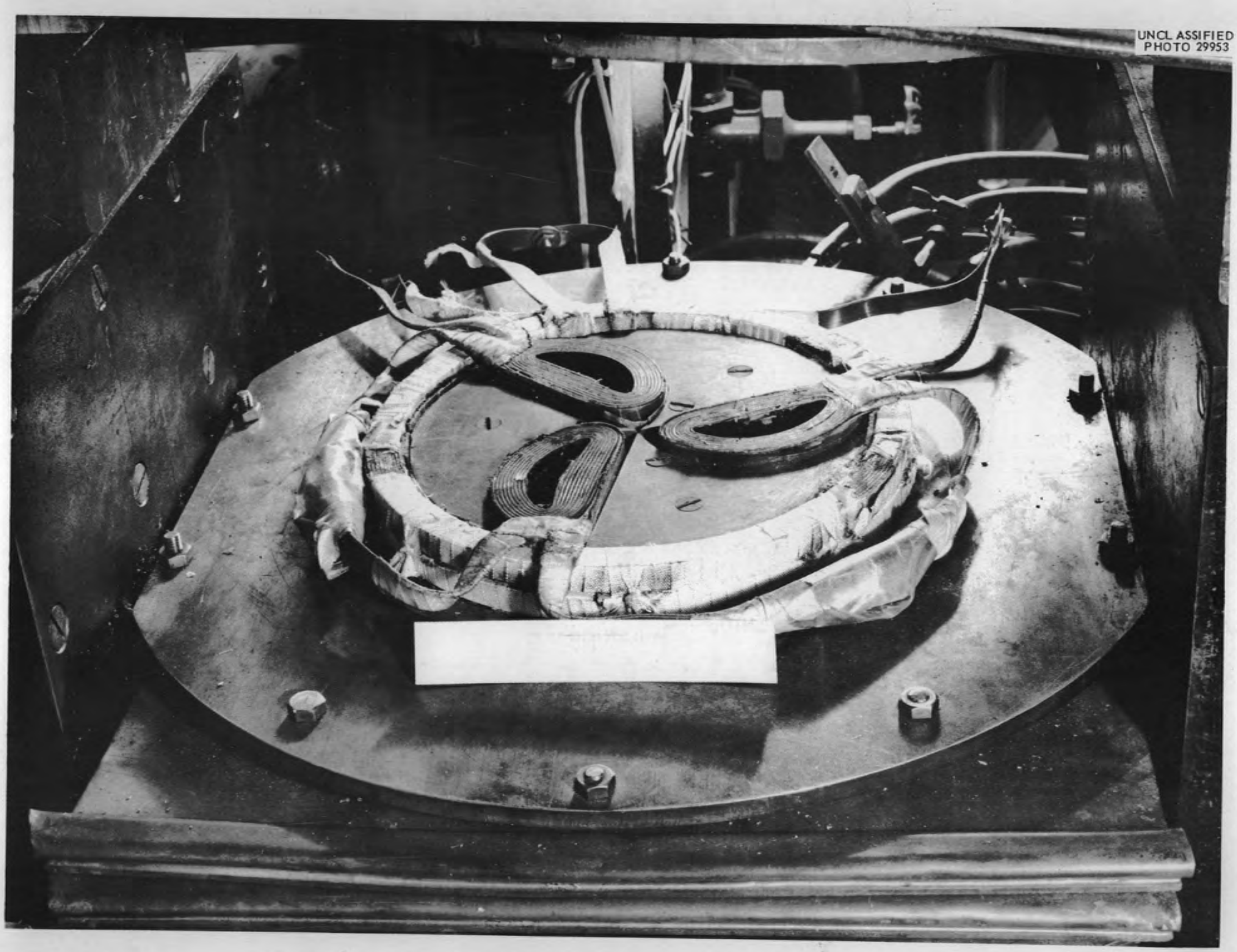

Fig. 8. Auxiliary Windings and Valley Coils of Three-Sector Model.

UNCLASSIFIED
ORNL-LR-DWG 30106

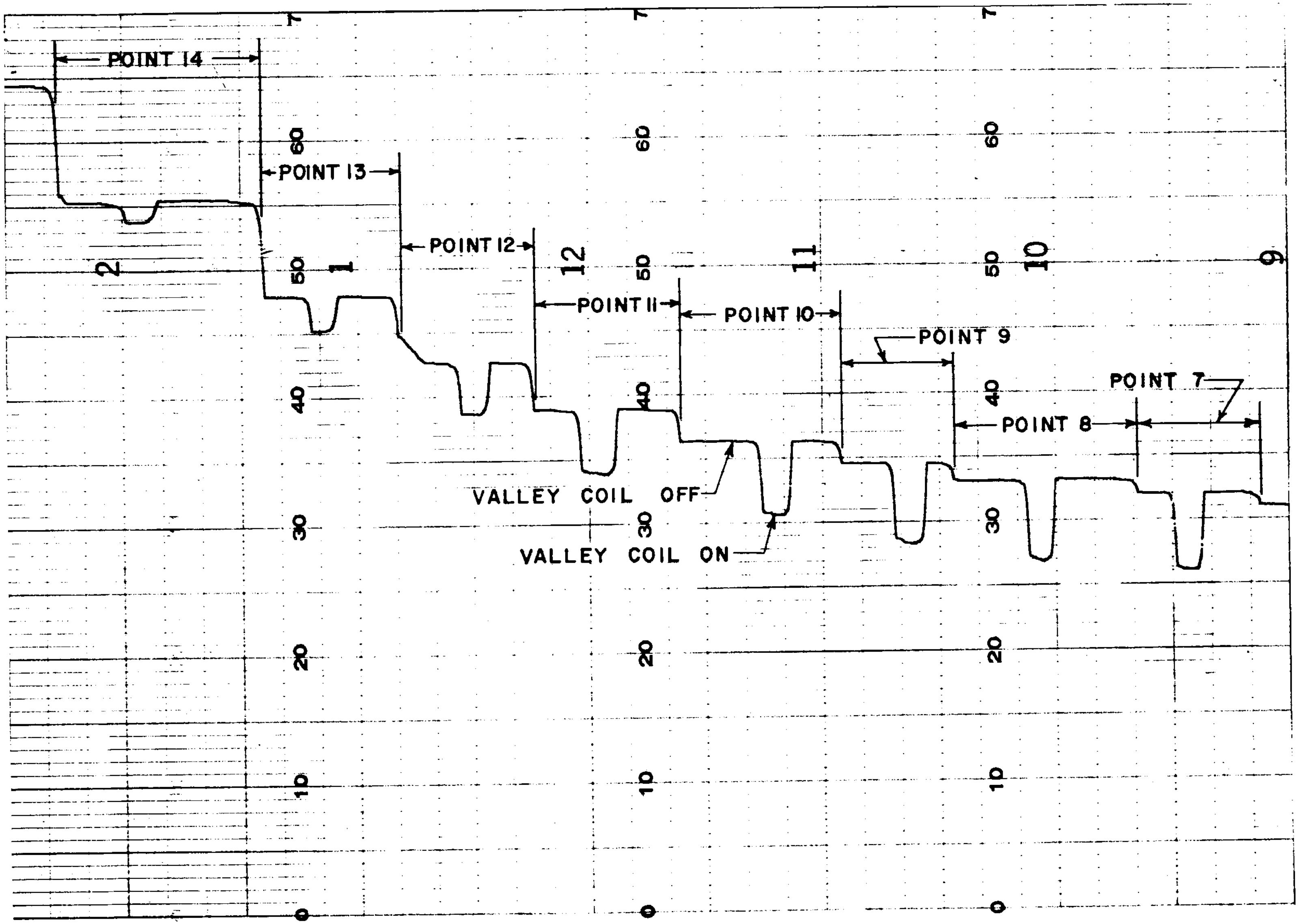

Fig. 9. Data from Recorder Showing Effect of Valley-Coil Currents.

UNCLASSIFIED
PHOTO 31579

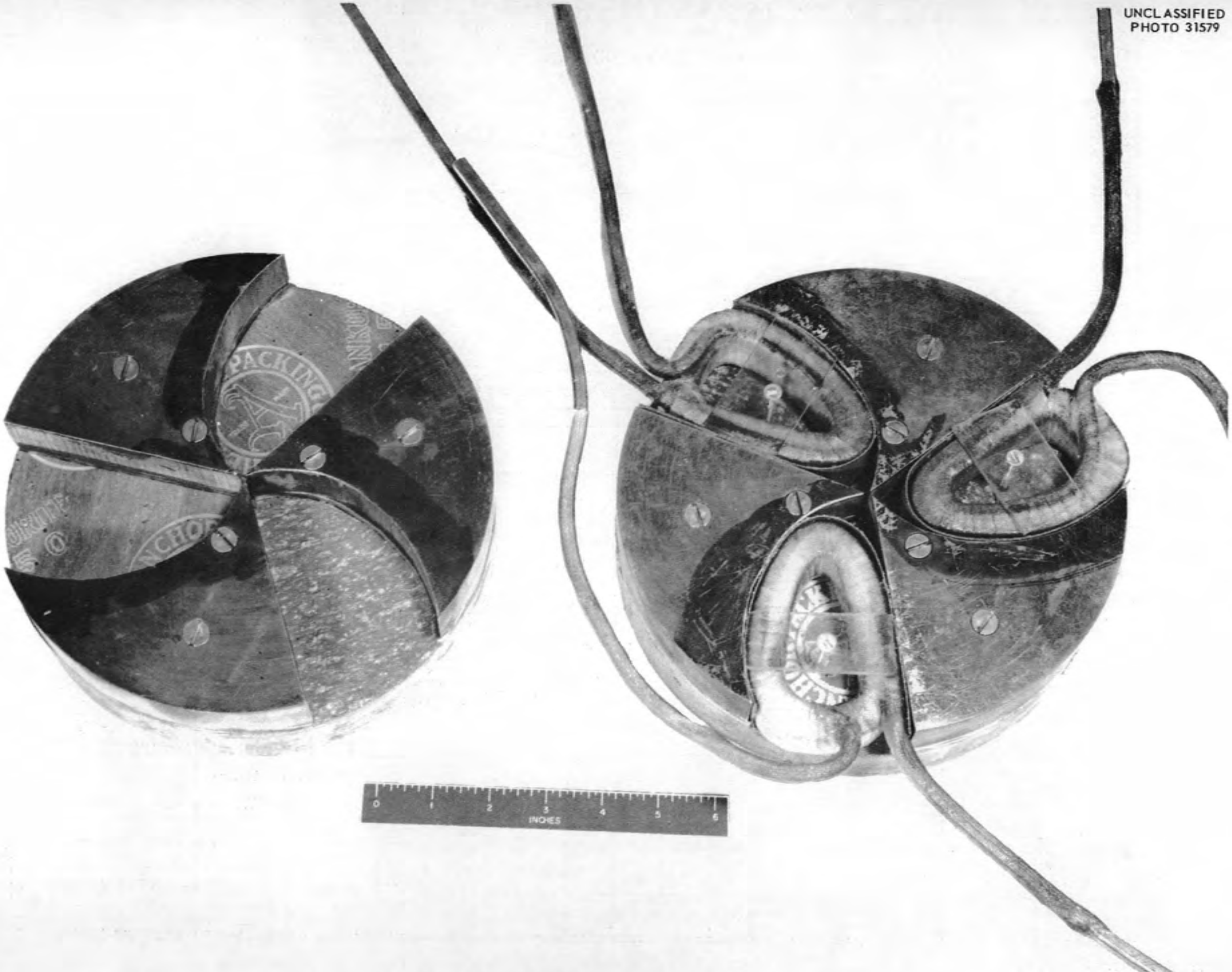

Fig. 10. Water-Cooled Valley Coils in Three-Sector Model.

UNCLASSIFIED
PHOTO 31643

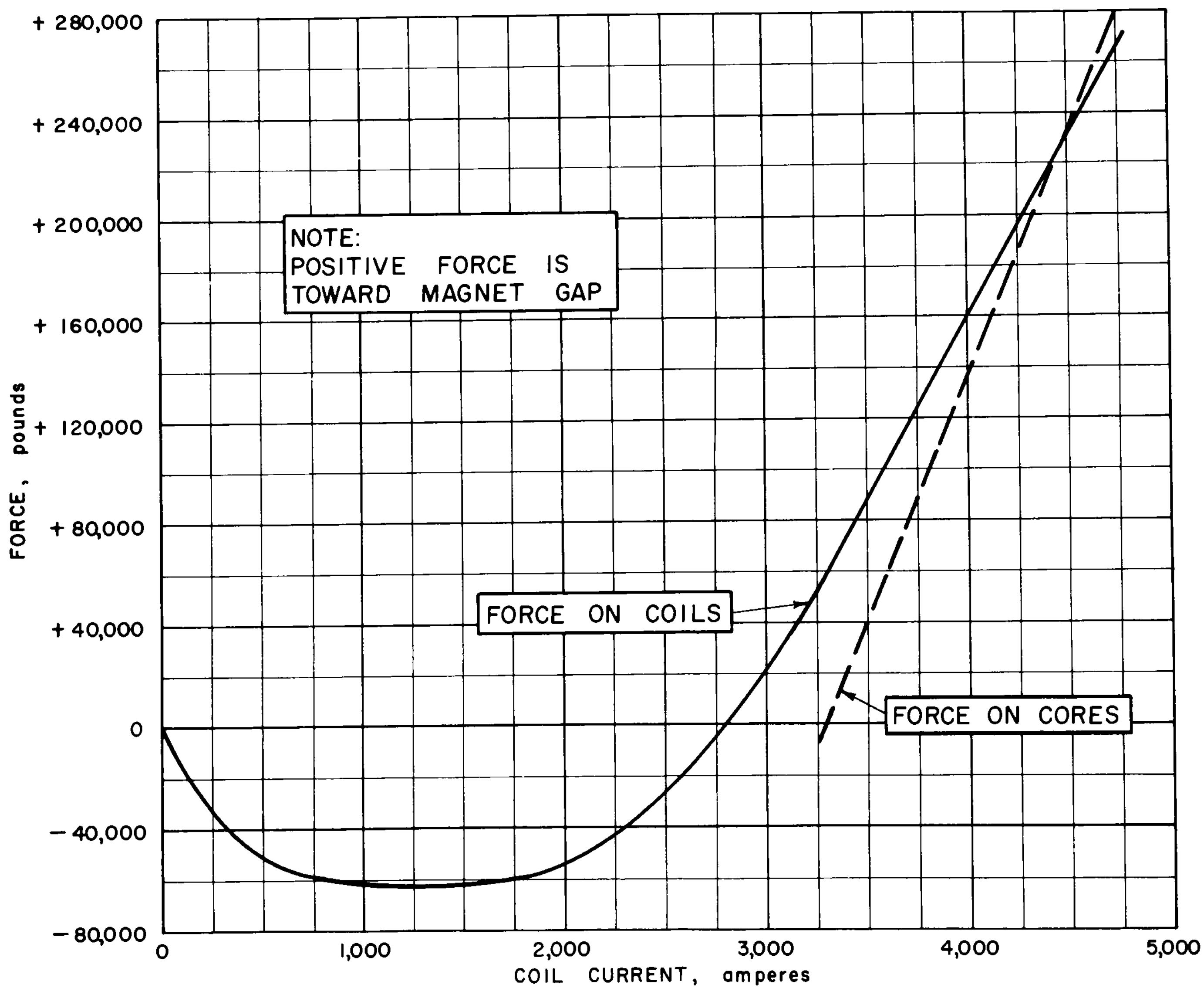

Fig. 11. Forces on the Coils and Cores.

that under certain fault conditions could drive the current up to 4,500 amperes where the force was nearly 240,000 pounds toward the gap. A similar condition existed for the core. In this case the core separated from the yoke and tended to move toward the median plane because the core extended through the coil about 11 in. This is the distance the coils were moved toward the gap to improve the efficiency, so that sufficient leakage at the high fields gave a larger H in the gap than between the yoke and the pole. These numbers are not presented to do any more than to point out that as magnets are designed and built to operate at higher and higher field intensities, the conventional direction of the forces for an iron core magnet may reverse and allowance for this reversal must be incorporated in the mechanical design of the system.

A 1/8-scale model of a 110-in. diameter, 4-in. gap, 4-sector magnet with individually energized sectors is shown in Fig. 12. This type of magnet would be used with accelerating cavities instead of a dee system. The cores are separated 12 in. to provide a 4-in. space for the cavity and 4 in. for each of the coils around the sectors. The coil cores were formed by sawing a 93-in. diameter disc into four equal parts and separating to 110 in. diameter. The shape of the pole tips required to produce the desired field would be similar to these tips. The tip separation is 2 in. at the center, in an attempt to obtain the desired average field. More measurements will be necessary to arrive at a suitable field in this region. The desired flutter was easily obtained in this type of magnet since the gap was 4 in. and since the main coils acted as valley coils.

Some consideration has been given to the use of the "Hall effect" as an alternate method of magnetic field measurement, both for the model studies and for the full scale machine. Hall generators with temperature coefficients of 0.04 to 0.06% per degree Centigrade are commercially available from Siemens and Halske in Germany, and were used at CERN for measuring the magnetic field of the synchrotron.

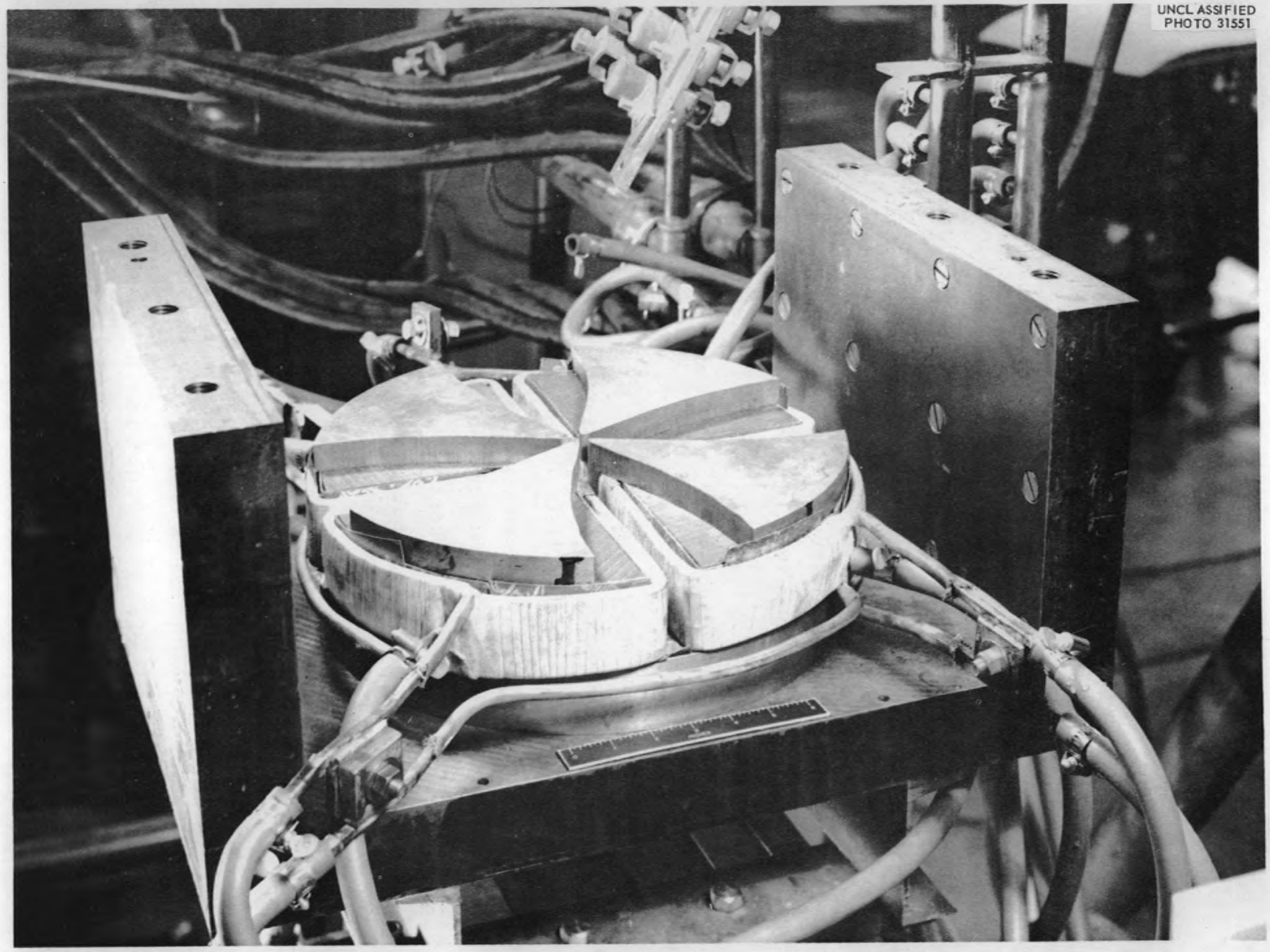

Fig. 12. Model Magnet with Four-Sector Main Coils.

Several of these Hall generators are on order; it is planned to incorporate one or more of them into a more automatic system of measurement. The output of the Hall generator is a d-c voltage of the order of 100 millivolts and is proportional to the magnetic field intensity. In principle, this voltage could be measured by a self-balancing potentiometer or digital voltmeter and punched on to paper tape or cards for input to a computer. This system would eliminate the time consuming operations of reading a chart and punching the data by hand, and at the same time eliminate errors that occur during these operations. It is possible that such a system would be considerably more accurate than the present method and would certainly be faster.

C. Design Study Procedure

The design of the AVF magnet is accomplished by a successive approximation procedure, as is standard in studies of this type. The magnetic field produced by a given magnet structure is determined (*via* the model magnet procedure described in the previous section), the orbit properties of this field are calculated, and corrections to the magnet structure are inferred from the orbit properties. The effectiveness of such procedures can vary enormously depending on the acumen with which choices are made in regard to magnet configuration and the subsequent revisions. The situation is complicated by the large number of parameters to be specified by the designer. A semi-empirical model of the field of a given magnet was effectively employed to guide the initial estimate and to gauge subsequent corrections.

The method is restricted to pole tips of right cylindrical form; for such, the tip geometry is completely prescribed by specification of pole diameter, number of sectors, hill gap, valley gap, angular width of hill as a function of radius, and spiral of the hill as a function of radius. Pole structures being investigated at nearly all sites have right cylindrical tips so that the restriction is small. (The University of Florida is, to our knowledge, the only location where poles of a different goemetry are being studied.) In addition to the magnet tip parameters, the location and number of ampere-turns of the various coils must be specified to complete the description of the magnet. It is assumed that the yoke is designed on the basis of standard practice, such that the magnetomotive drop in the yoke is small.

The analytical model of the field is a linear-edge approximation in which the field is assumed to be constant in hill and valley regions and to vary linearly in fringing regions. If the problem is an initial guess with no previous data available, the magnitude of hill and valley regions is estimated from empirical excitation curves such as those of Fig. 13. If the problem is one of gauging corrections to a previous run, the hill and valley magnitude is set from the previously observed values. The field is assumed to fall off linearly at all edges with $dH/ds = H_{max}/2g$, for ds perpendicular to the field edge, and where H_{max} is taken to be the value of the field in the flat region from which the falloff originated. The falloff is assumed to begin a distance of 0.6 g inside any edge of the magnet structure. Fig. 14 shows the contour map for one of the magnet configurations which results from the linear-edge approximation. This can be compared with typical field contours obtained for a four-sector magnet, Fig. 5. The two contours are considerably different in detail, but much less different in terms of the average properties $\langle B \rangle$ and F which are of primary concern, as is discussed subsequently. The approximate contour, moreover, can be calculated in 10 minutes whereas the measured contour represents approximately a man-month of work.

The approximate contour serves the important purpose of yielding a simple algebraic relationship between the magnet structure parameters (hill gap, valley gap, hill width, excitation, radius, etc.) and the $\langle B \rangle$ and F. If we define a_1 to be the fraction of circumference subtended by the hill region at a given radius, a_2 to be the fraction subtended by an average fringing edge and ζ to be the ratio of hill to valley field strengths, then $\langle B \rangle$ and $\langle B^2 \rangle$ are given by the expressions in Fig. 15, and F is, of course, simply

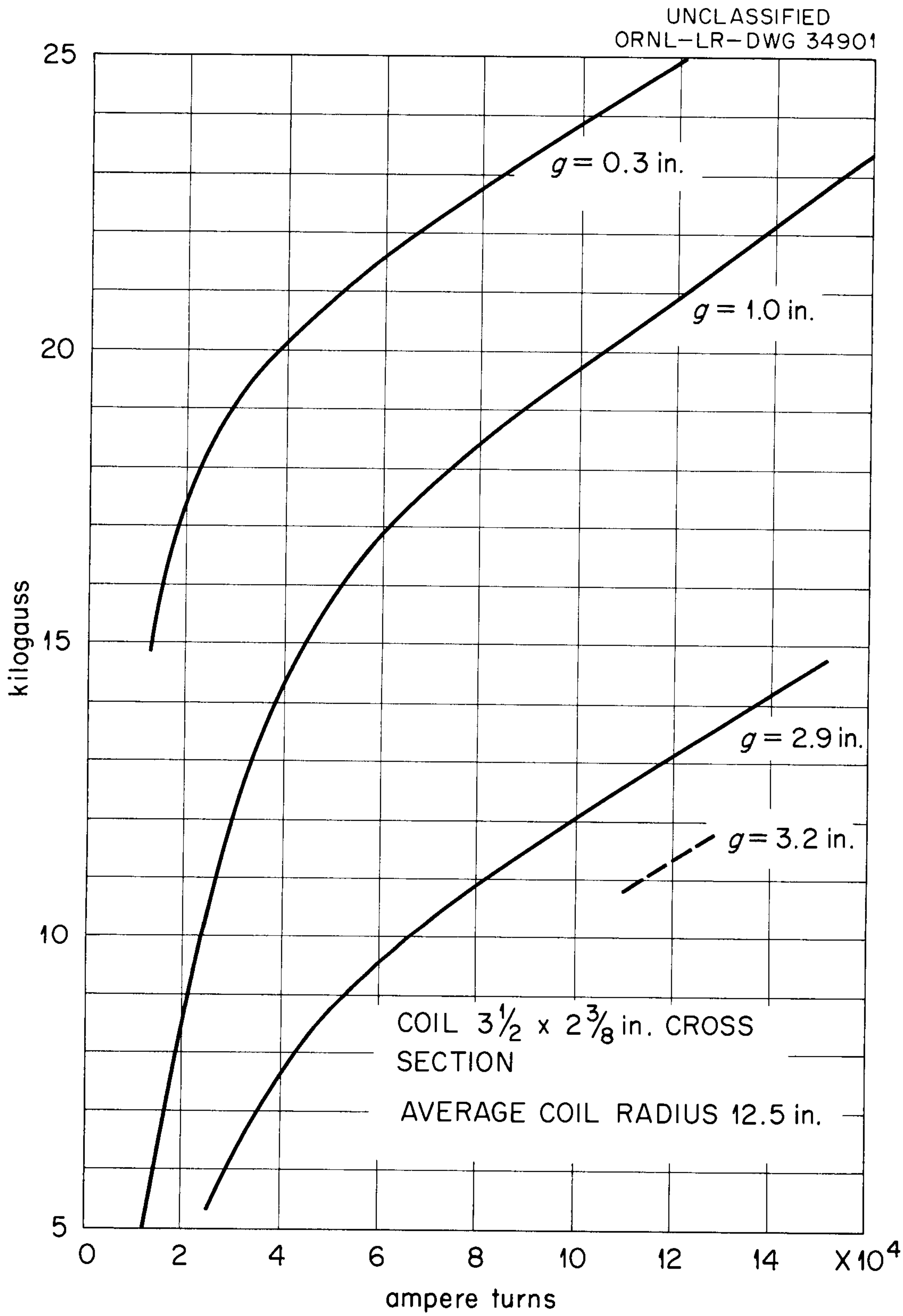

Fig. 13. Magnetization Curves for 8.75-in. dia Cylindrical Pole.

UNCLASSIFIED
ORNL-LR-DWG 34902

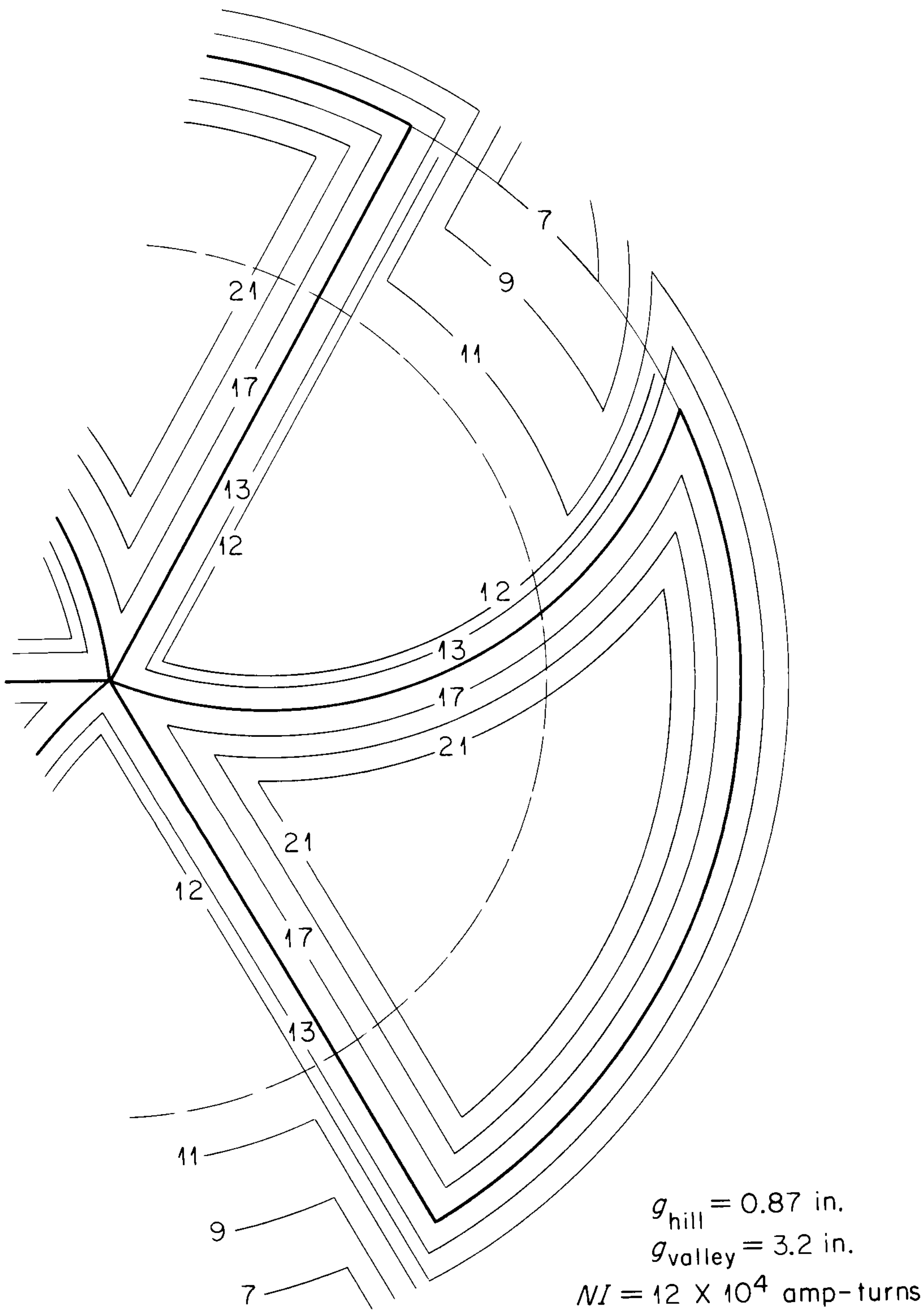

Fig. 14. Contour Map from Magnetization Data. Linear-edge approximation.

UNCLASSIFIED
ORNL-LR-DWG 28952R

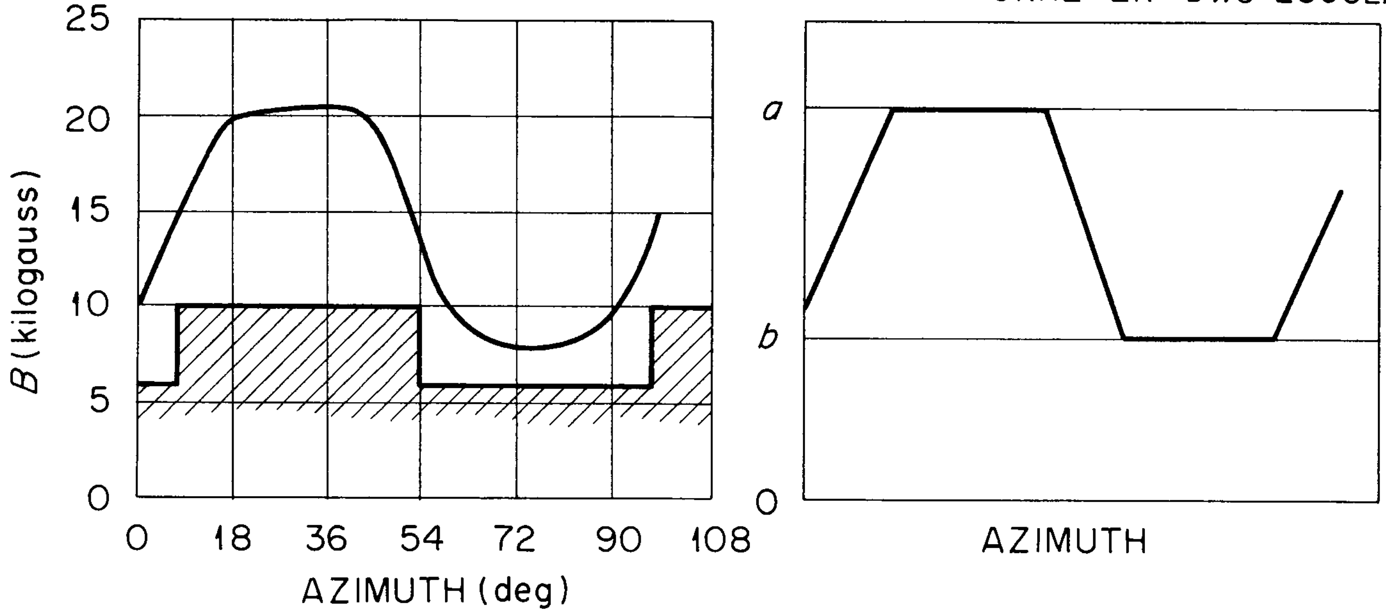

α_1 = RELATIVE WIDTH OF HILL

α_2 = RELATIVE WIDTH OF ONE FRINGING EDGE

$$\zeta = \frac{b}{a}$$

$$\langle B \rangle / a = (\alpha_1 + \alpha_2) + (1 - \alpha_1 - \alpha_2)\,\zeta$$

$$\langle B^2 \rangle / a^2 = (1 - \alpha_1 - \tfrac{4}{3}\alpha_2)\,\zeta^2 + \tfrac{2}{3}\alpha_2\,\zeta + \alpha_1 + \tfrac{2}{3}\alpha_2$$

Fig. 15. Definitions and Relationships.

$(\langle B^2 \rangle / \langle B \rangle^2) - 1$. By use of these expressions the $\langle B \rangle$ and F of new magnet configurations can be quickly computed and also corrections to parameters of magnets already tested can be computed to accomplish desired changes in $\langle B \rangle$ and F.

As an example of how the approximation is applied to new, untested magnet configurations, consider the configuration from which Fig. 14 is derived. First, by reference to the excitation curves of Fig. 13, the hill and valley field strengths are determined, and from this, a contour map such as Fig. 14 is plotted. From the contour map, the relative widths of hill and fringing edge are determined by measurement. These values are inserted in the formula for $\langle B \rangle$ and F. If, for example, we compute at the radius of the dotted curve in Fig. 14, the hill measures 47.5 deg and the two fringing edges 14 deg and 16.5 deg, which yield values for α_1 and α_2 of 0.396 and 0.127. The hill field $\underline{a}$ is 21 kilogauss and the fractional strength of the valley field ρ is 12/21 or 0.572, which gives:

$$\langle B \rangle / a = (0.396 + 0.127) + \left[1 - (0.396 + 0.127)\right] 0.572 = 0.796$$

$$\langle B \rangle = 16.7 \text{ kilogauss}$$

$$\langle B^2 \rangle / a^2 = (1 - 0.396 - 4/3 \times 0.127)(0.572)^2 + 2/3 \times 0.127 \times 0.572 + 0.396 + 2/3 \times 0.127 = 0.671$$

$$F = \frac{\langle B^2 \rangle}{\langle B \rangle^2} - 1 = \frac{0.671}{(0.796)^2} - 1 = 0.058$$

From the actual measurements made subsequently, $\langle B \rangle$ and F at this radius were found to be 17.3 kilogauss and 0.056, respectively, so that the approximate prediction is in error by about 4% in each case. Calculations of this type are then of great value in estimating the performance of magnet configurations for which previous data are unavailable. The calculations are substantially more accurate than the often used hard-edge approximation in which fringing is neglected and hill and valley fields are assumed to be of uniform strength over their complete respective areas of the poleface.

The application of the linear-edge approximation to obtain corrections to a previously measured configuration is illustrated in the upper part of Fig. 15. Here the observed field profile at some radius is shown on the left; a linear edge profile which gives a good fit to the observed profile is picked giving the curve on the right and from this, effective values of α_1, α_2, ζ and $\underline{a}$ are obtained. Correction terms are calculated by standard inversion of the formulas for $\langle B \rangle$ and F. If for example it is desired to correct $\langle B \rangle$ by a change in the width of the hill α_1, we have

$$\frac{2 \langle B \rangle}{2 \alpha_1} = 1 - \zeta \ ,$$

and hence,

$$\Delta \alpha_1 = \frac{1}{1 - \zeta} \quad \Delta \quad B \quad .$$

An actual application of this procedure is shown in Fig. 16. For lower solid curve in the figure $\langle B \rangle$ was taken from early model studies at the University of California. Corrections to this were computed, gauged to give the dashed curve in the figure. A set of pole tips with the corrected shape was fabricated and when tested in the model magnet yielded the upper solid curve in Fig. 16. The field of the iron should follow the desired contour to an accuracy of about 0.3%; the corrective procedure usually accomplishes this in 2 or 3 iterations.

UNCLASSIFIED
ORNL-LR-DWG 28954

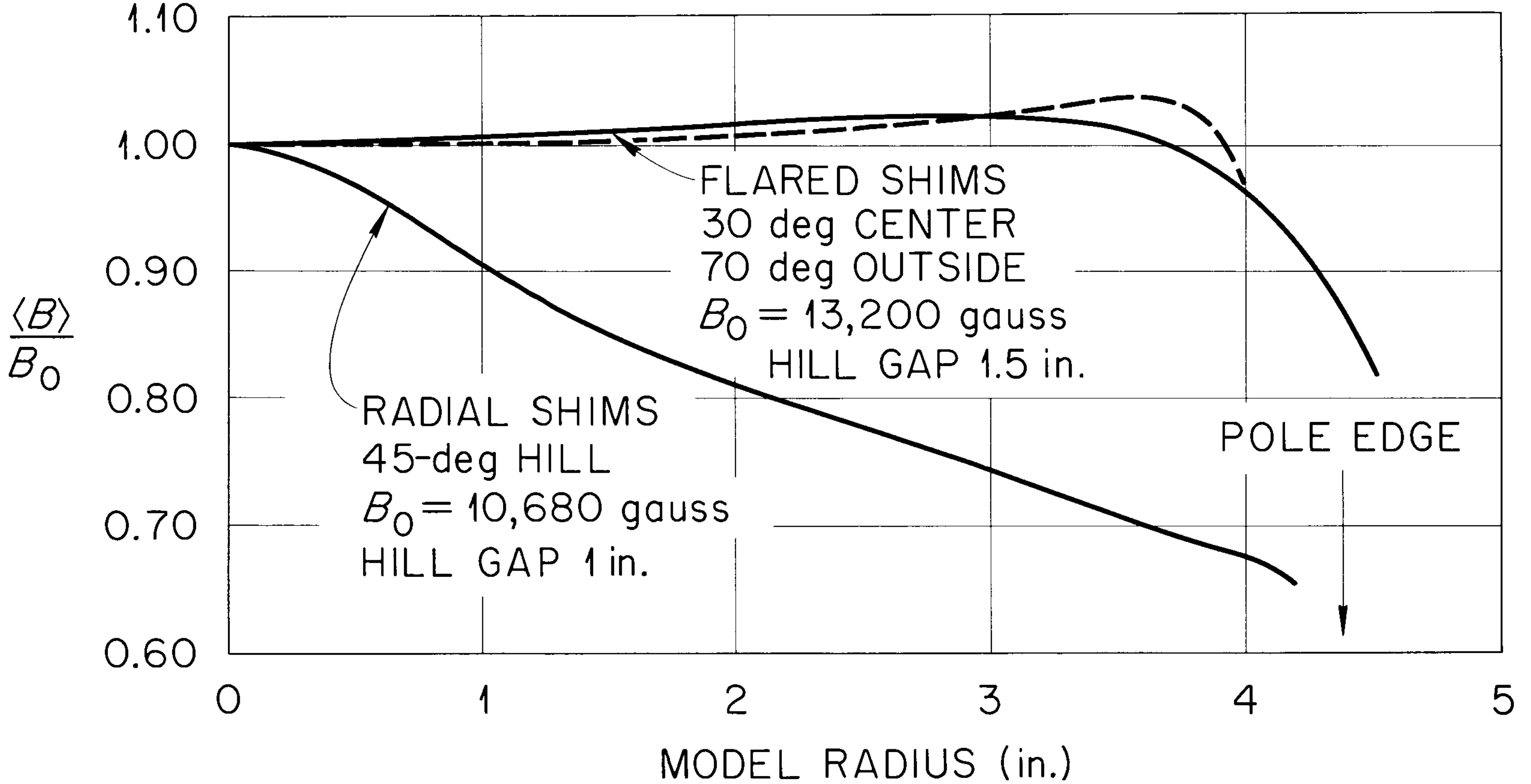

Fig. 16. Typical <B> Corrections.

In Figure 17 results of application of the procedure to correction of the flutter are shown. The lower solid curve in the figure labeled "0.90-in. gap" is a flutter curve from an early run. It was desired to convert this to a value of 0.11 at 3.5-in. radius* by changing the $\mathcal{F}$. Two independent procedures for changing $\mathcal{F}$ were used; the first increased the hill field by reducing the magnet gap giving the curve labeled "0.50-in. gap", the second decreased the valley field by means of deexciting coils around the periphery of the valley and gave the curve labeled "0.90-in. gap, valley coils on". For the large magnitude of the correction, both curves give values reasonably close to the desired 0.11 at 3.5 inches.

Another interesting feature of magnets with radial (or nearly radial) sectors and right cylindrical tips is illustrated in Figure 17. If the flutter curves are compared with the $\frac{R}{\langle B\rangle} \frac{d\langle B\rangle}{dR}$ curve the difference, which is ν_z^2, is seen to go through a maximum at intermediate radii. The behavior is illustrated schematically in Fig. 18, the focusing and defocusing terms being given in the left-hand graph and the resultant ν_z on the right-hand graph. The ν_z for H^+ goes through a pronounced maximum and ends at a final value of about 0.2. This intermediate maximum in the ν_z is an inherent property of tips of the type here considered in conjunction with the isochronism requirement. To remove it would require introduction of additional variables such as valley coils with an array of shunts which would vary the valley coil current as a function of radius. The maximum can also be eliminated by proper manipulation of the spiral angle; the fairly tight spirals required appear to be highly undesirable from the point of view of deflector design, as is discussed in a following section.

The effect of the maximum in the ν_z will be to reduce somewhat the radial stability limit for off-median plane motion due to proximity of the operating point to the Walkinshaw resonance. Radial stability limits in this region are quite large in the first place, however, so that this reduction will probably be of small consequence. This will be explored in detail in a subsequent calculation.

---

* An F of 0.11 along with the spiral term and the $(R/\langle B\rangle)\, d\langle B\rangle/dR$ shown, would give the desired 0.2 value for ν_z.

UNCLASSIFIED
ORNL-LR-DWG 28953

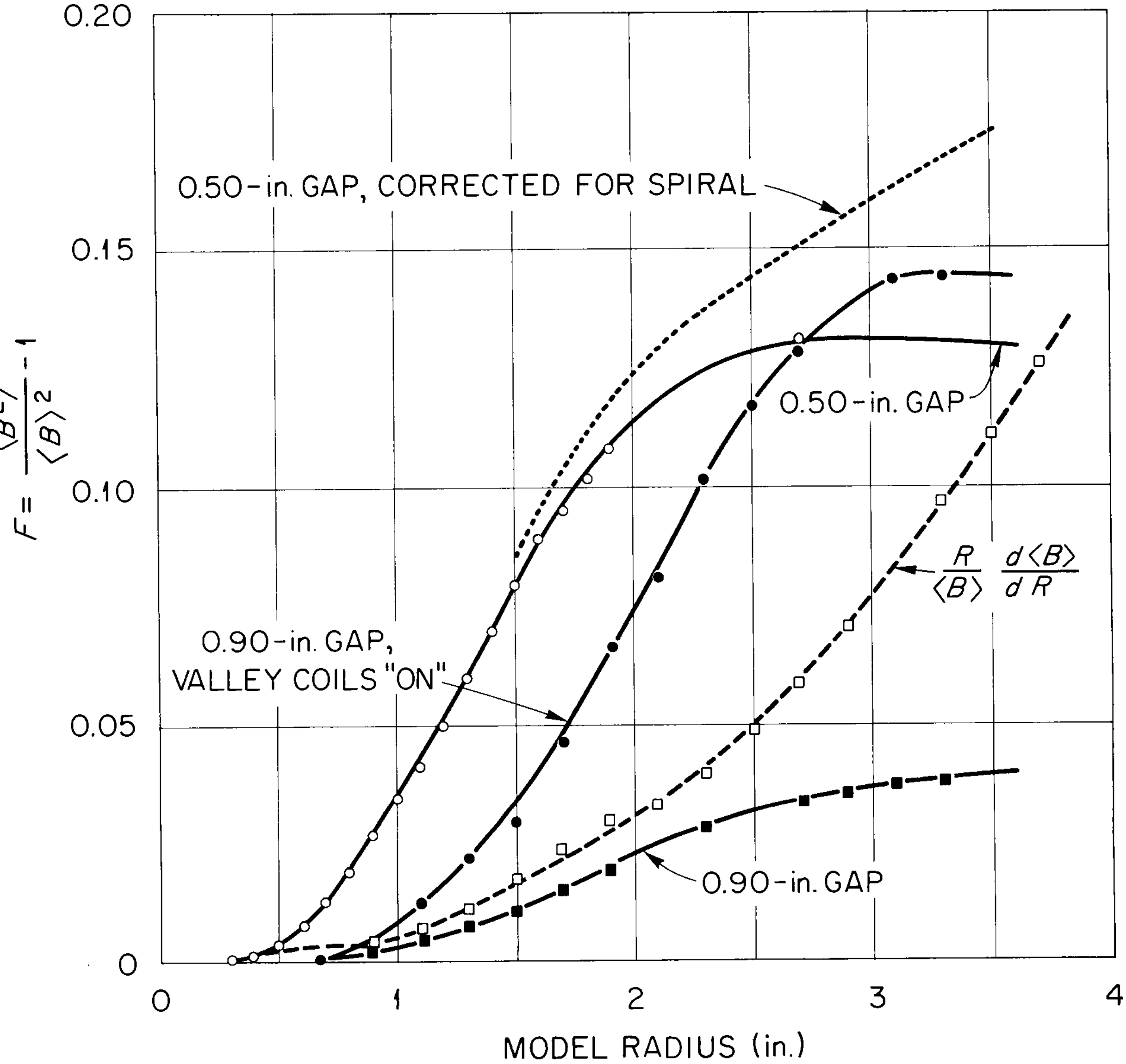

Fig. 17. Typical Flutter Corrections.

UNCLASSIFIED
ORNL-LR-DWG 30131R

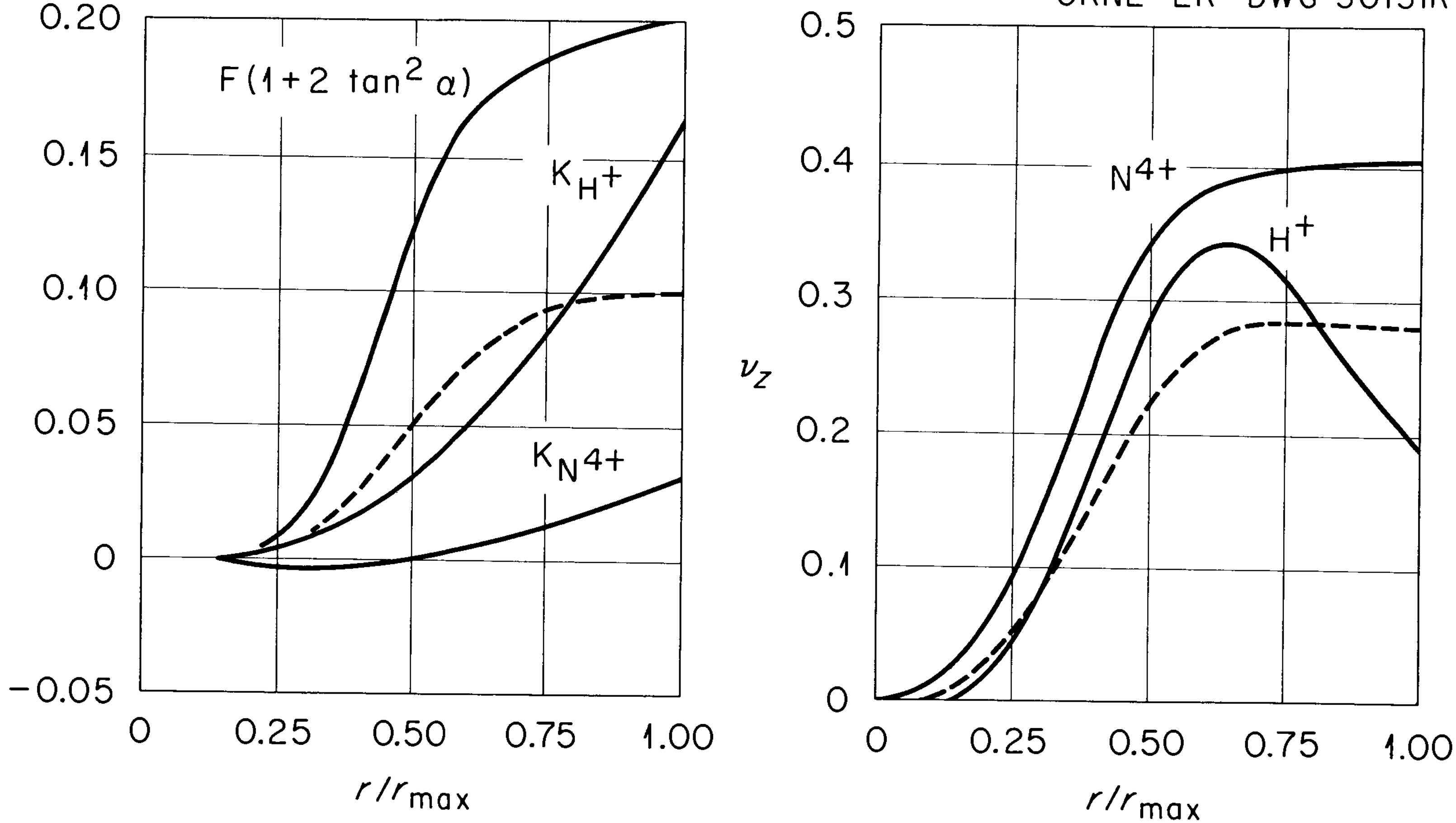

Fig. 18. Schematic Axial Focusing Behavior.

Figure 18 also shows the effect of change of the accelerated particle assuming an accompanying change in the average field to maintain isochronism. If the focusing term F $(1 + 2 \tan^2 \alpha)$ is left unchanged the solid curve on the right labeled "N^{4+}" results; the value of about 0.4 which this curve has at 3.5-in. radius is certain to cause difficulty in deflection due to proximity of the Walkinshaw line. If a portion of the focusing force is derived from supplementary coils such as the valley coils, then the focusing force can be reduced to a value such, as shown by the dotted curve on the left, by simply turning off the supplementary coils. For heavy ions a ν_z of the form shown by the dotted curve on the right results, which is more favorable for deflector design. The valley coils are invaluable for proper control over the ν_z as particles are changed.

In the design of the ORIC most of the magnet parameters were fixed on the basis of theoretical and economic considerations as discussed in other sections; after a particular choice of other variables had been made, the techniques here described were used to determine the hill gap and the angular width of the hill as a function of radius to give the proper $\langle B \rangle$ dependence on radius and the proper focusing at the maximum radius. The method is, however, quite flexible and could be used just as conveniently to fix other design parameters if the conditions of a particular problem made it desirable.

In the preceeding discussion it was assumed that orbit properties were determined, for a given field, by the approximate equations (1) and (5). This is purely a question of convenience. When a given magnet has evolved to a point where exact determination of orbit properties (via numerical integration of the equations of motion) is warranted, the exact results are used to fix the corrections $\Delta \nu_z$ and $\Delta \langle B \rangle$ which are required; these corrections are inserted, and the corrective procedure then procedes just as described.

A comment should be made, also, as to effects of coil position. At the field strengths employed in the ORIC such effects are large. As mentioned in the previous section, it was found that shifting the coils a distance of 1 in. in the model changed by 25% the ampere-turns (and hence power by 50%) required to obtain a given field strength. Curves such as those of Fig. 13 are hence substantially altered, particularly at high excitations if coils are moved. Care must be exercised to use curves applicable for the particular coil position under consideration.

In addition to the problem of obtaining a proper configuration of the iron and main coils, the multi-particle character of the cyclotron requires that trimming elements be available to shift the field shape to correspond to the different rates of mass increase of various particles. In the upper left sketch of Fig. 19 the curves labeled N^{4+} and H^{+} are the isochronous $\langle B \rangle$'s for N^{4+} and H^{+} ions of the same final $H\rho$. At small radii the two curves differ by more than a kilogauss. To obtain the necessary adjustment, the main magnet structure is designed to produce a $\langle B \rangle$ with radial variation corresponding to the curve labeled Fe in the Fig. 19, and a concentric layer of circular coils mounted on the pole face is used to shift the Fe profile up or down as required. These circular trimming coils must produce a maximum field of about 550 gauss with radial variation as shown in the lower left of Fig. 19. This trimming field must be continuously adjustable from "full on" to "full reverse", and in addition substantial changes in shape are required.

The desired corrections can be accomplished by arranging the circular trimming coils in a pancake extending from near the center to the outside of the magnet, with the turns divided into approximately seven separately excited sections. Standard least-square procedures are used to determine the currents in the various sections which give the best fit to the difference between a particular isochronous field and the $\langle B \rangle$ produced by the magnet at a given excitation. In the computation, it is of course necessary to know the radial dependence of the $\langle B \rangle$ produced by a given trimming coil. For present purposes, this dependence has been approximately measured by inserting trimming coils in the model magnet. More precise measurements will be made on the full-scale magnet. The least squares computation, in common with nearly all the computations herein described, have been coded for either the Oracle or the IBM 704. Flow sheets, in outline

UNCLASSIFIED
ORNL-LR-DWG 30130R

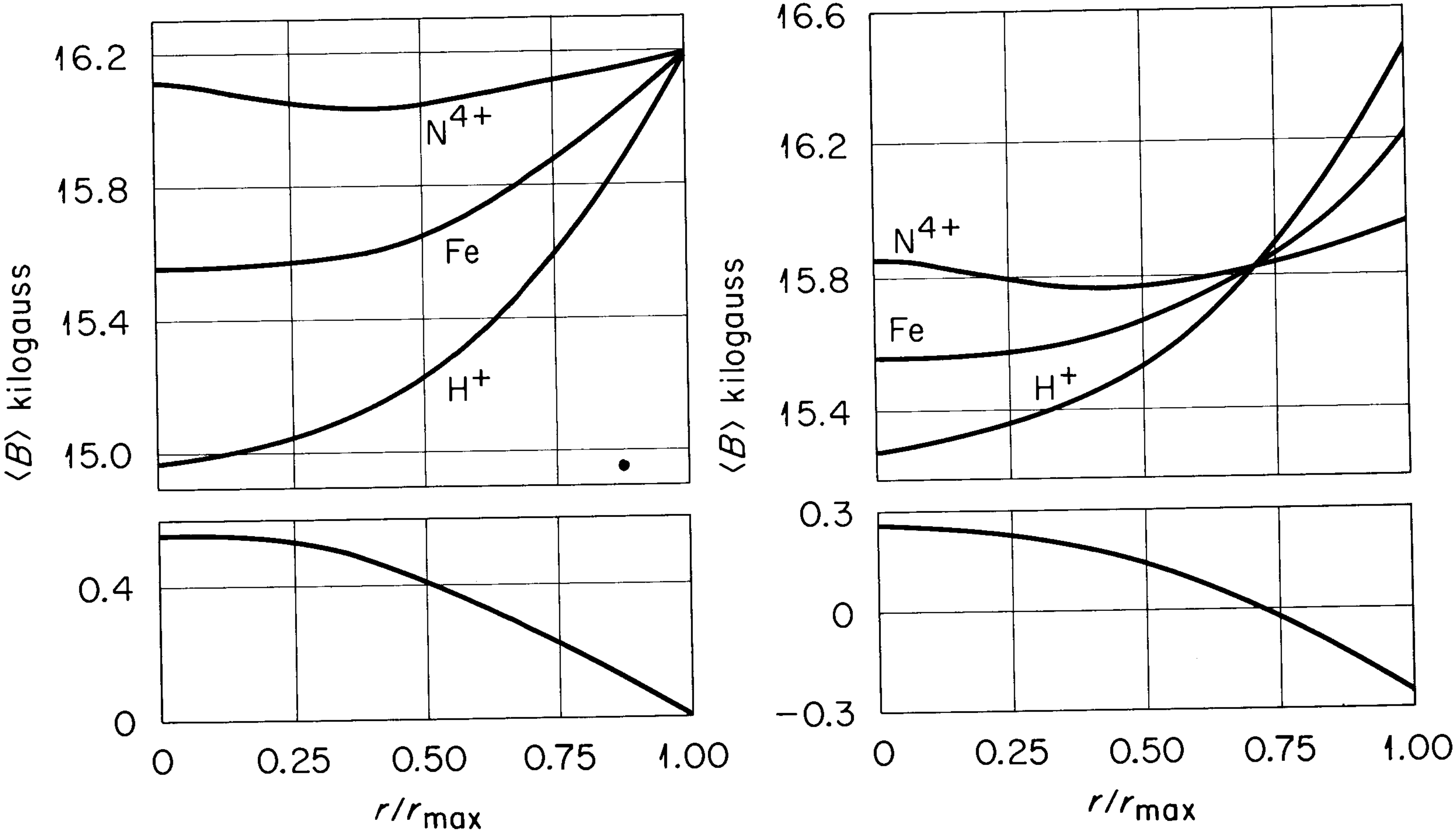

Fig. 19. <B> Trimming Requirements.

and in detail, of the computer program used in the least squares computation are given in Figs. 20 and 21. The program is a typical example of the many useful programs which have been developed in the course of accelerator design studies at ORNL.

The computation assumes the incremental field produced by a given coil to be a linear function of the coil current. For currents of the order required, the model studies indicate this to be a valid assumption. It is quite possible that situations will be encountered where the assumption breaks down, in which case a non-linear least-squares procedures will be substituted. A routine for this type of calculation has already been worked out and although three to four times longer than the linear routine, the added difficulty is not of major character. For the input to this code, the non-linear relationship between $\langle B \rangle$ and I for a particular coil would be determined by model measurements in the same fashion as for the linear problem except that measurements would have to be made at a number of different exciting currents.

Application of the fitting procedure to an actual situation is illustrated in Fig. 22. In the problem the curve labeled $\langle B \rangle$ (iron) is an actually observed set of values from a model run. The curve labeled $\langle B \rangle$ (isochronous) is a calculated curve for nitrogen ions. Best values for the trimming coil currents were computed and the deviation of the resulting field from the desired $\langle B \rangle$ isochronous is plotted on the lower curve, with scale on the right. Radial location of the coils is shown by the arrows along the radius axis. The residual area is quite small and mainly reflects errors in the model measurements. This is indicated by the lack of correlation between coil location and maxima and minima of the deviation, and has been further substantiated by runs in which analytical contours of form similar to the $\langle B \rangle$ (iron) were used in place of the $\langle B \rangle$ (iron). In these latter runs the deviations were a factor of 4 smaller and showed coherence with the coil location. The trimming procedures are hence of more than sufficient accuracy to meet the requirements. In operation the proper setting of the currents will be computed for every energy of every particle as needed.

UNCLASSIFIED
ORNL-LR-DWG 32319

(a) THE FIELDS FROM EACH COIL ARE CALCULATED AND STORED ON MAGNETIC TAPE IN MATRIX FORM, ONE COIL FOR EACH ROW. THIS IS THE MATRIX (F)

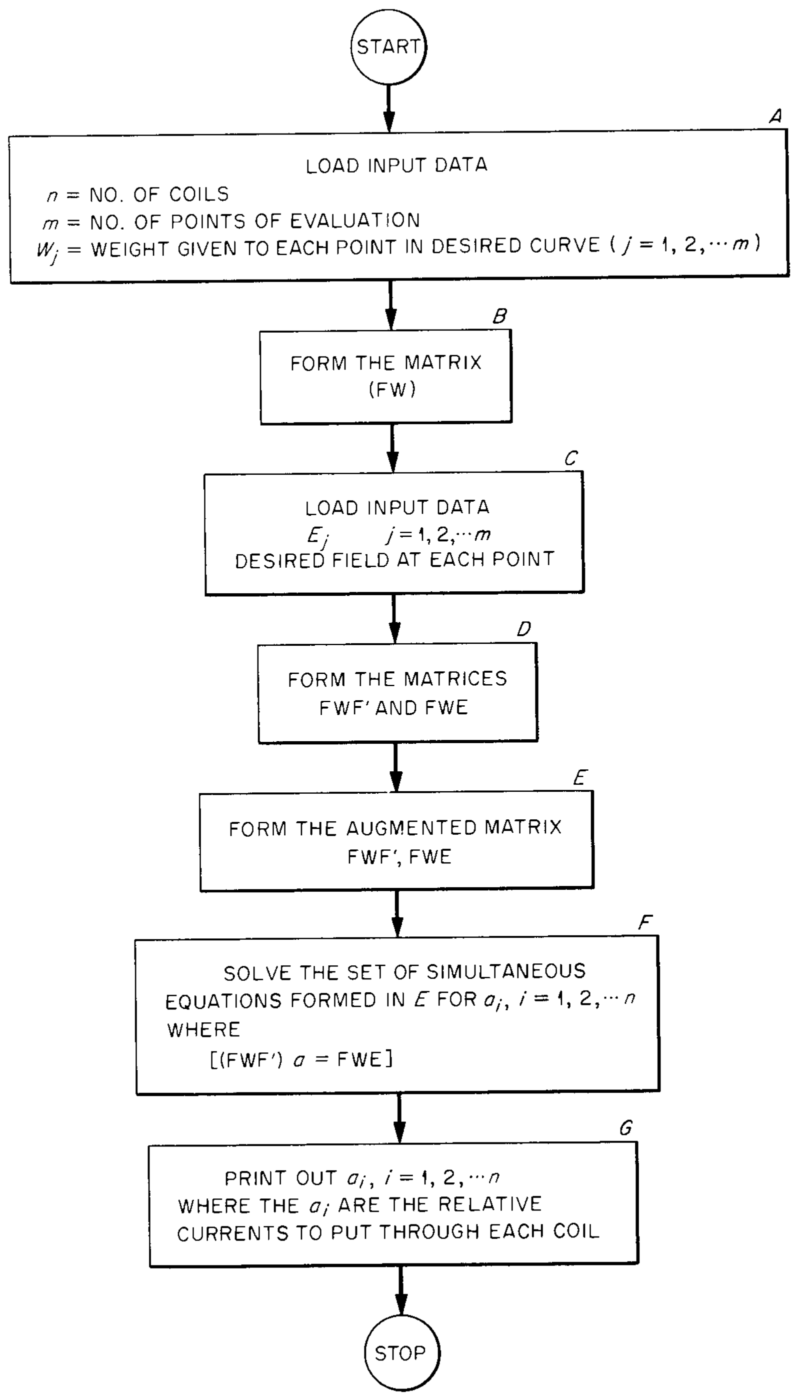

Fig. 20. Circular Coil Current Calculation, Outline.

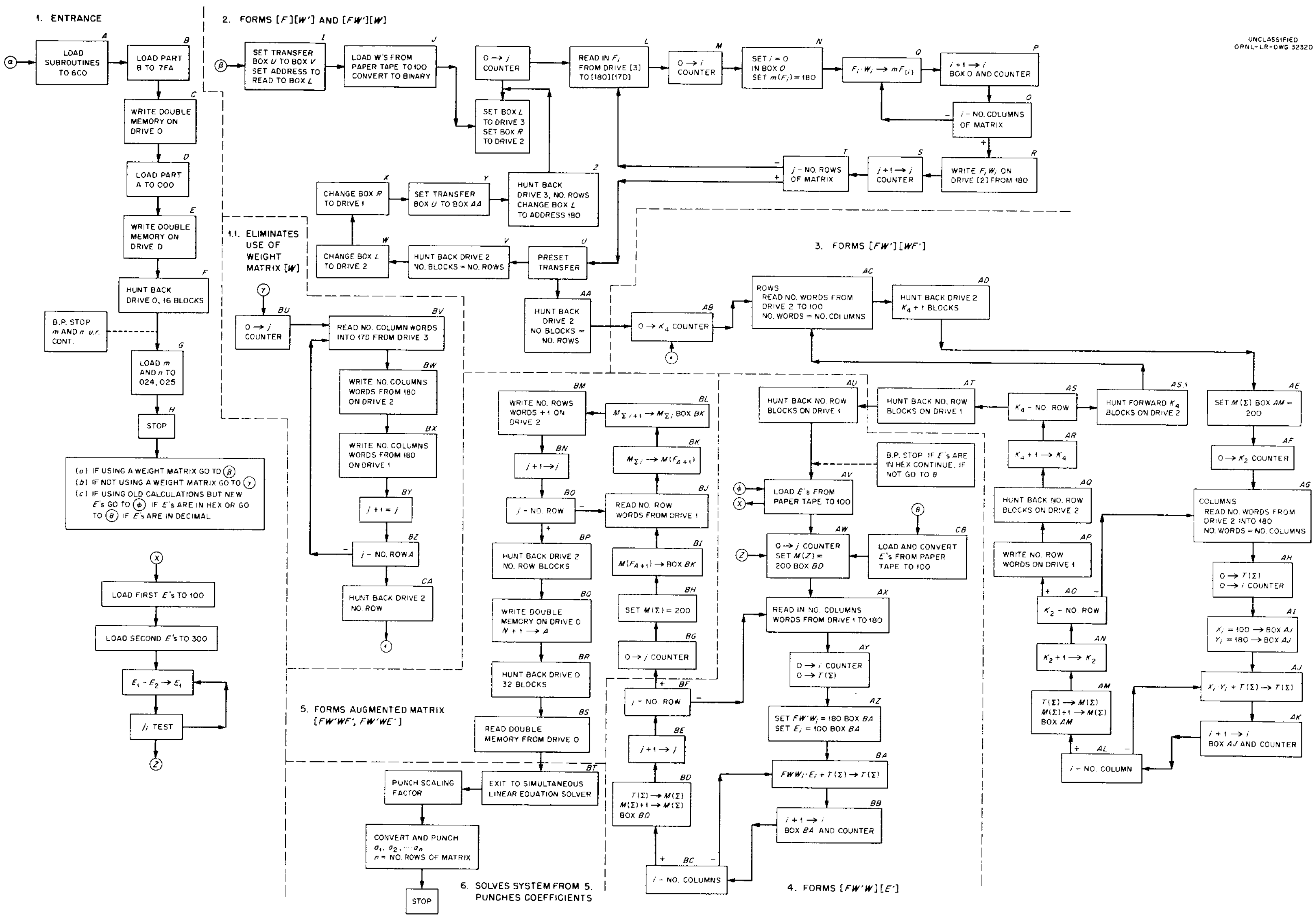

Fig. 21. Circular Coil Current Calculation, Detail.

UNCLASSIFIED
ORNL-LR-DWG 29324R

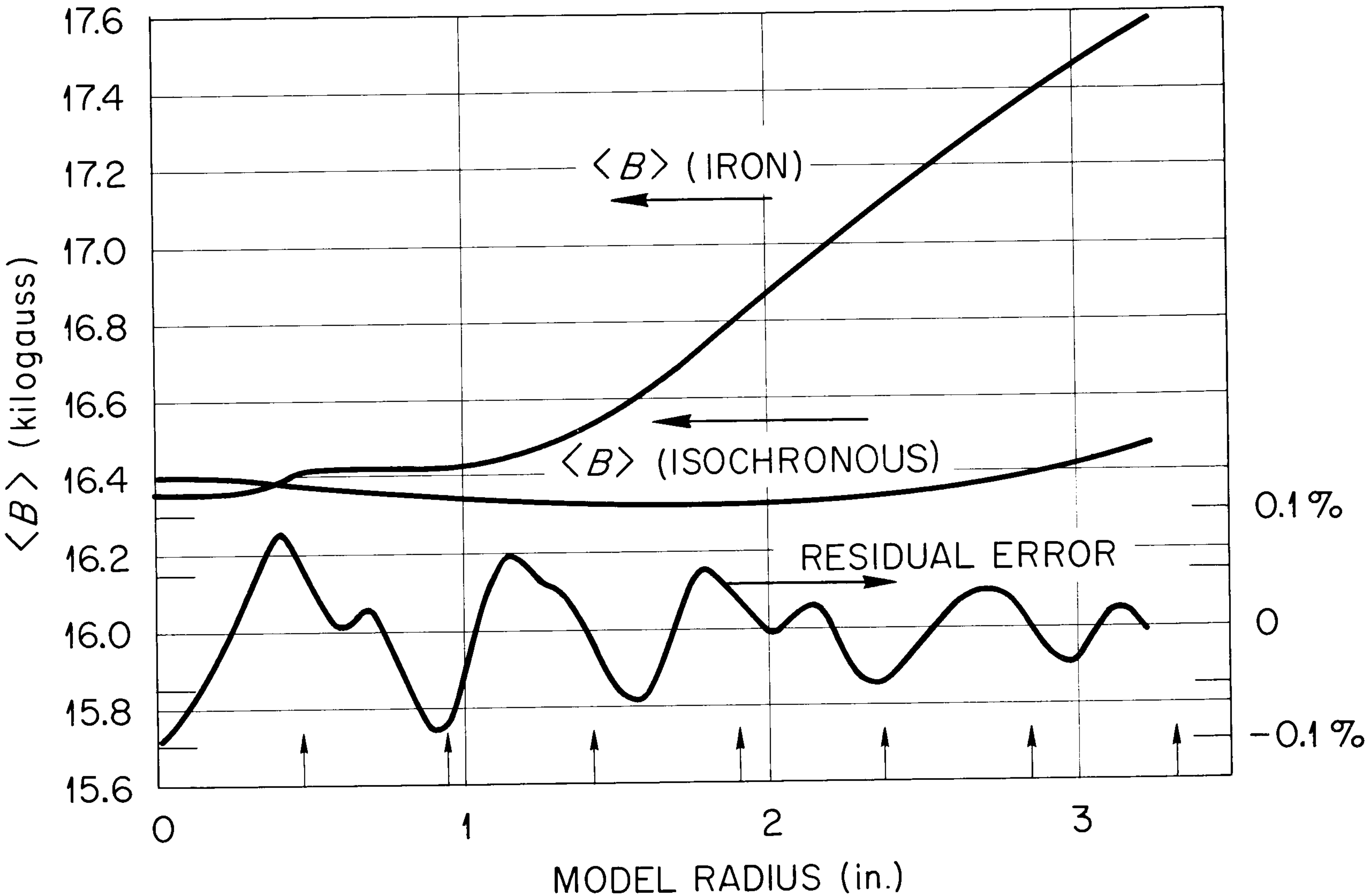

Fig. 22. An Example of the Accuracy to Which <B> Can Be Corrected to the Isochronous Value.

The least squares procedure occasionally gives an undesired result in that adjacent coils will be required to carry large oppositely directed currents which, to a large extent, cancel each other. When such situations arise, one of the pair of coils is removed from the problem and its current is adjusted individually to best fit the required $\Delta \langle B \rangle$; the remaining coils are then adjusted to fit the remaining difference. The residual is of course increased by the procedure, but in practice is still found to be small enough for the procedure to resolve the difficulty quite nicely.

In addition to providing a shift in field shape as required for change of particles, the trimming coils must also compensate for changes in field shape due to a shift in saturation effects as the field strength is varied. Measurements of the $\langle B \rangle$ produced by particular tip configurations were made over wide ranges of field strength. The field shape shifts considerably at reduced fields but also, of course, the range of adjustment required for change of particles narrows rapidly as the field is reduced. The combined behavior requires a trimming coil capacity of 600 gauss for adequate control, which is only slightly greater than the 550 gauss required for change of particles at the maximum field strength.

D. Model Magnet Studies - Results and Conclusions

The early model work was directed toward determining the H obtainable from the presently existing magnet* as a function of the magnet gap, the power dissipation, and the positioning of the main exciting coils. From these studies and from other considerations (Sec A, above), the design maximum energies were decided upon.

The next series of experiments was directed toward determing the conditions necessary for focusing 75-Mev protons. It was soon found that for hill gaps in the range considered practicable, either a three-sector, weak-spiral (3S-WS) or a four-sector, tight-spiral (4S-TS) configuration would be necessary. These were then investigated for radial stability first with theoretical fields and later with actual fields obtained from model measurements. As described in Sec V, both of these, 3S-WS and 4S-TS, were found to give sufficient stability.

At this point, a series of investigations was undertaken to determine with reasonable accuracy the design parameters for the 3S-WS and 4S-TS cases in order to reach a decision between the two. The principal problems in this program were in achieving adequate focusing at small radii and at the maximum radius (there is never any difficulty at intermediate radii) while still retaining a reasonable hill gap.

The space requirements for the various objects that must fit inside the hill gap are:

Pole face windings	1 in.
Liner structure	7/8 in.
R-f voltage breakdown gap (100 kv)	2-3/4 in.
Dee structure	7/8 in.
Total	5-1/2 in.

It is apparent that to leave a reasonable space for the circulating beam, the hill gap can be no less than 6-1/2in., and preferably as large as 8 or 9 in.

---

* At this time fabrication of the steel for what was then known as the "48-Inch Cyclotron" was already underway. The completed steel pieces for the yoke and poles of the magnet determine the basic dimensions of the newly designed accelerator.

The problem of achieving adequate focusing at the maximum radius is straightforward. In the 4S-TS case, since the spiral is already maximized and the geometry makes the use of valley coils difficult, the hill gap is the only variable. In the 3S-WS, the object was to keep the spiral very small. Since sufficient flutter could not be obtained by the iron alone, valley coils were necessary. Setting the power in the valley coils at 500 kw (the arbitrarily determined upper limit) and using as much spiral as seems prudent from stability considerations and compatible with simple valley coil design, we are left again with the hill gap as the only variable. The results of these investigations are shown in the first row of the table below:

Table 1. Maximum Magnetic Gaps (in inches) Which Give Adequate Focusing

	3-sector weak spiral	4-sector tight spiral	4-sector no spiral
Focusing at large radii	5.8 (7.5)*	9.5	4.3 (6.5)*
Focusing at small radii	9.0	7.0 (7.7)*	6.5 (7.2)*

* Values in parentheses are with 500 kw in valley coils.

The problem of achieving adequate focusing at small radii proved to be much more complex. Since $\langle B \rangle$ must increase approximately as r^2 to maintain isochronism while F rises initially as r^N, the first term in (5) predominates at small radii, giving a net defocusing. The situation in a 4S-TS machine is shown in Fig. 23; it is apparent that the difficulty is not easily overcome by decreasing the hill gap. Spiral is completely useless as it rises initially even less rapidly than flutter so that some defocusing seems inevitable. The defocusing impulse is proportional to the defocusing force times the number of

UNCLASSIFIED
ORNL-LR-DWG 30122R

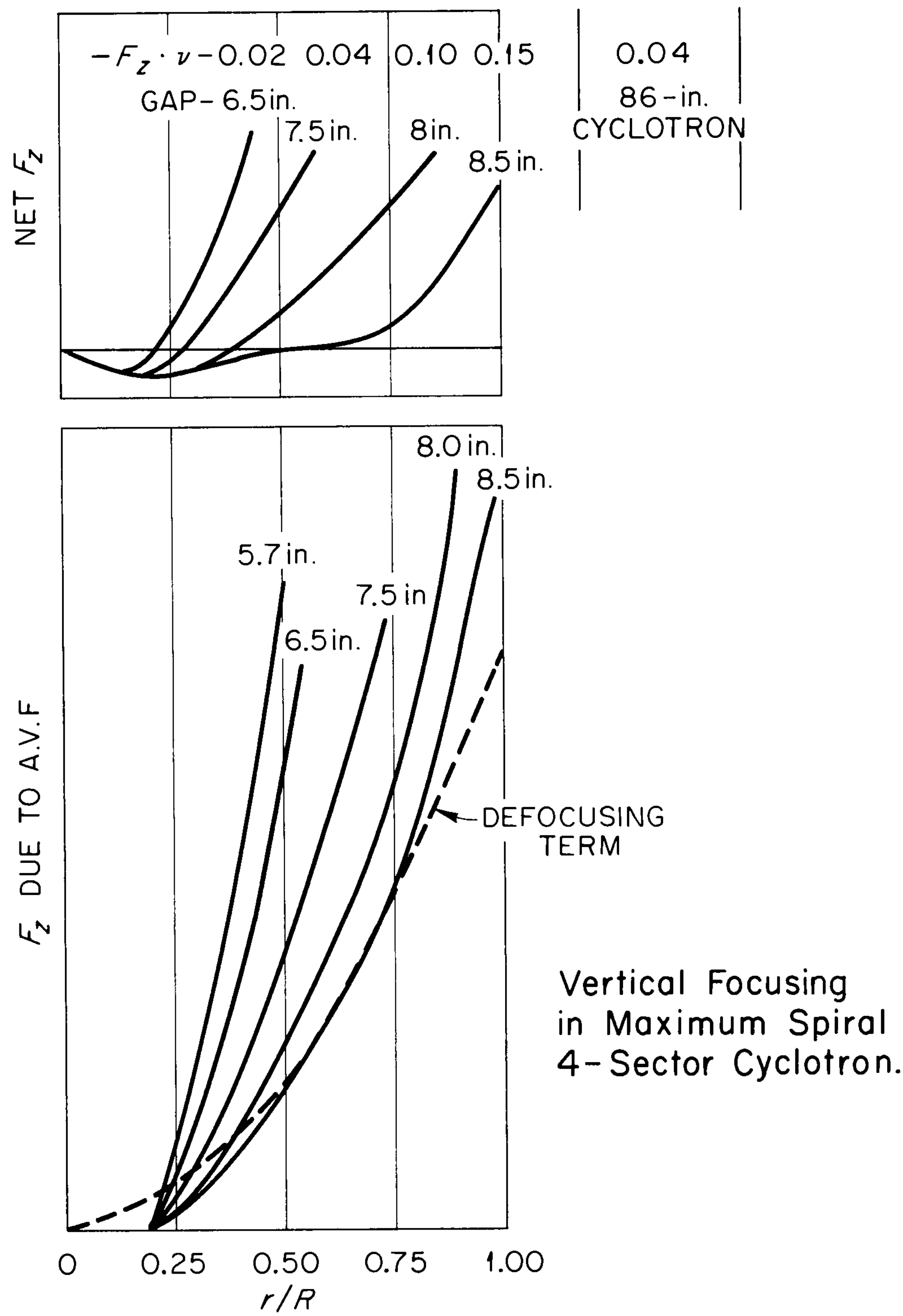

Fig. 23. Focusing in a Four-Sector, Tight-Spiral Field.

turns; values of this quantity are shown at the top of Fig. 23 where they are compared with this quantity in the ORNL 86-Inch Cyclotron. In the latter, as in all standard cyclotrons, axial defocusing is its greatest weakness; it would be highly desirable if this could be drastically reduced in AVF cyclotrons.

According to Fig. 23, the only possibility for doing this lies in the abandonment of isochronism at small radii; this procedure is, of course, severely limited by the requirement that ions do not get out of phase with the r-f voltage, or equivalently with a hypothetical ion in an isochronous cyclotron, by more than 90 deg.

The procedure for investigating nonisochronous magnetic fields was to (1) assume a field shape; (2) calculate the phase as a function of turn number (if it ever gets larger than 90 deg a new field shape must be assumed); (3) calculate the axial forces, both magnetic and electric; and (4) compute the net defocusing impulse as defined above. All calculations were numerical and on a turn-by-turn basis, although usually steps of five or even ten turns at a time could be used.

Two approaches were investigated by these calculations; in the first, the magnetic field was lowered in the center in order to shift the phases so as to cause the ions to arrive at the dee gaps after the electric field has passed its maximum (that is, the phase is positive); they thus experience electric phase focusing which, it was hoped, might overcome the magnetic defocusing. The difficulty with this approach is that the magnetic field must eventually reach (and even somewhat exceed) the isochronous field, and to do so, must increase with radius even more rapidly than the isochronous field. This gives magnetic defocusing from the first term of (5), and for all cases studied, this added defocusing was far larger than the electric focusing obtained.

In the second approach, the average magnetic field was made to decrease with increasing radius at small radii in order to obtain focusing from the first term in (5). Here again, the magnetic field must eventually reach the isochronous field and in order to do so must increase even more rapidly than the isochronous field so that an added defocusing is experienced. However, in some cases at least, this field increase could be postponed to radii where the AVF focusing is strong enough to overcome it. In order to achieve so long a postponement, it is necessary to make the magnetic field larger than the isochronous one at the center of the cyclotron, and let it fall-off with radius until it is well below the isochronous field before beginning to increase at radii where the AVF focusing becomes effective. The phase is thus shifted negative and then back through zero to positive just as in a standard cyclotron. The negative phase during the first several turns causes electric defocusing, but the net defocusing impulse can be substantially reduced relative to that in the corresponding isochronous field. The essential element in determining whether this method works is whether the magnetic field increase can be postponed long enough for the AVF focusing to overcome its effect. This is very senstive to the hill gap since this determines where the AVF becomes effective. The maximum hill gaps for which this method gives good results are listed in the second row of Table 1.

Actually, these values are also quite sensitive to the dee voltage, since this determines the number of turns required to reach a given radius, and thus the phase shifting. Increasing the dee voltage, however, requires increasing the required voltage breakdown gap and thus the magnet hill gap, so that some compromise must be reached. While these effects were not investigated in detail, it was determined that a dee voltage of 100 kv is not far from optimum, and since that voltage is most compatible with other requirements (especially radial stability) and achievability, it was used in the calculations.

The magnetic field fall-off method introduces still another problem; namely, that the ions must pass through a radial oscillation resonance. The radial oscillation frequency is given approximately by

$$\nu_r^2 = 1 + \frac{r}{\langle B \rangle} \frac{d\langle B \rangle}{dr}$$

so that at the radius where the magnetic field is flat in changing over from decreasing to increasing with increasing radius, $\nu_r = 1$. The particles spend only a small amount of time near this resonance so that it might be hoped that its effect may not be catastrophic. However, this point should be carefully investigated before this method of achieving axial focusing is used.

From Table 1 it is clear that either a 3S-WS or a 4S-TS cyclotron could be built with about a 7-1/2 in. hill gap; this corresponds to 2 in. of beam space, which is considered relatively adequate. In the 3S-WS case, valley coils would be needed, but the situation at small radii is much more favorable than in the 4S-TS. In the latter, a rather intricate and delicately balanced field shape must be obtained, an integral resonance for radial oscillations must be passed through, and there is still a moderate defocusing impulse during the first several turns. In the 3S-WS, the situation is so over-designed at small radii with a 7-1/2-in. hill gap that, it turns out, even an isochronous magnetic field gives no defocusing, and of course, avoids the other above-mentioned difficulties. The advantage would seem to easily justify the added constructional complication of valley coils.

In addition, it became apparent at this time that a tight spiral might well introduce serious difficulties into the deflection problem (Sec VI), whereas there are no apparent difficulties associated with the number of sectors. This again gives an advantage to the 3S-WS over the 4S-TS.

On the basis of these considerations, the 4S-TS design was abandoned in favor of the 3S-WS. However, as a result of all these investigations, it had become abundantly clear that a very high premium should be placed on hill gap space; practically every difficulty in the design can readily be overcome by reducing this gap. At this time, therefore, careful consideration was given to the fact that, in all of the designs that had been considered, about 2/3 of the gap (4-1/2 in.) is being used for the r-f system. This situation is difficult to change as long as a dee system is used; thus, consideration was given to an alternate method of applying the accelerating voltage, a method utilizing a resonant cavity[1]. This would allow the gap to be reduced sufficiently for a 4-sector machine with no spiral to give good focusing at all radii (Table 1). Such a machine would, of course, be ideal from the standpoint of radial stability.

It was finally decided, however, that in view of the fact that the 3S-WS machine with a 7-1/2-in. hill gap appeared to be completely feasible and was in a relatively advanced state of design and construction, it would not be profitable to undertake the numerous new engineering problems that would be introduced by so radical a change in design. The 3S-WS design was, therefore, adopted. The shape of the poles and the magnetic field contour are shown in Fig. 24 and 25 and the average field, flutter, and net focusing as a function of radius are shown for 75-Mev protons in Fig. 26 and for 90-Mev N^{4+} ions in Fig. 27.

---

(1) R. E. Worsham, to be published.

UNCLASSIFIED
ORNL-LR-DWG 29640-R

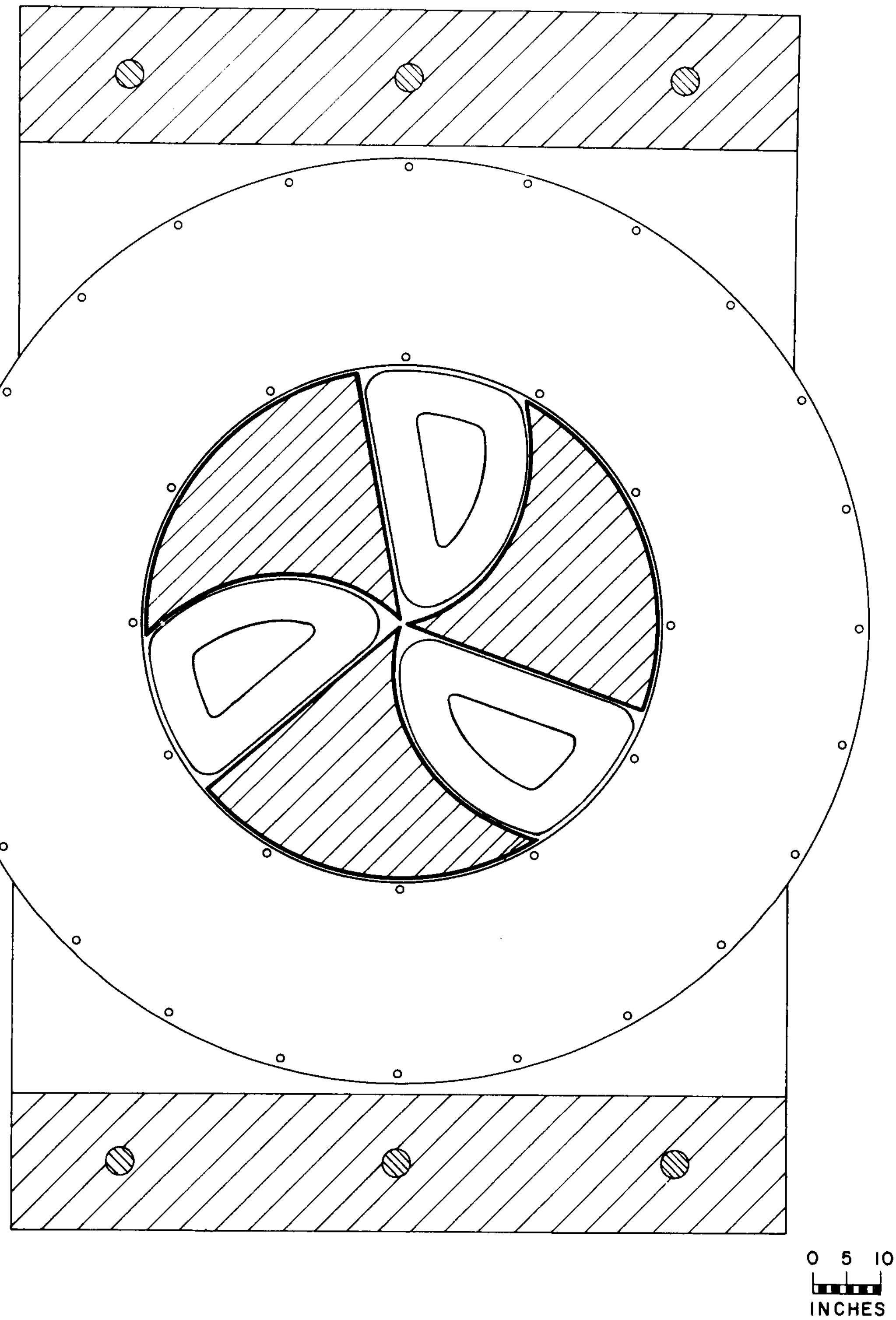

Fig. 24. Pole Configuration of the Three-Sector, Weak-Spiral Magnet.

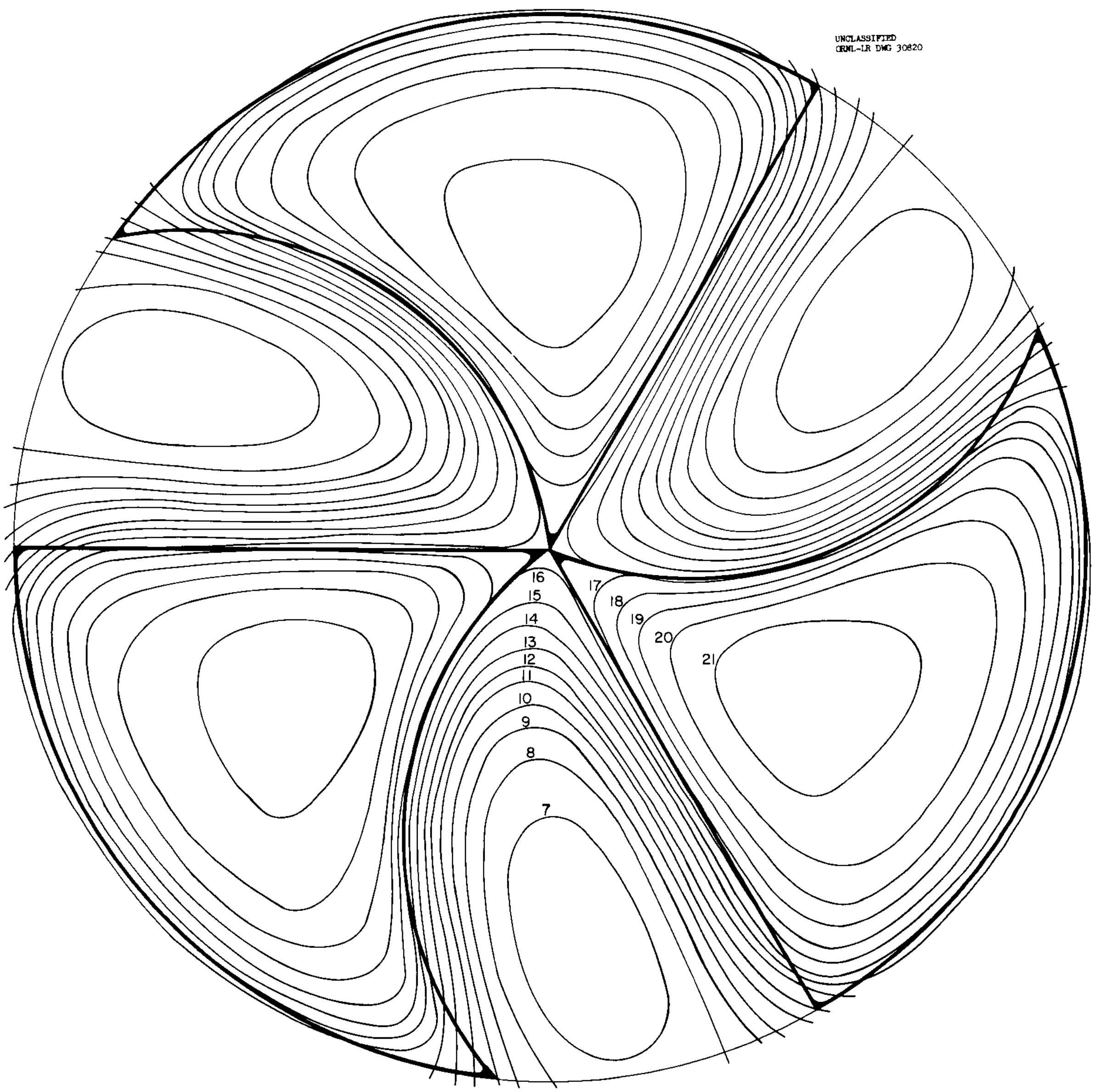

Fig. 25. Field Contours of the Three-Sector, Weak-Spiral Magnet, Sector Coils Energized. (Magnetic field in kilogauss.)

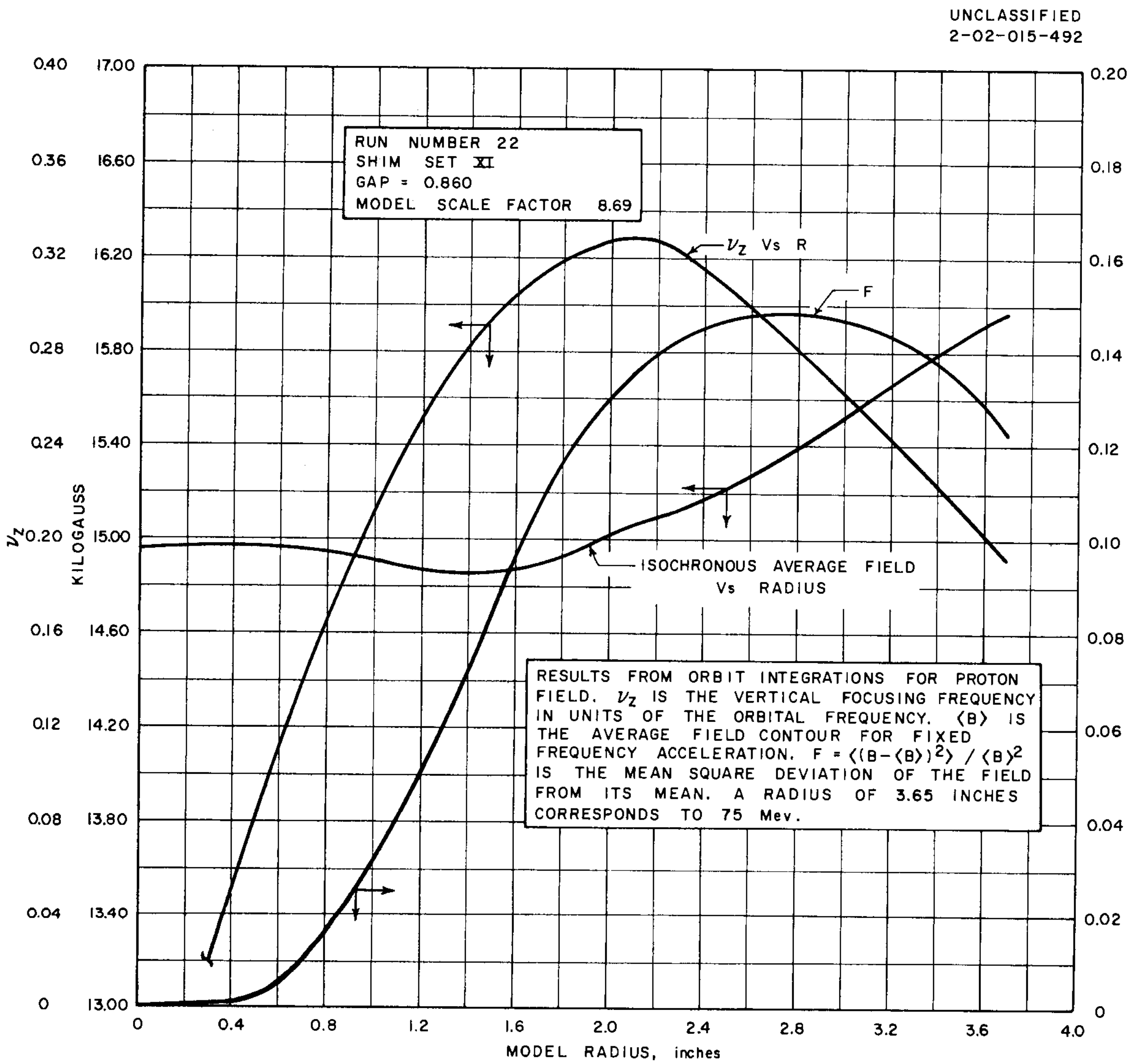

Fig. 26. Net Focusing for 75-Mev Protons.

UNCLASSIFIED
ORNL-LR-DWG 35085

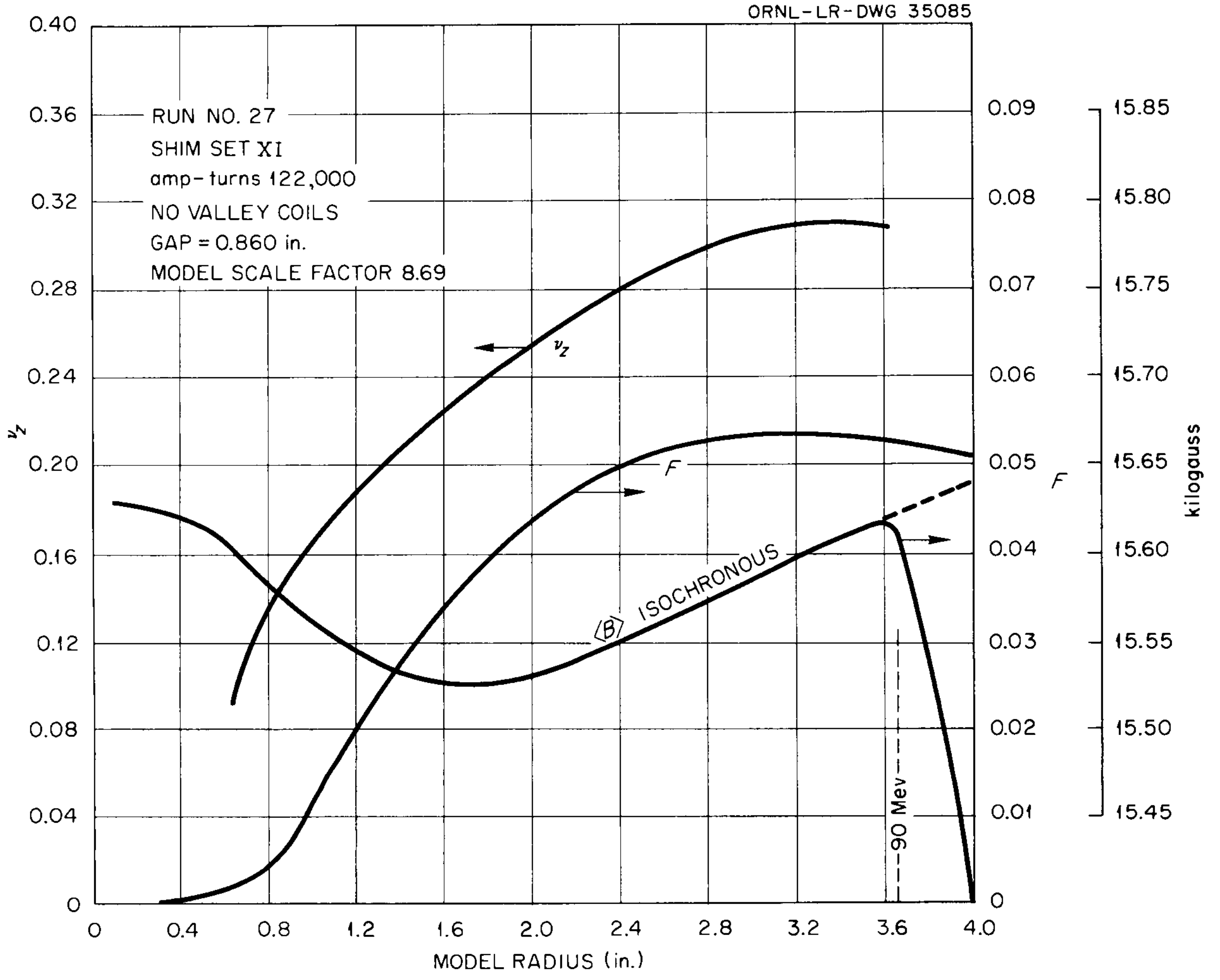

Fig. 27. Net Focusing for 90-Mev N^{4+} Ions.

V. RADIAL STABILITY

An important problem which arises in connection with an AVF cyclotron such as the ORIC is the question of radial stability of the orbits. Over most of the machine the radial oscillation frequency ν_r is close to unity. The periodic sector structure of the magnetic field leads, then, to the existence of nonlinear resonant driving forces acting on the radial oscillations of the particles. Under these conditions, particle orbits have absolute stability for only a finite range of oscillation amplitudes (orbit center displacements). In this section we shall discuss the results of our investigations into the radial stability of particle orbits in the ORIC.

The first part of our investigations was a preliminary study aimed at evaluating the relative performance of two machine types then being considered for the ORIC, namely, a four-sector, tight-spiral machine, and a three-sector, weak-spiral machine. In this study our attention was focused exclusively on the behavior of N^{4+} ions since for these ions ν_r is most closely equal to unity over the entire machine. Although a considerable amount of work had already been done especially at Harwell on the tight-spiral machines, hardly anything was known about the performance of a three-sector, weak-spiral machine. For three sectors the radial stability problem is much more acute since the resonance is of lower order (quadratic rather than cubic). As we shall show later, there are, however, mitigating circumstances in the three-sector machine such that the radial stability problem is not more severe than in the four-sector machine. On the basis of these results and other important considerations discussed elsewhere, it was decided that the ORIC should be a three-sector machine.

The second part of our investigation is a systematic study of radial stability for magnetic fields obtained directly from the three-sector magnet models described elsewhere. These studies have been reduced to a definite routine and will continue as an integral part of the magnet design procedure. All in all, the results of these studies show that radial stability limitations in the ORIC will be quite tolerable.

The theory of nonlinear resonances originated and was extensively developed in connection with AG synchrotrons by Moser at Brookhaven, Sturrock in England, Hagedorn at CERN, and others. This theory has been adapted to spiral-ridge cyclotrons by Stähelin at Illinois and the Harwell group. The results of their work considerably impressed us with the seriousness of the difficulties arising from the nonlinear resonances. These results, however, are directly applicable only to tight-spiral machines, and we are concerned with a much broader class of machines. Furthermore, the approximations made in this work, particularly by Stähelin, are not generally valid. Because of the difficulties involved in making an accurate analytical evaluation of the nonlinear resonance effects, our own work has been based on the use of a high-speed digital computer.

The two principal computer codes which are used in this work are the "equilibrium orbit" code and the "general orbit" code. These codes are specifically designed for handling problems connected with AVF cyclotrons. Two forms of each code are available: one in which the median plane field is given as an analytical function as follows:

$$B\,(r_1\theta) = \overline{B}\,(r)\left[1 + f\,(r)\cos N\,(\theta - \zeta\,(r)\right] \;; \qquad (1)$$

the other in which the median plane field is given at discrete points on a polar co-ordinate mesh. The first form of these codes is used principally for general theoretical studies and preliminary design work. The second form of these codes is used for detailed design work since it can take for its input field values obtained from model magnet measurements and the like.

The equilibrium orbit code takes a given median plane field and calculates the desired properties of the equilibrium orbits and the small amplitude oscillations as a function of momentum. With this code one can obtain such information as rotation period τ, radial oscillation frequency ν_r, and vertical oscillation frequency ν_z over an entire machine in less than 30 minutes. This code also provides input data for more general orbit studies.

The general orbit code takes a given median plane field and calculates orbit properties for given initial conditions. It is this code which is used in investigating such matters as nonlinear resonance effects on particle orbits. The procedure we have adopted for studying radial stability is as follows: The particle orbits are started out with specified deviations from the equilibrium orbit, and the computer then integrates the equations of motion until it is stopped. The output of the computer is in the form of "phase plots." If $\underline{x}$ is the radial displacement from the equilibrium orbit and p_x is its conjugate momentum, then a phase plot for a given orbit is obtained by plotting corresponding values of p_x against $\underline{x}$ at intervals of one sector during the orbit integration. The computer is equipped to make these plots automatically on its "curve-plotter" attachment while the calculation proceeds. At the same time the plotted curves can be observed on a "Memoscope" at the console. As a result, succeeding orbits can be arranged so as to "fill in" the phase space to best advantage. As we shall show later, these phase plots can be used directly to gauge the range of radial oscillation amplitude for which the orbits in a given field are effectively stable. The procedure for obtaining these phase plots has been reduced to a definite routine such that it requires only about two hours of computer time to complete the work on a given magnetic field.

We shall discuss first the results obtained for the four-sector tight-spiral machine. In this investigation we considered only N^{4+} ions because, as noted above, for these ions ν_r is most closely equal to unity over the entire machine and, hence, the greatest difficulty with radial stability could be expected. With the results of Stähelin as a guide, a median plane field having the maximum possible spiral consistent with the available magnet gap was derived. The parameters of this field were then fitted to B (r, θ) of Eq. (1) as follows:

$$
\begin{aligned}
f(r) &= 0.167 \left[r^2/(r^2 + a^2) \right]^2 \\
& \qquad a = 0.018 \\
\mathcal{C}(r) &= 24.0\, r \\
\overline{B}(r) &= (1 - r^2)^{-1/2}
\end{aligned}
\qquad (2)
$$

where f (r) is the "flutter", ζ (r) is the "spiral", and $\overline{B}$ (4) is the average field. The unit of length (cyclotron unit) for N^{4+} ions is in this case 280 inches. (Note that a field of this form is not quite proper as r $\rightarrow$ 0 since ζ (r) must go to zero at least as r^2. We may overlook this difficulty by stipulating that this field does not extend all the way in to r = 0.) This field was run through the equilibrium orbit code with results shown below:

Table 2. Four-Sector, Tight-Spiral Machine with N^{4+} Ions

p	E_k	τ	ν_z	ν_r	$\overset{o}{\nu}_r$
0.020	2.6	0.9998	0.0403	1.0011	1.0002
0.045	13.2	0.9992	0.1581	1.0038	1.0010
0.070	31.9	0.9991	0.2635	1.0082	1.0024
0.095	58.7	0.9991	0.3653	1.0147	1.0045
0.120	93.5	0.9991	0.4660	1.0230	1.0072

p = momentum in Mc units
E_k = kinetic energy in Mev
τ = ratio of particle rotation period to r-f period
ν_z = axial oscillation frequency
ν_r = radial oscillation frequency
$\overset{o}{\nu}_r$ = "smooth approximation" values of ν_r

As can be seen, the momentum values chosen cover the machine from inside to out. The values of τ shown indicate that the form of $\overline{B}$ (r) is close enough to that required for isochronism ($\tau \equiv 1$) for our purposes here. The values of ν_z shown increase steadily and reach a rather large value near the outside of the machine, a result which is made necessary by the fact that the same flutter field must also focus vertically 75-Mev protons. This result is rather unfortunate since it means that the operating point of the N^{4+} machine comes close to the $\nu_r = 2\nu_z$ coupling resonance line and, as we shall show in the next section, this has important effects on the problem of beam deflection. Since we are concerned here, however, only with the question of radial stability we shall, for the present, overlook this difficulty. The last two columns of Table 2 give ν_r as obtained by the computer and ν_r^o, the corresponding values as obtained from the smooth approximation $(\nu_r^o)^2 = 1 + k = 1 + p^2$ for $\overline{B}$ as given). As far as the question of radial stability is concerned, the important quantity is $(\nu_r - 1)$, and we see from this table that the smooth approximation values of $(\nu_r - 1)$ are off by a factor of about three. This is not surprising considering the degree of validity of this approximation; however we have emphasized this matter here to point out that the analytical treatments of radial stability which have used this approximation for ν_r cannot be considered very reliable. The deviation of ν_r from the smooth approximation value arises not only from the flutter and noncircularity of the orbits, but especially from the flutter derivatives (as first noted by L. Teng), and these derivatives are particularly important near the machine center. These deviations vary as N^{-2} and, as we shall see, are therefore even larger in the three-sector machines.

We turn now to the radial phase plots obtained for the four-sector, tight-spiral machines just described above. These phase plots are shown in Fig. 28; the method by which they are obtained has already been discussed. The nature and significance of these plots can best be understood from the theory of nonlinear resonances and so we shall delay the discussion of our results to present a brief, qualitative sketch of this theory as it applies to the present situation. For the nonlinear driving force acting on the radial oscillations, we shall write

$$F = 32\,C\,x^3 \cos 4\theta$$

where $\underline{x}$ is the displacement from the equilibrium orbit, C is a constant characterizing the strength of the force (the factor 32 is included here merely to simplify other equations to follow), and the

UNCLASSIFIED
ORNL-LR-DWG 32311

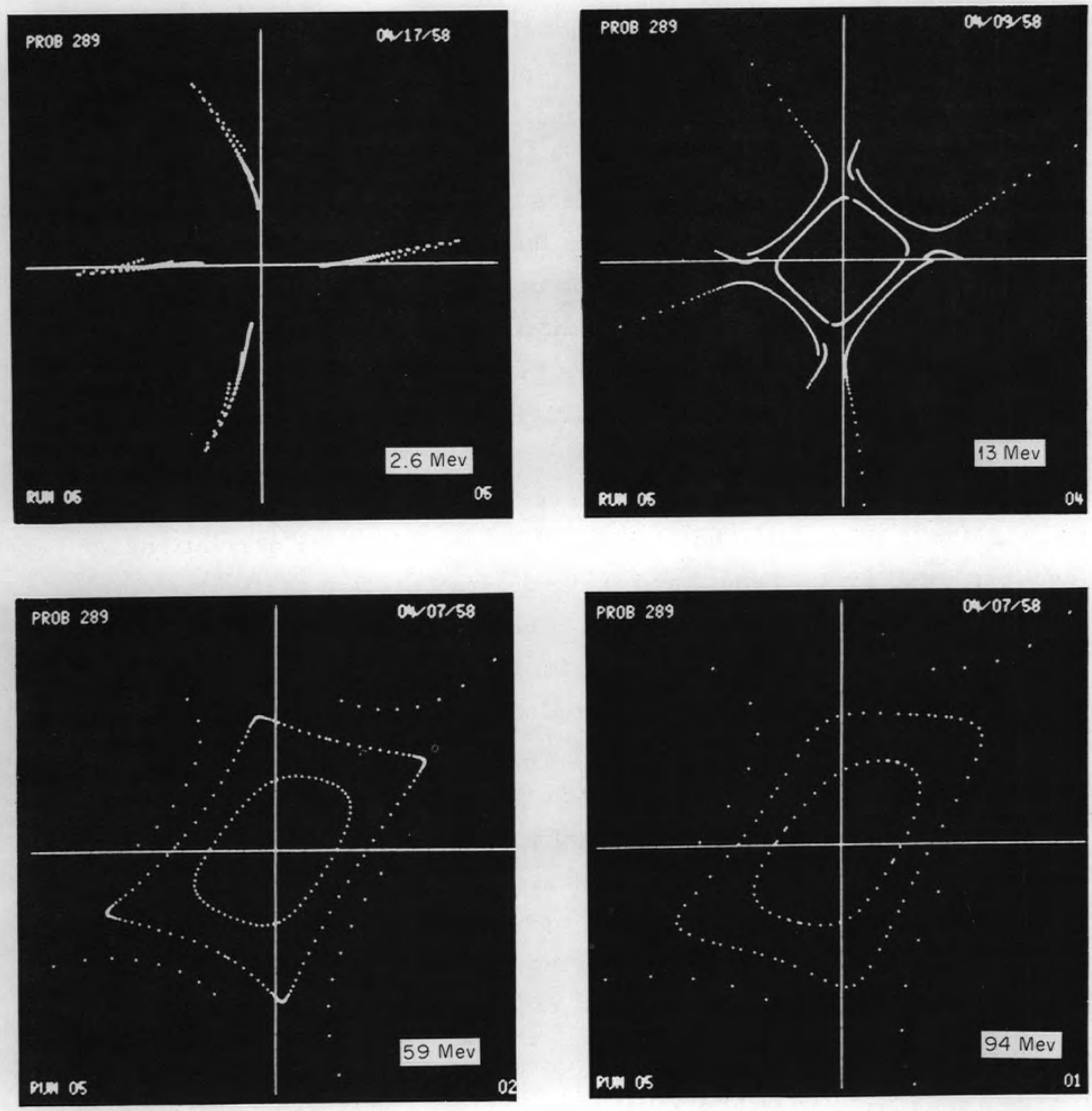

Fig. 28. Phase Plots for N^{4+} Ions in a Four-Sector, Tight-Spiral Machine.

cos 4 θ factor arises from the four-sector periodicity of the field. (For simplicity we are omitting other terms in F, for example the one in x^3 alone, since we are interested here only in the qualitative results of the theory.) Instead of $\underline{x}$ and p_x, we introduce the variable A and ϕ defined as follows: $x = A \cos (\theta + \phi)$, with p_x being proportional to $(dx/d\theta)$. We may consider that the phase plots are constructed from a given orbit by plotting p_x against $\underline{x}$ once per revolution at $\theta = 0$ so that (A, ϕ) are essentially the "polar coordinates" of the points in these plots. If the nonlinear forces are negligible the A is constant and $(d\phi/d\theta) = (\nu_r - 1)$ so that successive points in the phase plot will fall on an ellipse, the "invariant ellipse" characteristic of the linear motion. The number of revolutions required for the ellipse to close will then be $(\nu_r - 1)^{-1}$ since the angular velocity of the plotted points in the phase plane is $2\pi\, (d\phi/d\theta)$. (Actually, the points in the phase plots are plotted at the rate of once per sector rather than once per revolution, but we can consider the resultant plots as four separate plots superimposed.) Considering F as a perturbation on the linear motions, the first-order equations for the adiabatic variation of A and ϕ are then as follows:

$$\begin{cases} (dA/d\theta) = C\, A^3 \sin 4\,\theta \\ (d\,\phi/d\theta) = (\nu_r - 1) - C\, A^2 \cos 4\,\phi \end{cases}$$

The following is then a first integral or invariant of these "equations of motion"

$$(\nu_r - 1)\, A^2 - 1/2\, C\, A^4 \cos 4\,\phi = H. \qquad (3)$$

The significance of this result is that the points in a phase plot for a given orbit will lie on a curve for which H is a constant. Even though the theory is only approximate, it does provide a valuable qualitative guide in interpreting the results obtained in these phase plots. Equation (3) for the invariant makes the following predictions: For small amplitudes A is a constant independent of ϕ so that the curves are ellipses (linear motion). As the amplitues A increase these ellipses will develop "corners" and become quadrangular in shape. For still larger amplitudes the corners become sharper and the sides of the quadrangular figures become concave. It is these figures which mark the boundary between stable orbits with closed invariant curves and unstable orbits with open invariant curves. The limiting case is the "unstable fixed point" which occurs when $A = \left[(\gamma_r - 1)/C \right]^{1/2} =$ constant, ϕ = constant. The open invariant curves corresponding to unstable orbits are characterized by asymptotes along which points move in or out. There are four asymptotes of each kind roughly 90 deg apart.

We return now to the phase plots shown in Fig. 28. Each picture contains a series of phase plots at a given fixed energy shown on the picture. The center of each picture (zero amplitude point) is the equilibrium orbit location at the given θ value chosen here to be at the field maximum. Full scale for these pictures is a displacement of 1/64 cyclotron units = 4.4 inches. Each picture shows phase plots for three orbits which were chosen to give a fairly good estimate of the configuration of the invariant curves. As can be seen, the forms of the curves traced out by the plotted points are quite consistent with the theory sketched above. The plotted points move generally in the clockwise direction about the origin; the angular speed with which the points move is greater at the higher energies since $(\gamma_r - 1)$ is greater there. Examination of the pictures at 69 and 94 Mev shows that radial oscillation amplitudes up to about two inches are definitely stable. The same is true for the picture obtained at 32 Mev, which is not shown. Although the picture at 13 Mev is qualitatively different, we would still estimate the maximum stable amplitude as about two inches. The "knees" of the two curves, one flowing in, the other out, mark out fairly definitely the position of the unstable fixed point which must lie between these knees. The picture at 2.6 Mev is quite different; all these orbits are unstable and it is evident that the stable orbit region must be quite small. However, the information that can be gleaned from these curves is quite encouraging. First of all let us note that the points on these curves lie very close to "outflowing asymptotes" and, hence, the amplitude growth rate at these ϕ values is a maximum. If we examine, then, the history of these plots we find the following: The three plots start at displacements of 1.1, 1.65, and 2.2 in. and run for 51, 20, and 9 revolutions, respectively. Since they all terminate at nearly the same displacement, we may conclude that the minimum number of revolutions required for an amplitude growth from 1.1 to 1.65 in. is 31 revolutions, and from 1.65 to 2.2 inches is 11 revolutions. Now since the energy gain per revolution for N^{4+} ions is about 1.6 Mev, it will require only about 7 revolutions for ions at 2.6 Mev to reach 13 Mev where the amplitude stability limit is 2 inches. Therefore, those ions at 2.6 Mev with amplitudes less than 1 1/2 in. will certainly survive. The "effective" stable amplitude limit will actually be larger since only a minority of the ions will have unfavorable ϕ values at 2.6 Mev and, as we shall discuss later, the acceleration process will at any rate keep changing the ϕ values. In summary then, we find that over the last 85% of this machine, radial stability is assured for amplitude up to 2 in.; over the first 15% this limit is probably not less than 1 in. and may be larger, depending on acceleration effect. These amplitude limits are considered adequately large.

We turn next to the discussion of the results obtained for three-sector, weak-spiral machines. These investigations have included N^{4+} ions, as above, and also protons. We divide this work into two parts the first of which, along with the four-sector work described above, was a preliminary investigation of the problem, and the second of which is the work being done in connection with the model magnet design work. The first part of these investigations which dealt only with N^{4+} ions was carried out using a field in the form given by Eq. (1). The parameters for this field were obtained from measurements on a preliminary three-sector model magnet. The resultant field parameter are as follows:

$$f(r) = -0.096 + 14.0r - 91.8\, r^2$$
$$\zeta(r) = 32.2\, r^2$$
$$\overline{B}(r) = 0.998383 + .00655 \cos (57.8\, r)$$

These parameters are appropriate to N^{4+} ions for which the cyclotron length unit is 280 inches. Although the extent of the actual machine is $0 \lesssim r \leq 0.12$, this f(r) is valid only over the range $0.012 \gtrsim r \gtrsim 0.100$ so that our range of calculations was thereby restricted. Values of f are given below:

Table 3. Three-Sector, Weak-Spiral Machine with N^{4+} Ions

p	E_k	τ	ν_z	ν_r	ν_r^o	f
0.02	2.6	1.0005	0.1420	1.0090	0.9965	0.147
0.03	5.9	1.0004	0.2140	1.0202	0.9944	0.241
0.04	10.4	1.0002	0.2677	1.0315	0.9944	0.317
0.05	16.3	0.9998	0.3043	1.0409	0.9977	0.375
0.06	23.4	0.9992	0.3293	1.0463	1.0036	0.414
0.07	31.9	0.9988	0.3503	1.0445	1.0104	0.434
0.08	41.6	0.9993	0.3754	1.0341	1.0150	0.436
0.09	52.7	1.0017	0.4086	1.0150	1.0149	0.420

p = momentum in Mc units

E_k = kinetic energy in Mev

τ = ratio of particle rotation period to r-f period

ν_z = axial oscillation frequency

ν_r = radial oscillation frequency

ν_r^o = "smooth approximation" value of ν_r

f = f(p), value of flutter

The spiral here is "weak" and is really only needed at the outside of the machine where f(r) begins to fall off. The total spiral in this machine is only 0.46 radians whereas in the four-sector machine described above it is 2.88 radians. The value of $\overline{B}$ was chosen to produce a condition of near isochronism. Note that $\overline{B}(r)$ falls off with increasing r (negative k value) near the center of the machine. This behavior is a result of the fact that the orbits here are appreciably noncircular.

This field was run through the equilibrium orbit code with results which are shown in Table 3. The energy range (2.6 to 52.7 Mev) here is restricted to about half the full energy because the validity of this field extends only out to r = 0.1. As can be seen from the values of $\mathcal{T}$ shown, the degree of isochronism is quite good. Here again the values of ν_z reach rather large values at the outside of the machine for reasons given before. As can be seen the values of ν_r given by the computer are significantly larger than those obtained from the smooth approximation. This difference is much more striking here than in the four-sector case as a result of the larger $\underline{f}$ and smaller N. The importance of the flutter derivatives on ν_r is apparent near the end of the table where ν_r decreases along with $\underline{f}$.

Before discussing the phase plots obtained in this case, we again give a brief sketch of the theoretical background required to interpret these plots. Most of the discussion given in connection with the four-sector machine will also apply here so we shall note here only the changes necessary for a three-sector machine. For the nonlinear driving force acting on the radial oscillation, we write

$$F = 16\, C\, x^2 \cos 3\,\theta.$$

For the first-order equations giving the adiabatic variation in the variables A and ϕ we now have

$$\begin{cases} (dA/d\phi) = C\, A^2 \sin 3\,\phi \\ (d\phi/d\theta) = (\nu_r - 1) - C\, A \cos 3\,\phi. \end{cases}$$

For the invariant associated with these equations, we then have

$$(\nu_r - 1)\, A^2 - 2/3\, C\, A^3 \cos 3\,\phi = H, \tag{4}$$

which may be compared with Eq. (3) for a four-sector machine. The discussion of the form of the curves obtained from the phase plots is quite similar to that for the four-sector machine except that here the figures will be triangular rather than quadrangular. The unstable fixed points, where the amplitude of stable motion has its largest value, is here given by $A = (\nu_r - 1)/C$, ϕ = constant. The unstable orbits here will again be characterized by open curves with asymptotes along which the points move in and out. There will be three asymptotes of each kind (inflowing and outflowing) spaced about 120 deg apart.

We return now to the three-sector machine described above. The phase plots obtained in this case are shown in Fig. 29. Each picture contains a series of phase plots obtained at a given fixed energy as shown. As can be seen, the centers of these pictures are almost, but not quite, on the equilibrium orbit. Full scale on these pictures is a displacement of 1/64 cyclotron units = 4.4 in. The picture obtained at 41.6 Mev contains phase plots for four orbits, three stable and one unstable. The "knees" in the plots for the unstable orbit (where the points are closely spaced) give a good indication of the location of the fixed points in this case. The maximum stable amplitude is about 4 in., almost twice that of the four-sector machine. The picture obtained at 23.4 Mev is similar to that at 41.6 Mev, although the maximum stable amplitude is down to somewhat less than 3 in. The picture obtained at 10.4 Mev contains plots for one stable orbit and three unstable orbits (close together). The stability region is pretty well delineated and the maximum stable amplitude is about 1.5 in. The picture obtained at 2.6 Mev contains plots made from three orbits all unstable. An estimate of the size of the stability region leads to the conclusion that the maximum stable amplitude is about 1 in. However, the results at this energy are not considered reliable since the flutter $\underline{f}$ used here does not approach zero properly at small $\underline{r}$ values and, hence, the driving force (which depends essentially on d^2f/dr^2) is very likely incorrect. The over-all results of this preliminary investigation of radial stability in the three-sector machine were very encouraging. In the middle of the machine the orbits are more stable than in the four-sector machine, while at lower energies the results were at least comparable in the two cases.

UNCLASSIFIED
ORNL-LR-DWG 32312

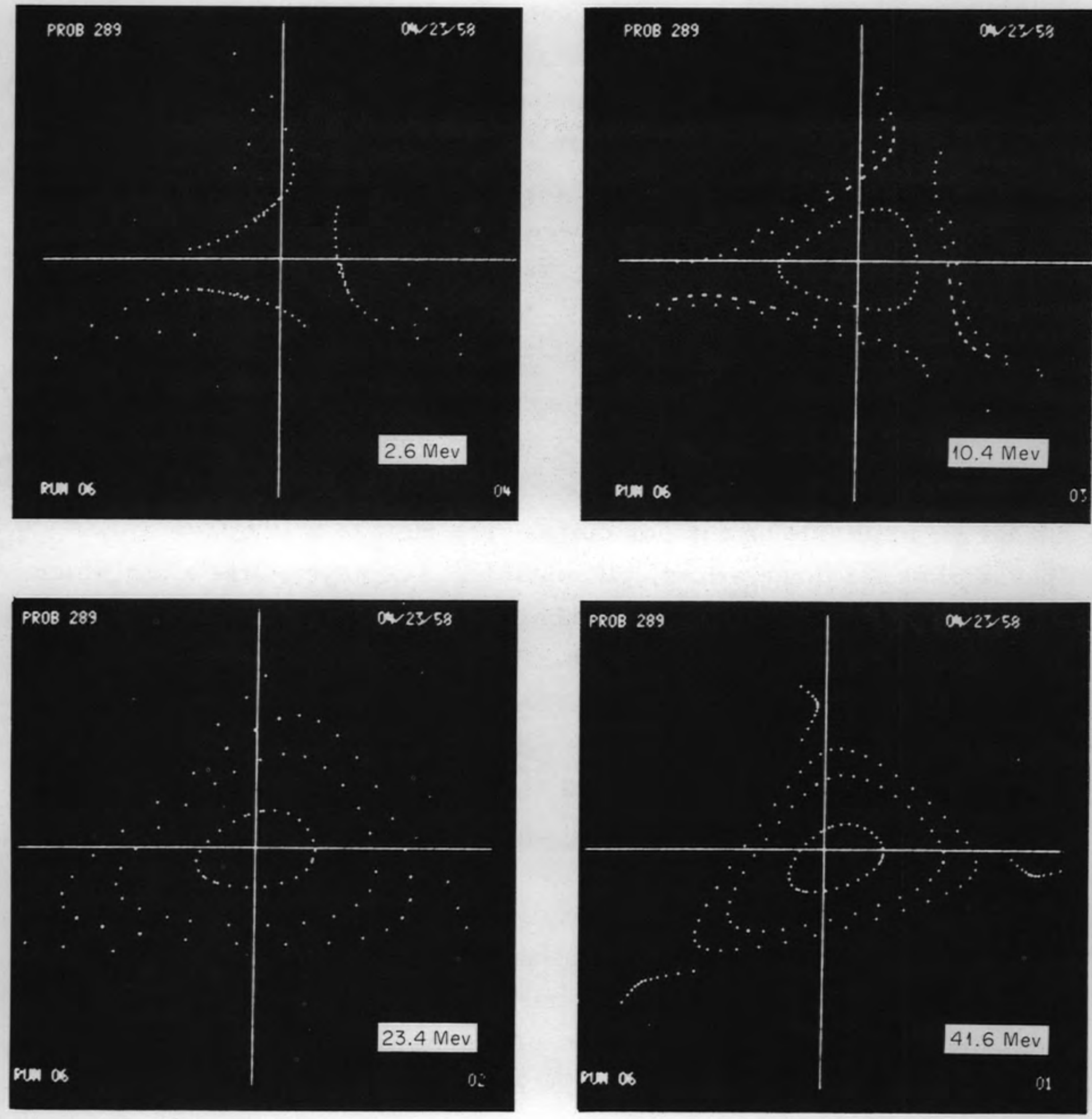

Fig. 29. Radial Phase Plots for N^{4+} Ions in a Three-Sector, Weak-Spiral Machine.

Having completed the discussion of the preliminary investigation of the radial stability problem, we turn now to discuss the work done using magnetic fields obtained directly from the three-sector magnet models. This work has included both protons and N^{4+} ions, which represent the two extreme cases. The results obtained with N^{4+} ions have generally verified those discussed above. In the middle and upper energy regions of this machine the limiting stable amplitudes range from 3 to 5 in. so that the orbit stability is quite good. For the sake of brevity we shall discuss here only the results obtained near the center of the machine. In Fig. 30 we have two sets of phase plots obtained at 2.6 Mev and 16.3 Mev. In these pictures $\underline{x}$ is plotted vertically and p_x horizontally. The cyclotron unit here is 265 in. so that full scale in these pictures is a displacement of 1/64 cyclotron unit = 4.14 in. The picture at 16.3 Mev shows phase plots (slightly off center) for three orbits, all stable. The stability limit indicated here is for an amplitude of 2 in. or more. The picture at 2.6 Mev shows phase plots for three orbits, all unstable. The asymptotes along which the points move outward are clearly indicated. For the plot nearest the center we found that an amplitude growth from 0.5 to 1.0 in. requires about 20 revolutions. Note that since the energy gain per turn for N^{4+} ions is about 1.6 Mev, it requires only about 9 revolutions for the particles at 2.6 Mev to reach 16.3 Mev.

Turning now to the results obtained with protons we find that orbit stability over most of the machine is no problem at all. The values of $\gamma/_r$ rise significantly above unity for energies over 15 Mev. Beyond this energy the orbits are stable for amplitudes up to 5 in. and more. This being the case, we shall describe here only those results which pertain to the lowest energy region of the machine. Pictures of phase plots obtained at energies of 1.7, 6.7 and 15.1 Mev are shown in Fig. 31. In these pictures $\underline{x}$ is plotted vertically, p_x horizontally. In two pictures (6.7 and 15.1 Mev) the equilibrium orbit position is somewhat off center. The cyclotron unit here is 84.9 in. so that full scale deflection in these pictures = 1/16 cyclotron unit = 5.3 in.

UNCLASSIFIED
ORNL-LR-DWG 32313

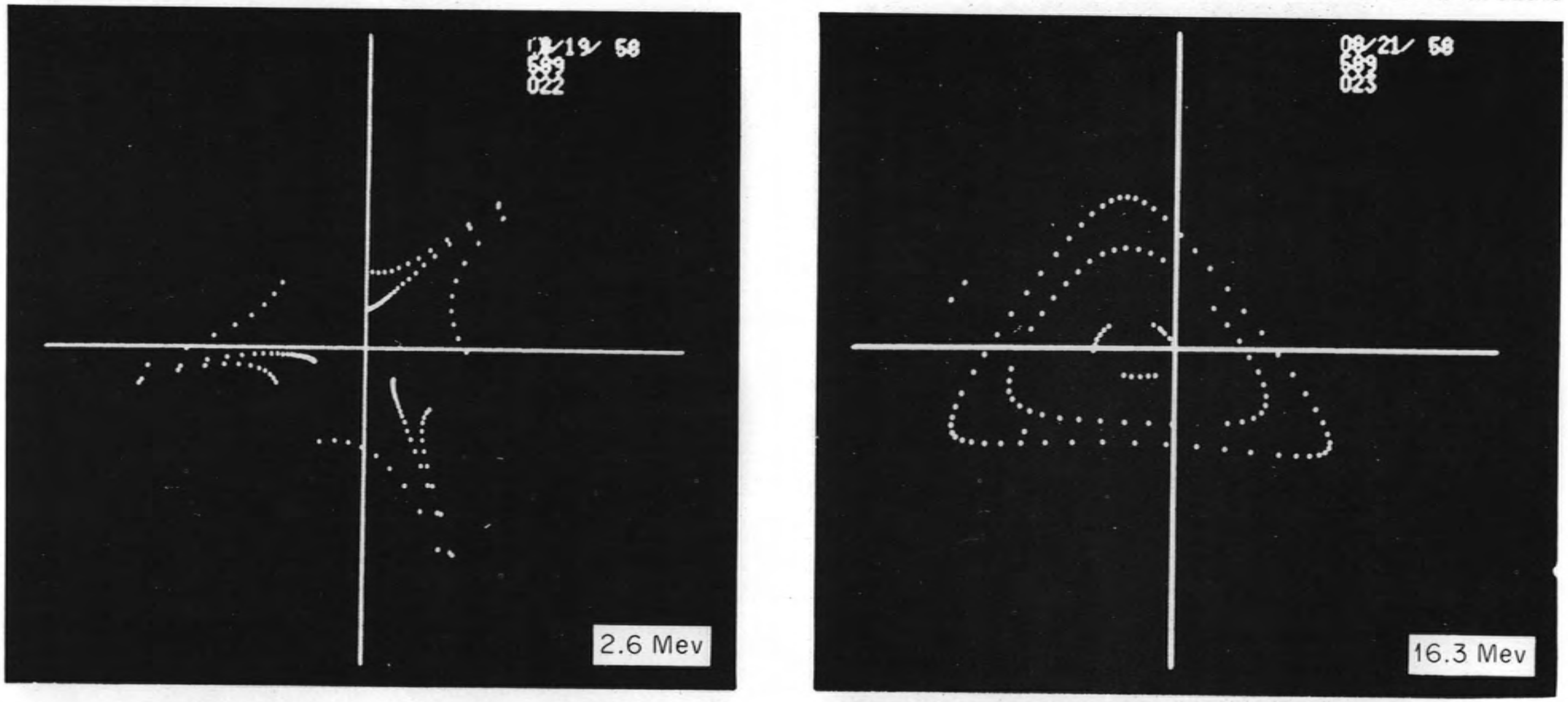

Fig. 30. Radial Phase Plots for N^{4+} Ions for Fields Obtained from Three-Sector Model Magnet.

UNCLASSIFIED
ORNL-LR-DWG 32314

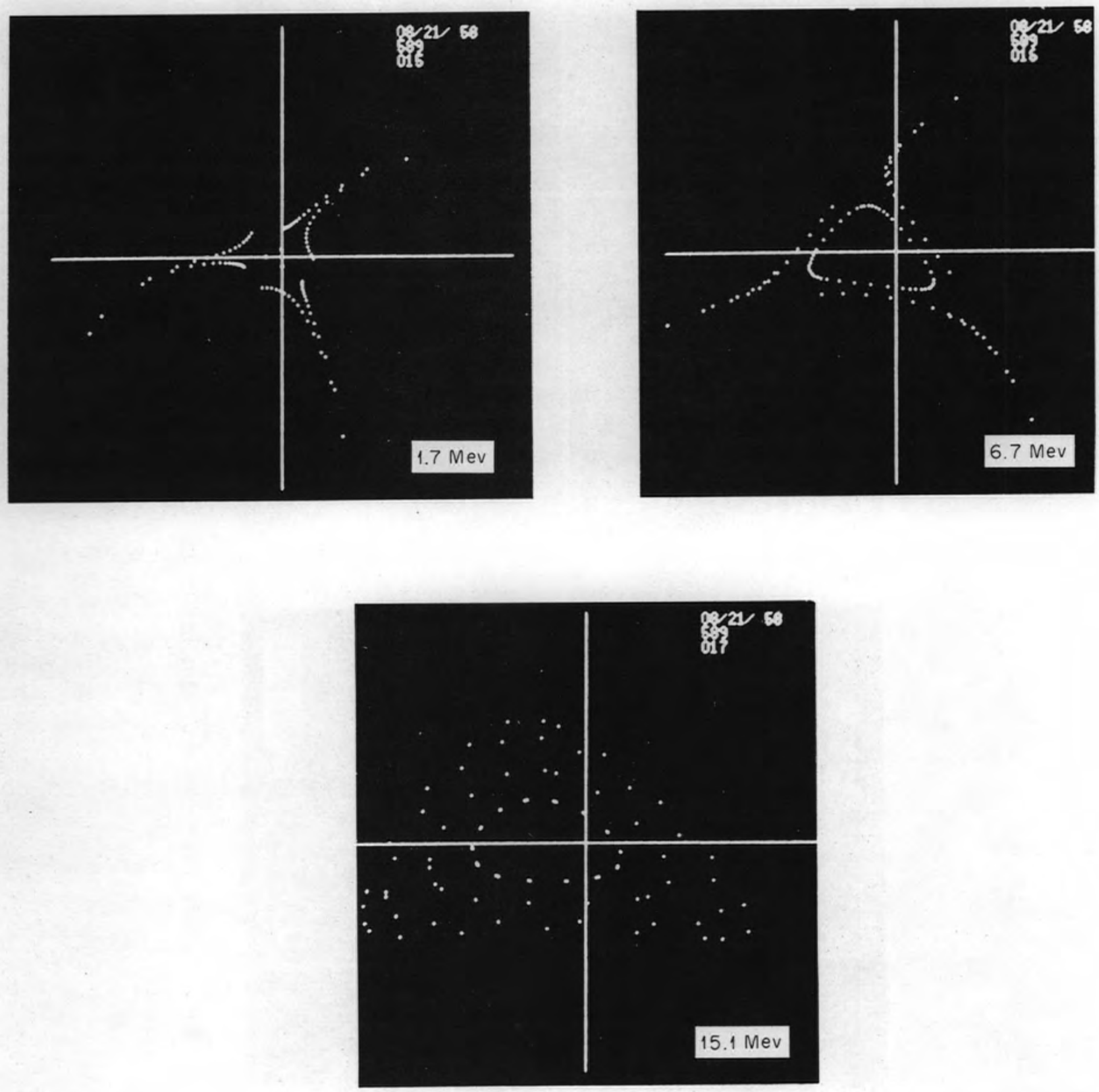

Fig. 31. Radial Phase Plots for Protons for Fields Obtained from Three-Sector Model Magnet.

The picture obtained at 15.1 Mev shows plots for four orbits, all of which are stable. In this case the stability limit corresponds to an amplitude of at least 3.5 in. Note that $\nu_r = 1.07$ here. The picture obtained at 6.7 Mev contains plots for three orbits, one stable and the others, which overlap, unstable. The stability limit here corresponds to an amplitude of about one inch. For protons the energy gain per turn is 0.4 Mev so that it requires 21 revolutions for a particle at 6.7 Mev to reach 15.1 Mev where the limiting amplitude is over 3.5 in.

The picture obtained at 1.7 Mev contains plots for two orbits both of which are unstable. The asymptotes along which the points flow outward are clearly defined. One orbit with an initial displacement of 0.6 in. runs for 16 revolutions, the other with an initial amplitude of 0.9 in. runs for 15 revolutions.

We may summarize the preceding discussions by saying that radial stability of the orbits is not much of a problem for the proposed three-sector machine except close to the center. Our investigations thus far have been made by means of phase plots obtained at constant energy. Close to the center of the machine we can expect the acceleration process to have a pronounced effect on the radial oscillations. Each time the particle crosses an accelerating gap there will occur a nearly discontinuous change in the amplitude and phase of its oscillation. These changes arise because of the outward shift of the equilibrium orbit and the increase of ν_r with increase of energy. The changes which occur in the phase are partiuclarly important. As the results we have discussed show, the resonance phenomenon may cause either a growth or shrinkage in amplitude depending on the phase of the oscillation, so that a shifting of the phase tends to ameliorate the effects of the instability.

The radial stability problem at low energies can be viewed in the following way: If the particles reach an energy of 20 Mev or so, such that their (r, p_r) values lie within a certain area of phase space, then their orbits thereafter will be stable. If these particles are decelerated and retraced back down to near zero energy, their resultant (r, p_r)

values must cover an area in phase space which includes the area occupied by the (r, p_r) values of the particles emitted by the ion source. Present computer codes have facilities for including acceleration effects on particle orbits and we plan to perform computations of this kind. The matching of the two phase space areas is then the solution of the stability problem. This can partly be accomplished by proper location of the ion source, although a location suited to protons, for example, will probably not be suited to N^{4+} ions. What is usually needed is a system of field coils which will produce a "cos θ" perturbation on the beam. If such a first-harmonic field has sufficient variability in strength and phase, it will serve to displace the (r, p_r) values of the particles in the beam to the proper area of phase space. With the computer facilities available here it should be possible to design a workable system.

VI. BEAM DEFLECTION

The problem of beam deflection from a machine such as the ORIC is a rather difficult one. Whatever deflection scheme is used, it must work equally for low-energy heavy ions all the way up to the highest energy protons. Although the conventional electric deflection system would work for the low-energy ions, it is quite unlikely that it would also work for 75-Mev protons. The beam deflection studies we have carried out so far are aimed at investigating the possibilities of magnetic deflection schemes. It is intended that the design of the beam deflection system will be worked out simultaneously with the design of the magnet. In this way it is hoped that a workable deflection system can be built right into the machine from the start. As a result, all the problems which arise from trying to obtain deflected beams after the machine is built would be avoided.

Our investigation of a magnetic deflection system is based on the Le Couteur system, with appropriate modifications for use in an AVF cyclotron. In the section on radial stability we discussed the fact that the sector structure of the magnetic field, together with the closeness of ν_r to unity, gives rise to nonlinear resonance effects which limit the radial stability of the orbits. One may hope then to make use of this instability to help achieve beam deflection. The basic requirement for a deflection system is that it must produce a sufficient separation between successive turns so that most of the ions in each pulse can clear a septum and enter the exit channel. The nonlinear resonance effects have the required property. For a three-sector machine the increase in amplitude per turn is proportional to the square of the amplitude so that if a small radial oscillation is induced in the beam, the resonance can amplify this amplitude to achieve a large increase per turn.

A considerable amount of work on the nonlinear resonance deflection system has been done at ORNL in connection with the design of an eight-sector, 850-Mev, AVF cyclotron.[1] The results of this work show that such a deflection system can work quite well.

For the ORIC the first requirement for this system to work is a manipulation of ν_r. As pointed out in the section on radial stability, the value of ν_r for protons is significantly greater than unity (~ 1.1) near the outside of the machine. As a result, radial oscillations with amplitudes up to 5 in. and more are stable. For deflection purposes this considerable degree of stability is undesirable. To shrink the range of stable oscillation amplitudes it is necessary to have the average field fall off near the outside. This field fall-off will reduce the value of $\underline{k}$ and hence also ν_r. One additional consequence of having the average field fall off is that the particles will lose phase. However, if a good degree of isochronism is maintained over the rest of the machine, then the total phase loss during extraction should not be enough to cause the particles to decelerate. Accompanying the decrease in $\underline{k}$ should be a corresponding decrease in flutter such that ν_z does not get too large. A decrease in flutter will also aid in dropping ν_r toward unity.

The second requirement for the success of the nonlinear resonance deflection system is a suitable field bump. The radial phase plots associated with the resonance are characterized by a central region of small oscillation amplitudes which is stable and a peripheral region of open phase plots of unstable orbits. Before the deflection process begins the beam will be located in the central stable region of phase space. Part of the deflection system must, therefore, contain a mechanism for shifting the beam from a stable area of phase space into a region of instability. After this has been done, the nonlinear resonance force will then act on the beam to increase its radial amplitude at a steadily increasing rate. The mechanism for shifting the phase space location

(1) ORNL-2501, and
M.M. Gordon and T. A. Welton, Bull. of APS, 3, 57 (January 1958).

of the beam is the so-called "field bump". The purpose of this field bump is to produce a force acting on the radial oscillations of the following form:

$$F = \epsilon_o \cos\theta + \epsilon_1 x \cos 2\theta + \ldots$$

At resonance ($\nu_r = 1$), the first term in F (which is the most important here) causes the oscillation amplitude to grow at the rate of $\pi\epsilon_o R$ per revolution, where R is the radius of the orbit. The parameter ϵ_o here is the ratio of the strength of the bump to the strength of the average field. Thus, for $\epsilon_o = 10^{-3}$ and $R \gtrsim 30$ in., the amplitude gain per turn will be about 0.1 in. If the stability region in phase space is sufficiently reduced when deflection begins, then a relatively weak bump can be used. In addition to the strength of this bump, its azimuthal location is quite important. The region of phase space where the orbits are unstable is characterized by asymptotes along which the points representing particle orbits move either in or out, corresponding to growth or decrease in oscillation amplitude. The field bump must not only displace the phase space points of the particles into the region of instability, but must also displace them so that they move toward one of the asymptotes along which the amplitudes will continue to grow at an accelerated rate. This can be accomplished by a suitable choice of the azimuth at which the bump is located.

To summarize, the resonance deflection system consists of two parts. As the particles arrive at the outer orbits they are acted upon by a suitable field bump which builds up their radial oscillations. As these oscillations grow in amplitude the nonlinear driving forces take over and accelerate the rate of growth. This growth rate will eventually reach a point where the particles can in one turn clear a septum and enter the exit channel. This system differs from the usual Le Couteur system in that use is made here of the nonlinear driving forces already present in the machine so that the additional field bumps required need not be so large.

There is a very serious danger in this deflection system (as in the Le Couteur system also), namely the possibility that the beam will lose its axial stability during deflection. An essential part of the deflection process is the induction of large radial oscillation amplitudes in the beam. Whenever large radial amplitudes are present certain nonlinear coupling resonances become important and may lead to a disastrous growth in the axial oscillations. The coupling resonances which are important here are

$$\nu_r - 2\,\nu_z = 0; \quad (N-1)\,\nu_r + 2\,\nu_z = N$$

where N is the number of sectors. As the radial oscillations grow in amplitude the nonlinear terms in the orbit equations cause ν_z to shift toward the resonant value given above, about 0.5. When ν_z reaches a resonant value, the amplitude of the axial oscillations then begins to increase. Since the amount of axial gap space available to the beam is quite limited, any such growth is harmful and may be disastrous. This effect has been studied extensively in connection with our work on beam deflection from the 850-Mev proton machine mentioned above. There we found that the effects of the coupling resonances limit the amount of radial amplitude build-up that can be achieved during the deflection process. These effects are considerably worse for tight-spiral machines since the spiral makes a large contribution to the nonlinearity of the machine. The work at Harwell on the four-sector, tight-spiral machine has amply demonstrated this point.

Our first study of this problem was made for the four-sector, tight-spiral machine with N^{4+} ions discussed in the preceding section on radial stability. We chose the energy for this orbit test run to be 58.7 Mev since other orbit data had already been collected there. We did not use the higher energy (94 Mev) since we wanted to be sure that the orbits would remain inside the machine for large radial displacements. The initial values of r and p_r for this orbit were so chosen that the orbit would be radially unstable. In addition, the orbit was given an initial vertical displacement of about 1 in. from the median plane. (Since the axial motion is nearly linear, the results for other displacements are roughly proportional.) The radial phase plot for this orbit is the open (unstable) plot in Fig. 28, at this same energy. The corresponding axial motion is shown in Fig. 32. Points for this curve were obtained from the computed z values plotted once per sector. During this run the radial amplitude increased from about 2 in. to about 6.5 in. in ten revolutions. As can be seen in Fig. 32, the axial frequency shifts in and out of resonance with successively larger growths in amplitude. Our conclusion from this run is that coupling resonance effects would be disastrous during beam deflection in this type of machine. This conclusion is consistent with the results obtained at Harwell.

A similar study has also been made for the three-sector, weak-spiral machine with results which are much more encouraging. For this work we used fields obtained from the three-sector magnet model. For comparison with the above results we again considered N^{4+} ions, this time at an energy of 64.9 Mev. The equilibrium orbit code gave for this energy $\nu_r = 1.045$ and $\nu_z = 0.330$. Radial phase plots obtained at this energy are shown in Fig. 33. Full scale in this figure corresponds to a deviation of about 4 in. from the equilibrium orbit. Two orbits are shown, one stable and the other unstable. The unstable orbit begins with a radial displacement of 1.0 in. and runs off the edge of the picture. This orbit was run again with an initial vertical displacement of 0.5 inches from the median plane. In this run the particle went 15 revolutions before running off the outer end of the magnetic field. The z-motion of this orbit is shown in Fig. 34. The curve shown was obtained from points plotted at intervals of once per sector. As can be seen, in this case the amplitude and frequency of the vertical oscillations held quite steady over the entire length of the orbit. At the same time the amplitude of the radial oscillations grew from 1.0 in. to 7.2 in.

UNCLASSIFIED
ORNL-LR-DWG 30282R2

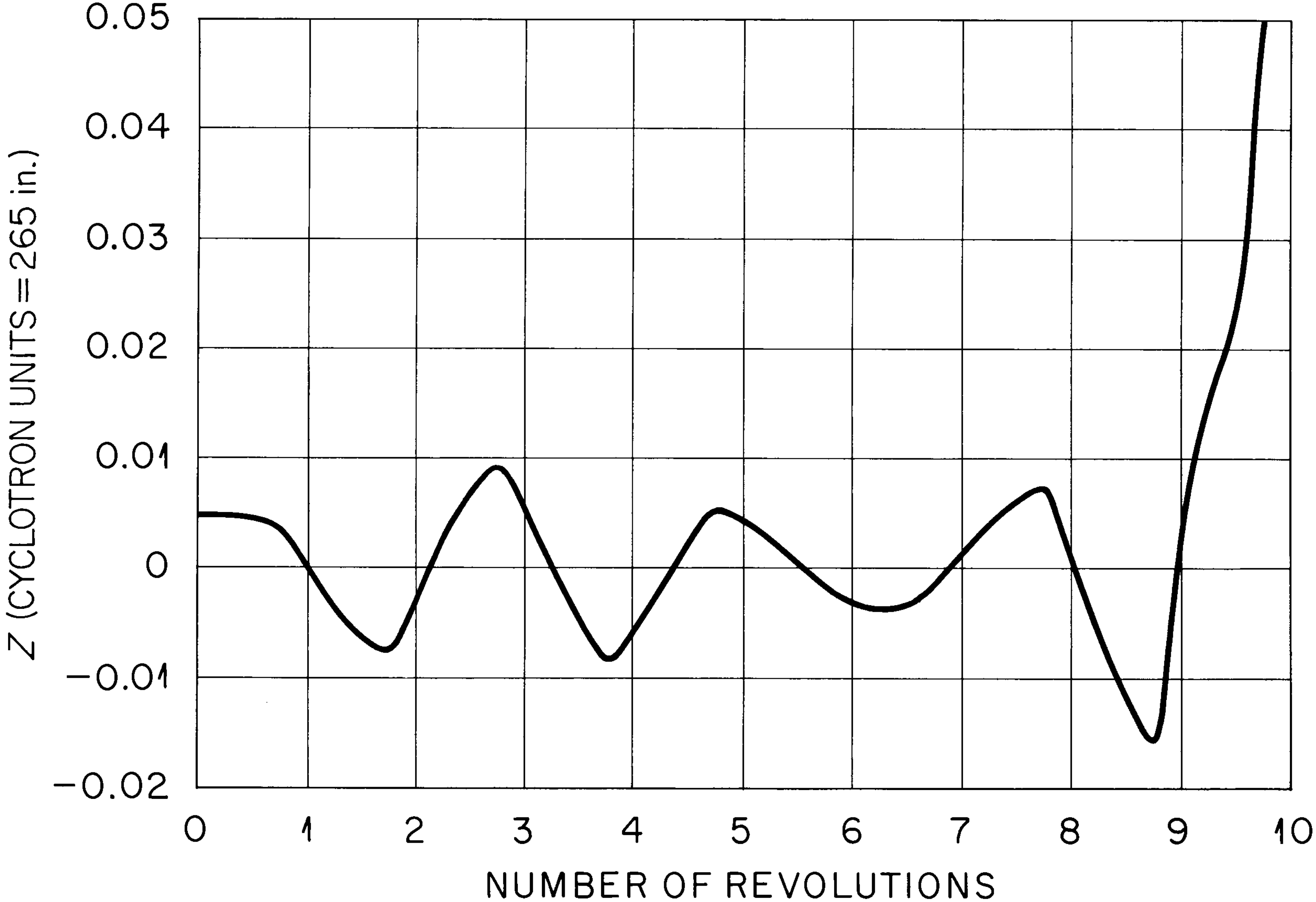

Fig. 32. The Effect of Coupling Resonances on Axial Oscillations.

UNCLASSIFIED
PHOTO 44837

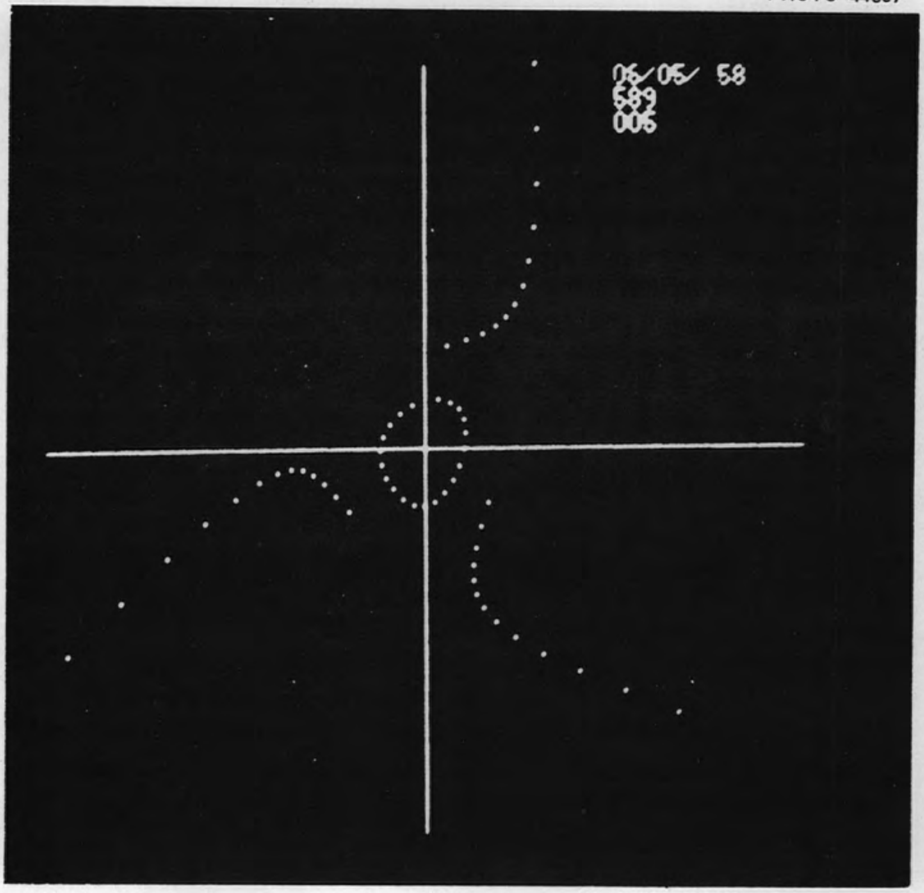

Fig. 33. Radial Phase Plots Obtained with Fields from Three-Sector Model Magnet for N^{4+} Ions at 65 Mev, in Connection with Beam Deflection Studies.

UNCLASSIFIED
ORNL-LR-DWG 32529

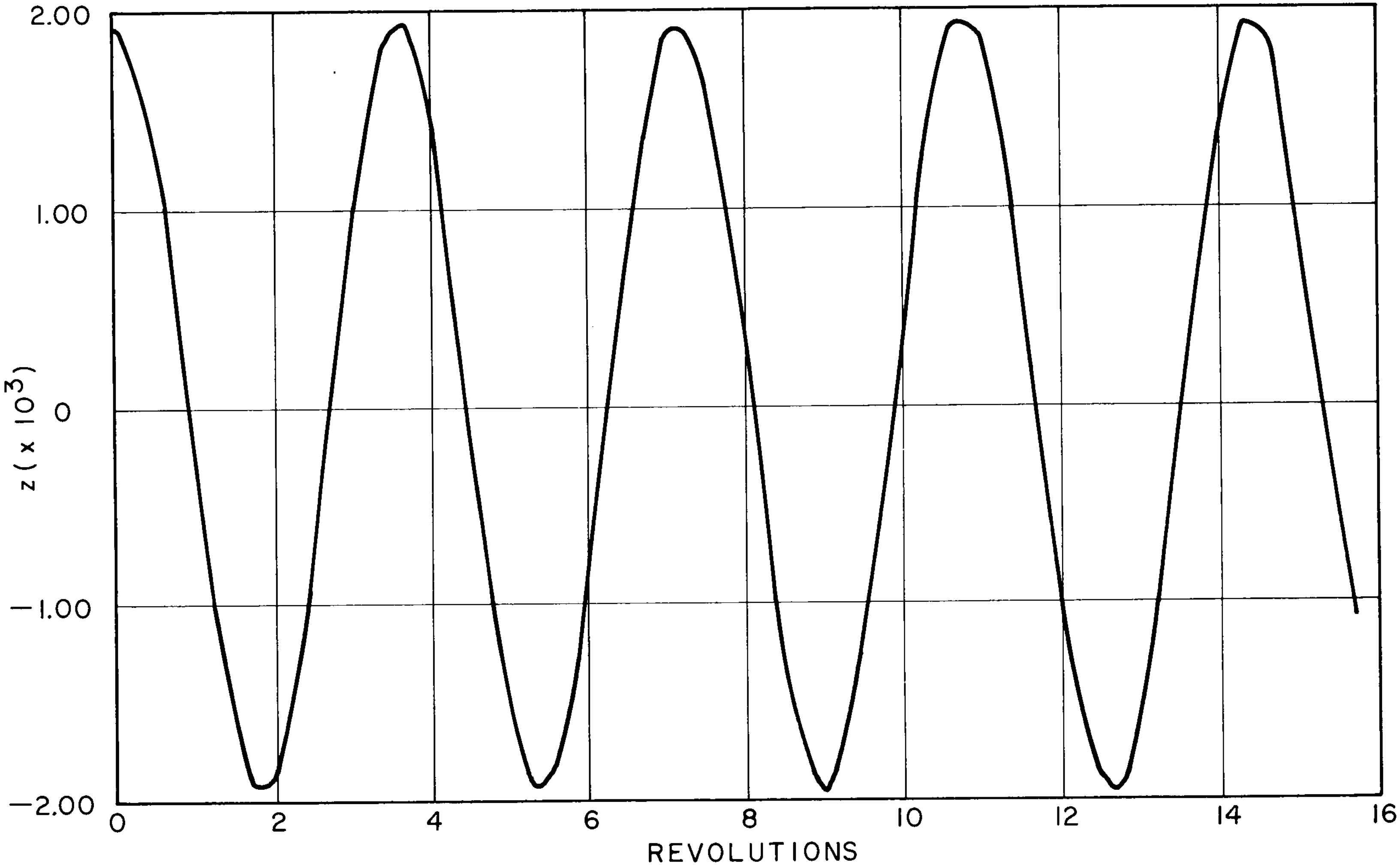

Fig. 34. Axial Oscillations of Orbit with Unstable Radial Oscillations, in Three-Sector Machine. N^{4+} Ions at 65 Mev (Beam Deflection Study).

In the table below we give the history of the radial motion over the last several revolutions of this orbit.

Rev. No.	r (in.)	Δr (in.)
10	30.178	
11	30.769	0.59
12	31.479	0.71
13	32.309	0.83
14	33.287	0.98
15	34.482	1.20

The particular θ value at which this data was recorded was such that the value of p_r did not change very much so that the increase in radial oscillation amplitude here goes almost entirely into increasing $\underline{r}$. The Δr shown in this table was calculated by taking the cyclotron unit as 265 in. The effect of the nonlinear driving force on Δr is quite apparent. For comparison, the Δr produced at this energy by an energy gain per revolution of 1.6 Mev is 0.3 inches.

Further work of this kind is now in progress with protons.

VII. RADIO-FREQUENCY SYSTEM

A. Requirements and Specifications

1. Frequency Range: In order to provide a continuous energy range, a continuous frequency range is required of the radio-frequency accelerating system. Since it is possible to use harmonics, that is, to accelerate particles with the radio frequency at certain multiples of the ion rotation frequency, the frequency range actually required is considerably reduced. In the case of 180-deg dees, operation of the dees in the out-of-phase (or push-pull) mode makes possible the use of the first and all odd harmonics. Thus, the r-f system need tune only over a 3:1 range. Use of the in-phase (or push-push) mode on the dees would allow the even harmonics to accelerate particles and the required tuning range would be only 2:1. However, this mode is impractical in many configurations for resonators since it requires high r-f current connections between the dee stems and liner. Therefore, it is impossible to bias the dees to prevent multipactoring, and a more complex booster oscillator circuit is required.

A 3:1 tuning range with the dees operating in the push-pull mode appears to be the first choice. The specified range is from 7.5 to 22.5 Mc/s. Operating with the r-f at the third and fifth harmonic of the orbit frequency would, in effect, bring the lower limit of the frequency range down to 2.5 and 1.5 Mc/s, respectively.

2. Energy Gain/Turn: The maximum energy gain/turn for this machine was chosen as 400 kev, see page 60. Thus, with two 180-deg dees, the dee-to-ground voltage must be 100 kv peak.

3. Angular Width of Dees and Dee Voltage: The particles gain the maximum energy in passing through a dee, of angular width θ, if the phase is as shown:

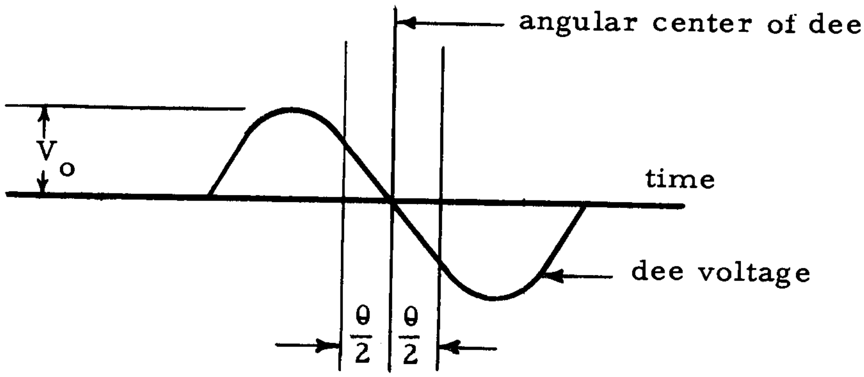

Thus, for particles of the same frequency as the r-f, the maximum voltage gain/dee is $V_d = 2V_o \sin \theta/2$; for particles rotating on sub-harmonics of the dee frequency, the angular width of the dee is $n\theta$ to the particle where n is the order of the sub-harmonic, and the energy gain is $2V_o \sin n\theta/2$. It is interesting to note that even a 15-deg wedge removed from the dee lip would cut the voltage gain/turn of the heavy (third harmonic) particles by 30%. The choice of 180-deg dees fixes the dee voltage as 100 kv peak.

4. Dee-to-Liner Separation: The selected value of 100 kv peak voltage requires about 1.5-in. clearance from dee-to-liner, Fig. 35. Since the magnetic gap is so precious in a machine of this type, this minimum value is taken for design.

5. Dee Voltage Standing Wave, Impedance, and Current: In the lower part of the frequency range, the dee may be treated to sufficient accuracy as a lumped capacitance. That is to say, the VSW along the dee is nearly flat at 100 kv peak. However, with the dee geometry chosen and at the high end of the frequency range, the VSW has been computed to be

$$V = 64.5 + 6.5(r/28) - 2.5(r/28)^2 - 1.5(r/28)^3 \; . \; . \; . \; . \; ,$$

UNCLASSIFIED
ORNL-LR-DWG. 30818 R

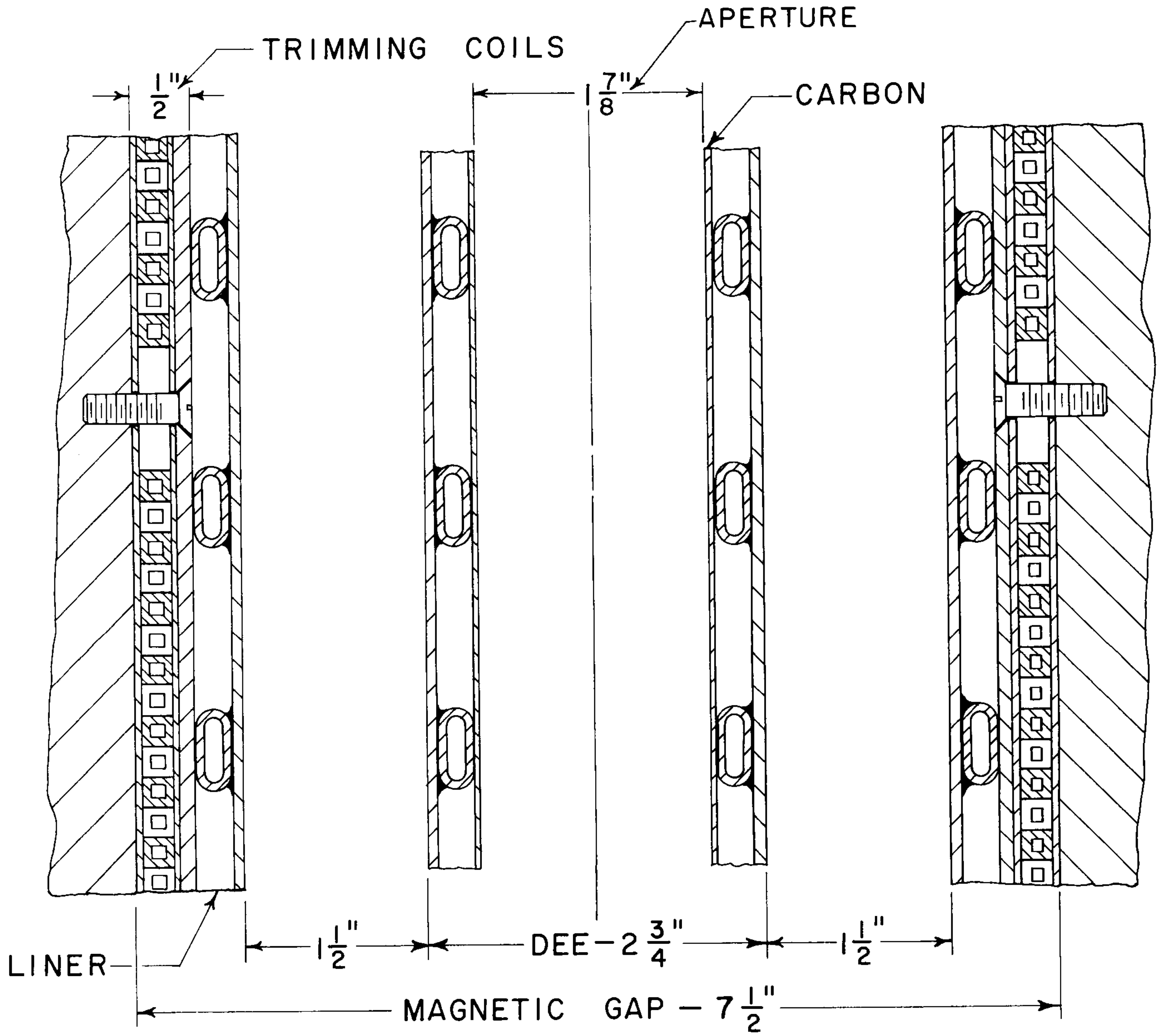

Fig. 35. Spacing of Dees and Liner in Magnet Gap.

where the voltage is in rms kilovolts and r is the distance from the center of the dee in inches. Thus, a first harmonic exists in the r-f voltage.

The capacity of the dee is about 700 μμf. The exact value cannot be known at this time, since the final shape of the dee should be chosen as the smallest value possible to enclose the orbits. The equilibrium orbits are known, of course, but the paths of the particles during deflection are not yet fully known.

For a dee capacity of 730 μμf, a figure chosen as an outside limit, the dee input impedance is given in Fig. 36. The total current to the dee is plotted on the same figure.

Resonator Design Considerations

1. Quarter-Wave Resonator: To make the system resonant as a quarter-wave line over the range 7.5 to 22.5 Mc, an inductive stub must connect from each dee to ground and present an impedance to the dee equal to the impedance of the dee as shown in Fig. 36. This dee stem, which extends between the magnet coils, may have a characteristic impedance of about 20 Ω in its location between the coils and, of course, a much larger value once outside the coils. The input impedance of the stub is $+jZ_o \tan \beta \ell$. Thus, at 22.5 Mc, ℓ would have to be about 28 inches. This length which, further, neglects the inductance of the shorting bar is much too short for the stem since it would require the shorting bar to be between the magnet coils. Since a quarter-wave resonator is impossible with the 180-deg dees, the system must be made more complicated.

2. Half-Wave Resonator: The next simplest resonator would be one-half wave length long. That is, the dee stem would be capacitively loaded at each end; one end would be the dee capacitance, and the other would be a tuning capacitor. The dee stem for this configuration must be supported on insulators and the cooling water supplied through r-f chokes. Since there are insulator commercially available with maximum compressive stress up to 300,000 psi and good r-f properties, this type of system might be feasible. Experiments to determine the heating of the insulators in such a system would be essential.

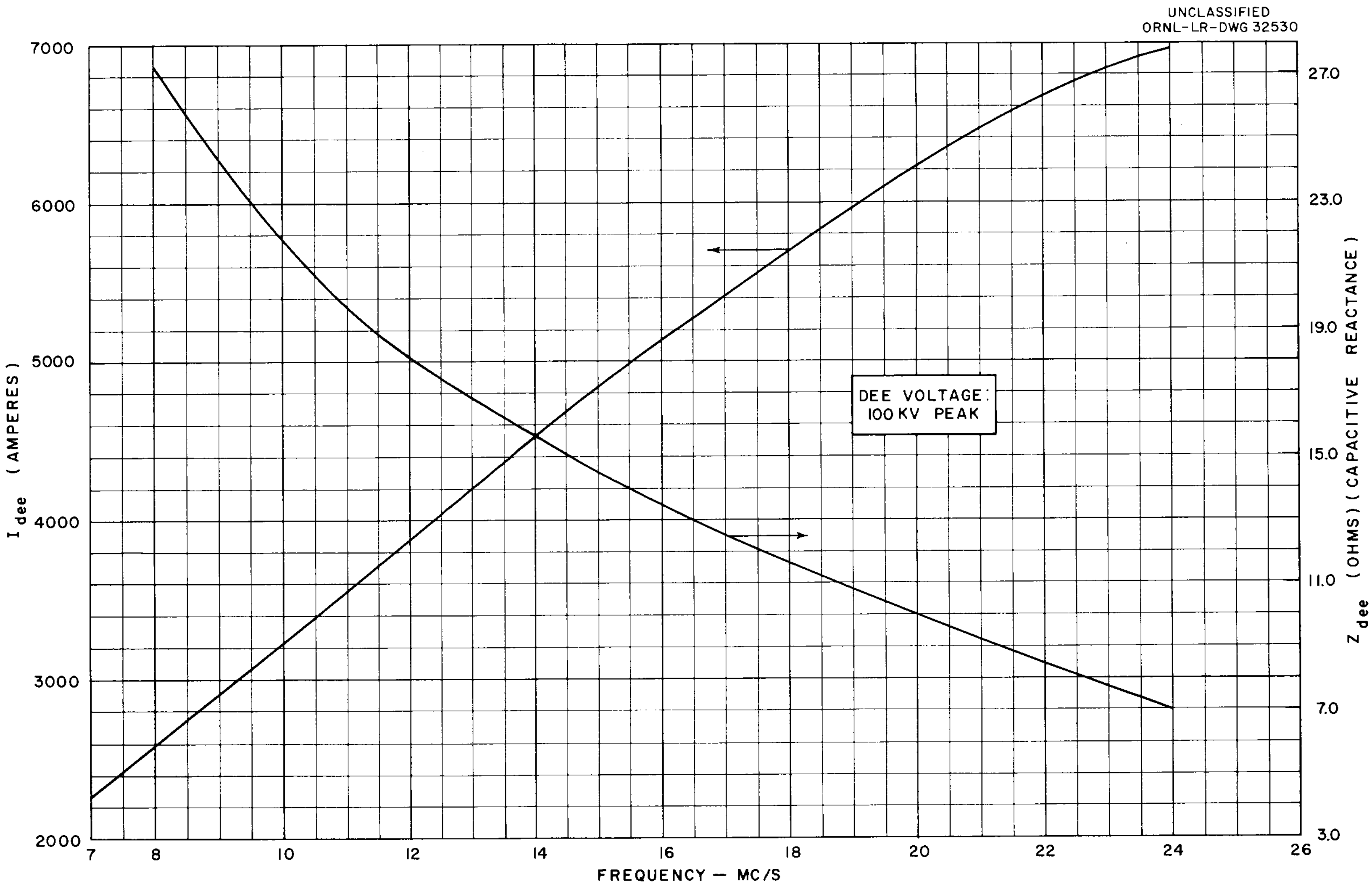

Fig. 36. Dee Impedance and Current (rms) as a Function of Frequency.

The total power to excite a half-wave system, consisting of the 180-deg dee, 18.8-Ω dee stem, and a 100-in. 60-Ω line outside the coils terminated in a large variable capacitor, has been computed as 360 kw for 100 kv dee-to-ground voltage.

In addition to the question about insulators mentioned above, there is a question about the tuning capacitor because of its large size, wide range of capacity, and voltage breakdown. Models and further analysis should answer these questions.

3. Two-Coupled Circuit Resonator: The properties of two-coupled lumped circuits are shown in Fig. 37; the circuits have two natural modes of oscillation. In one case the currents are in phase, and in the second case they are opposite in phase. Thus, considering the effect of the second circuit back on the first, it is seen that in one mode the inductive reactance is increased lowering the frequency from the value when the two circuits are isolated, and in the other mode the opposite situation occurs. The frequency of resonance is plotted on Fig. 37 with the ratio of the separate natural frequencies as variable and k, the coefficient of coupling, as a parameter.

The physical dimensions (dee size and stem length) of the ORIC are such that the dee and stems can form one circuit with a resonant frequency about 10 Mc. It is possible to tune this circuit over but a small range. The second circuit can then be inductively coupled to the dee stems. Since this second circuit can be located outside the magnet, it can be made large with a very high Q.

Two variations of this circuit are being considered. The first, chosen largely for mechanical reasons, has a fixed mutual inductance between the two circuits as shown in Fig. 38. The disadvantages of this circuit are that a wide tuning range is required of the tuned circuit and that is impossible to tune to frequencies close to the natural frequency of the fixed (dee) circuit. Thus, since the dee-circuit frequency is within the required frequency range, a dead band would occur. A greater disadvantage is that to obtain maximum frequency range, the inductance as well as capacity must be variable; this

UNCLASSIFIED
ORNL-LR-DWG 32531R

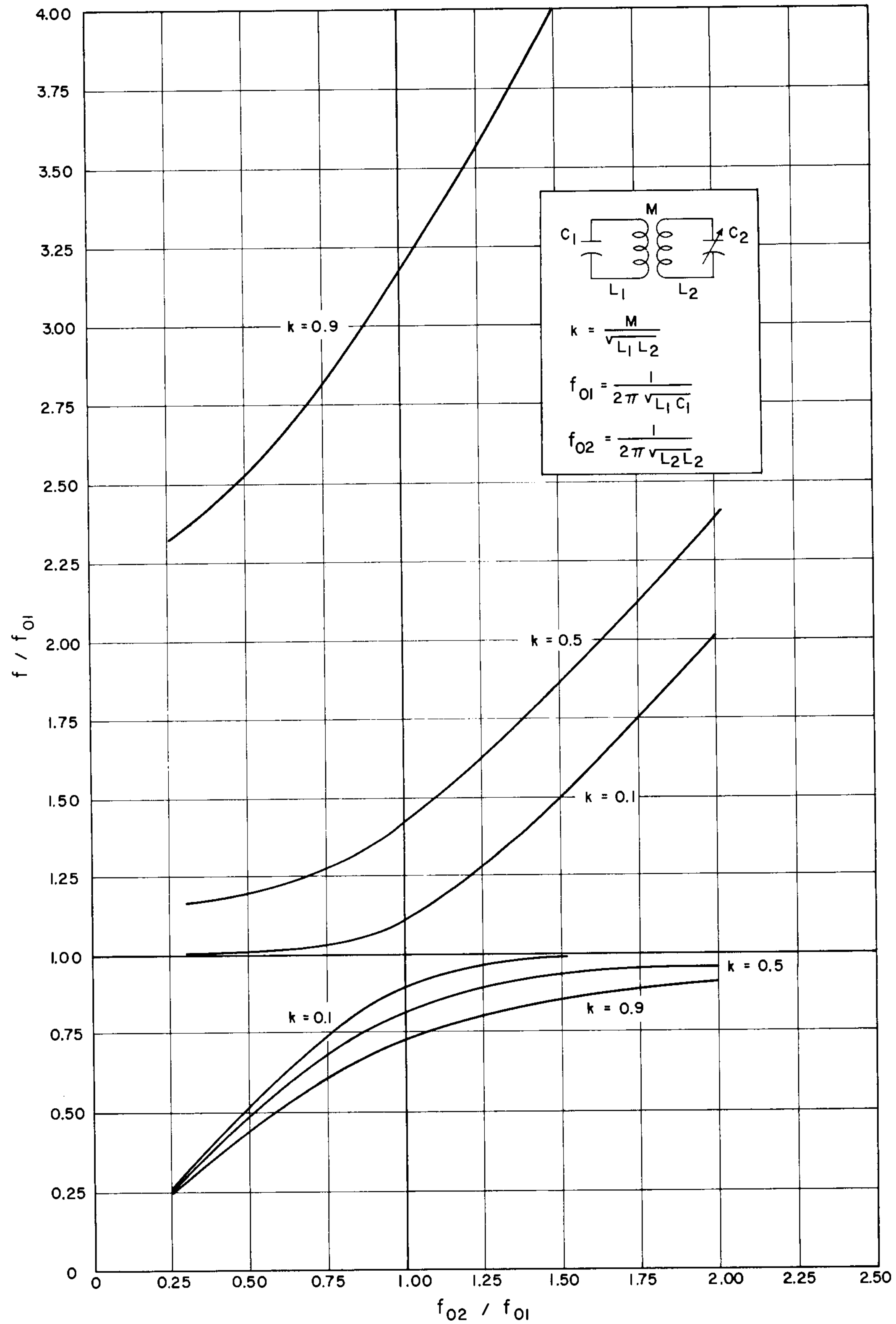

Fig. 37. Natural Frequencies of Two Coupled Circuits.

UNCLASSIFIED

2-02-015-499

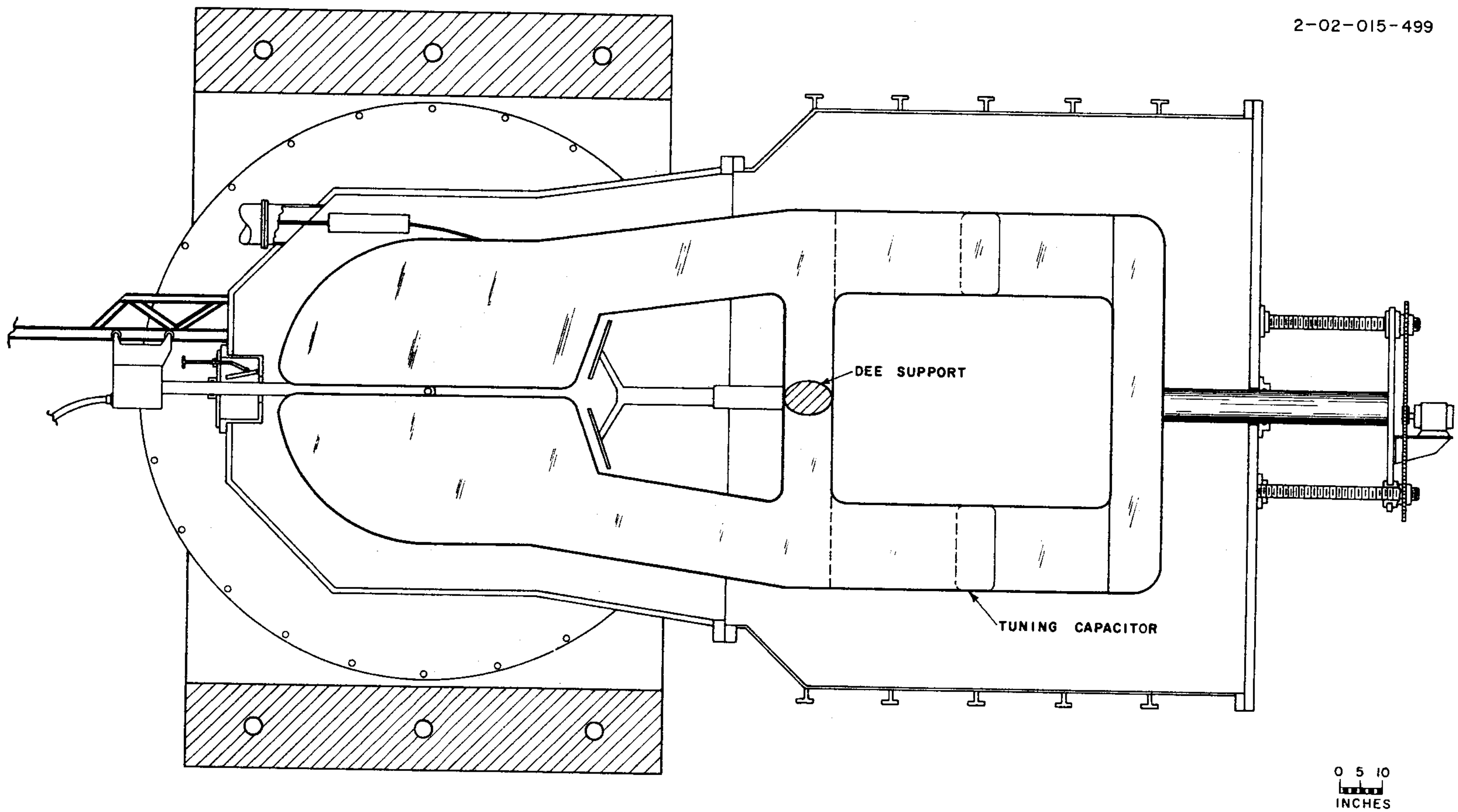

Fig. 38. Resonant System with Fixed Mutual Inductance.

requires a movable shorting bar as shown in the modification of Fig. 39. The current density required at the shorting clamp exceeds that of present designs by a factor of two to three. Computation indicates the power into this system would be about 500 kw.

The second variation of the two-coupled circuit scheme involves variable mutual inductance as shown in Fig. 40 along with variable frequency of the tuned circuit. This arrangement requires that the dee circuit be driven if the system is to be tuned to all frequencies in the band specified since the mutual inductance must go to zero. A model is being constructed to measure the properties of this system. Unfortunately, there is no reason to expect the maximum driving power to be any less than that required in the first variation described, 500 kw. However, there are no current carrying joints which would have to be movable and there are tubes readily available for service at this power level.

UNCLASSIFIED

2-02-015-503

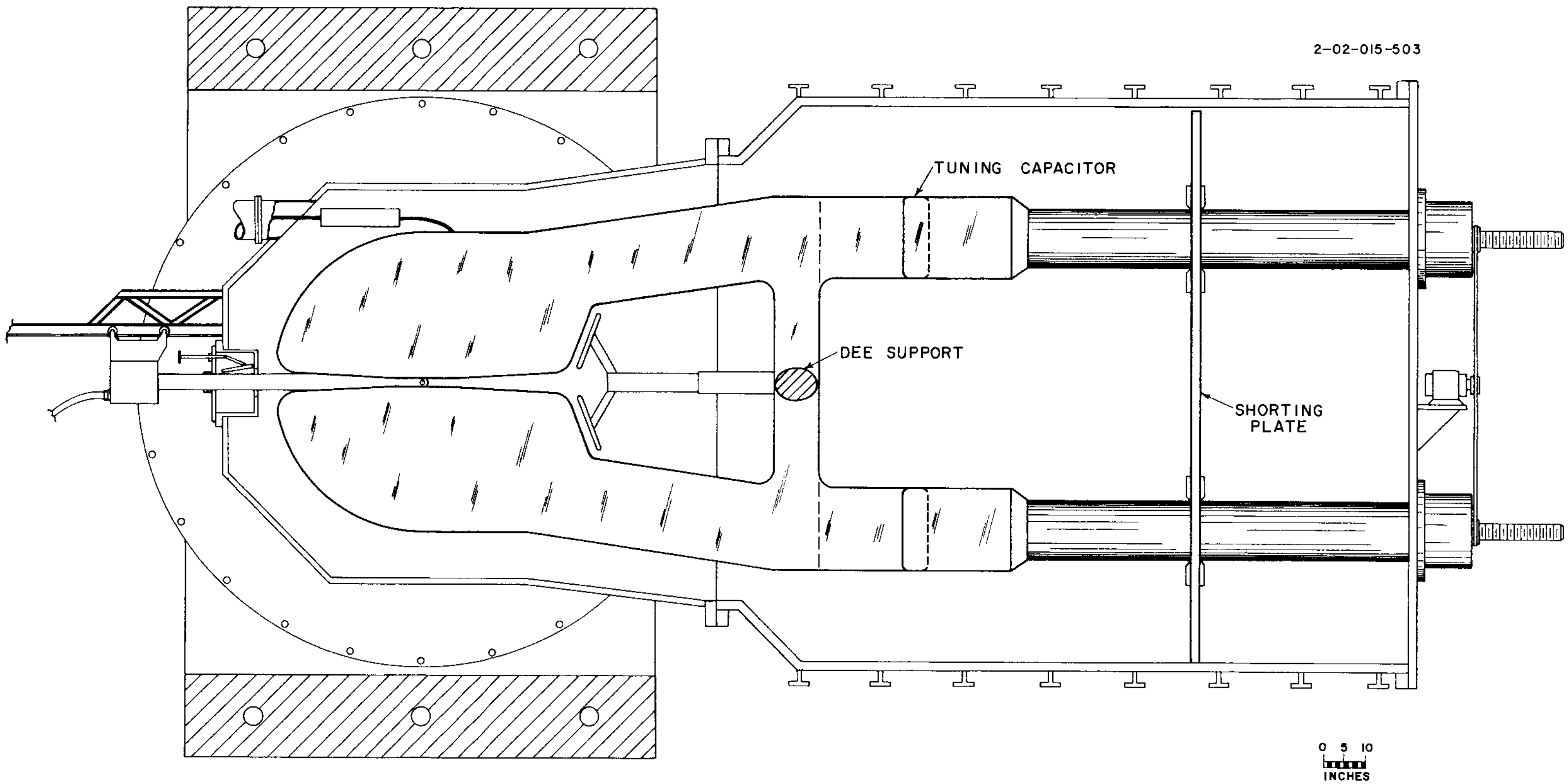

Fig. 39. Resonant System with Movable Shorting Bar.

UNCLASSIFIED
2-02-015-499-R1

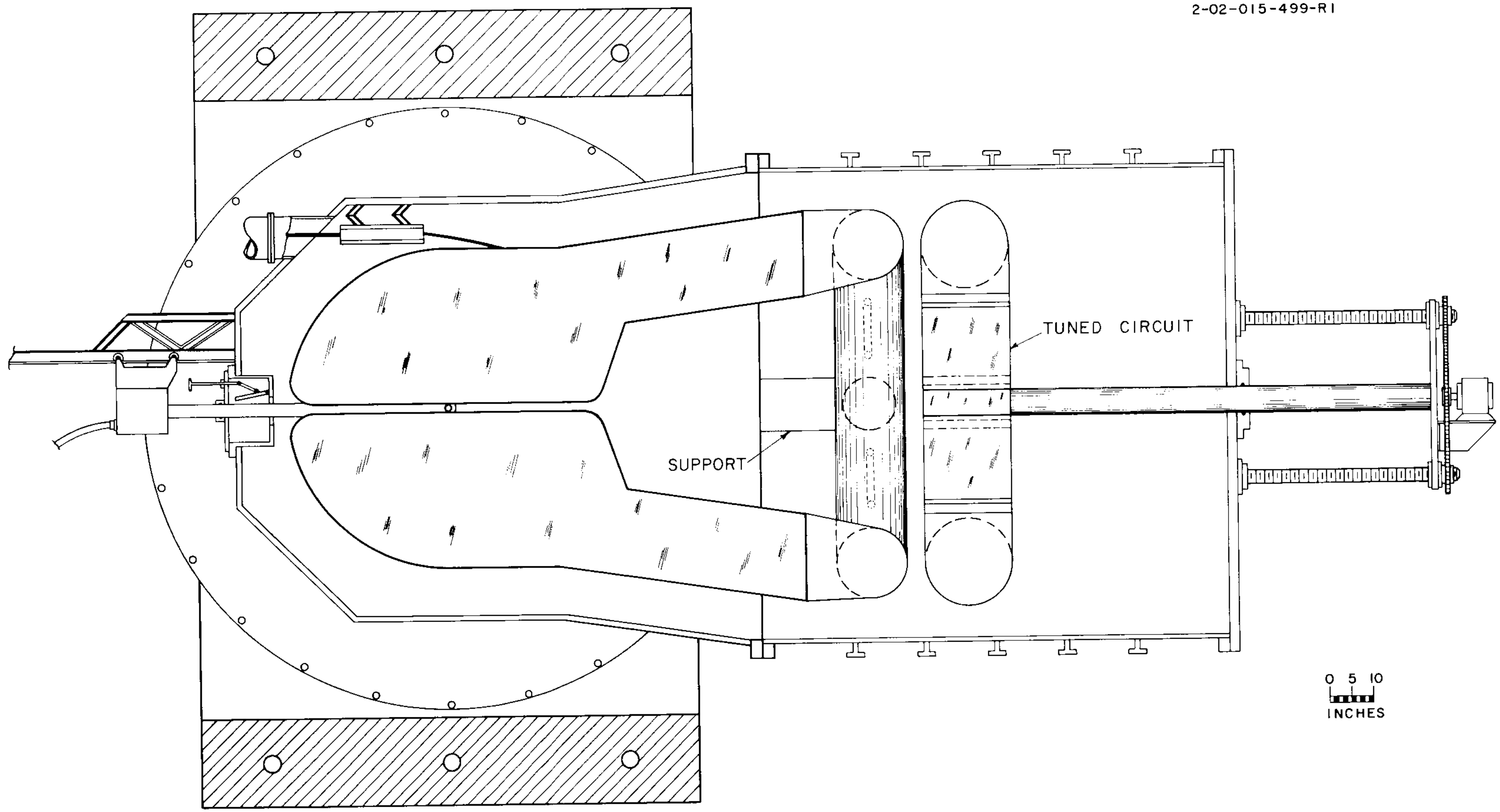

Fig. 40. Resonant System with Variable Mutual Inductance.

VIII. ENGINEERING STUDIES AND DESIGN FEATURES

Engineering studies have been completed for the ORIC magnet and its design is essentially complete except for details of the pole tips and auxiliary coils. Preliminary design studies have been made for the resonant system, vacuum system, and ion source. Each of these components is discussed below.

Magnet

The specifications for a cyclotron magnet involve relations between many dependent parameters. It is necessary, therefore, to make both successive approximations and compromises in the preparation of firm specifications. The process of selecting the specifications involves the determination of the following parameters: 1) basic criteria, 2) ampere-turns, 3) operating power, 4) choice of conductor material, 5) specification of conductor material, 6) coil design, 7) yoke specifications, 8) yoke design, and 9) the design of auxiliary coils for the AVF feature of the ORIC.

Design Criteria

The basic design criteria for a cyclotron magnet evolves from a consideration of the $H\rho$ and beam aperture required for the transmission of the desired ion currents to a given maximum energy. These criteria are usually selected by a suitable compromise between desired maximum energies and currents and those obtainable practically, at a reasonable cost. The design latitude of the ORIC magnet was slightly, but not seriously, restricted by the availability and usefulness of existing equipment obtained for an earlier machine. Thus, after a review of previous calculations and model work, an energy of 75 Mev for protons, a maximum beam radius of 31.5 in., a pole diameter of 76 in., and a minimum gap of 7.5 in. were chosen. A horizontal section through the magnet is shown in Fig. 41.

UNCLASSIFIED
ORNL-LR-DWG 34924

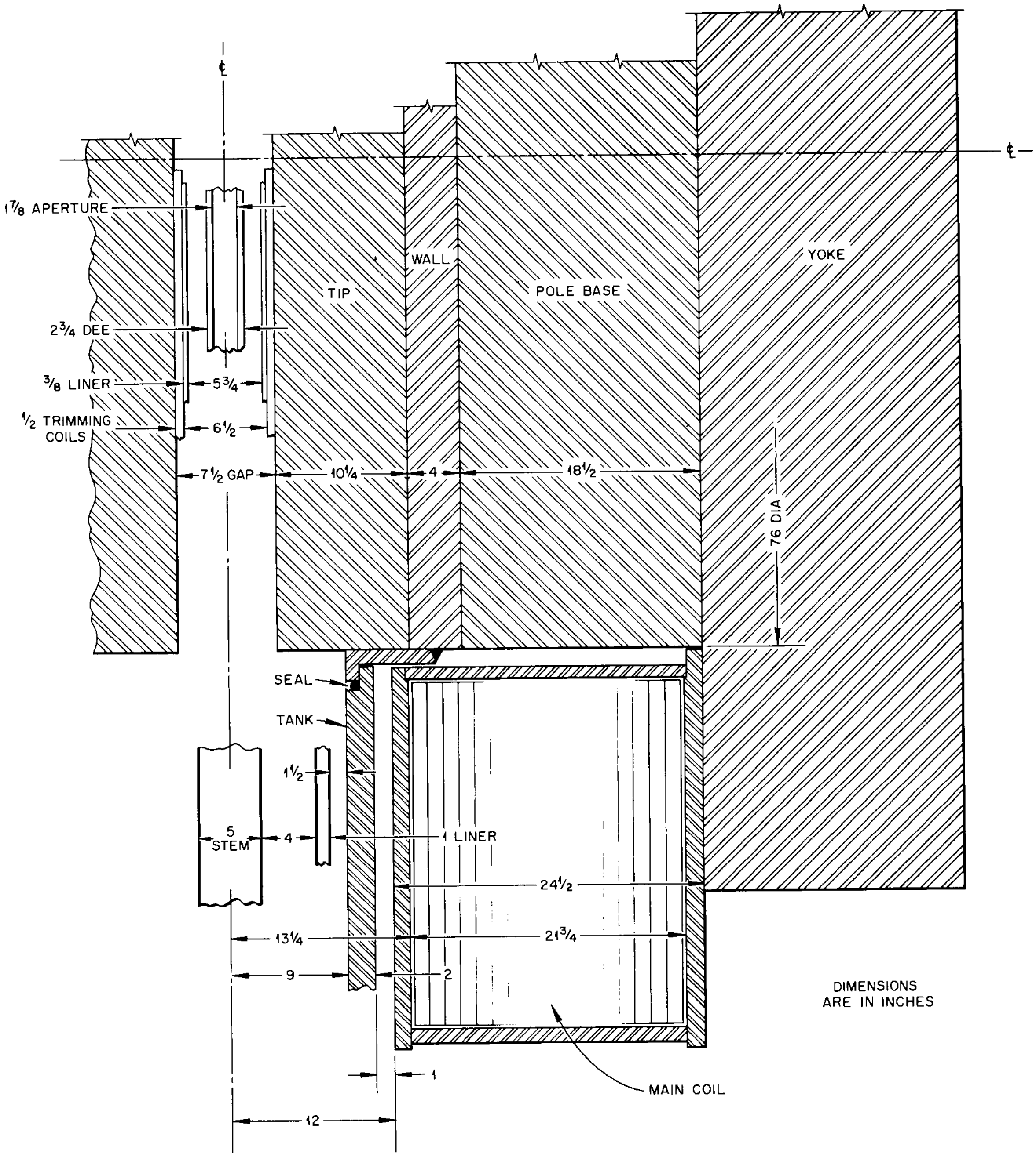

Fig. 41. Horizontal Section with Assigned Dimensions.

Ampere-Turns

The number of ampere-turns required to obtain the magnetic field specified by the basic criteria was determined by model magnet measurements. First, an estimate of the ampere-turns was obtained by assuming a magnet with an efficiency of 60% and substituting in the relationship

$$NI = \frac{2.02\, Hg}{\eta}$$

where NI is the ampere-turns, H the magnetic field strength in kilogauss, g the magnetic gap in inches, and η the efficiency.

With this estimate, a 1/8.69 scale model was constructed for use in investigating field shapes and for determining a reliable value for ampere-turns. The value obtained was 1.09×10^6 ampere-turns at an efficiency of 52.4%. This value was adjusted for possible errors, which were all assumed to be in the direction to increase the ampere-turns required, as follows:

Items	% As Estimated	As % of Total Current
Iron (μ)	1.5	1.0
Current measurement error	0.2	0.2
Winding end effects	0.1	0.1
Dimensional errors of model	1 to 2.0	6.0
Field measurement errors	1.0	3.0
Contingencies	1.0	3.0
		13.3%

After this 13% adjustment for errors the value for use in subsequent calculations became 1.23×10^6 ampere-turns.

Power Level

The operating power level for the magnet was selected to provide the minimum-cost magnet that meets the basic criteria. The choice of operating power level is related to the amortization time of initial costs. This time was arbitrarily chosen as 10 years, and a range of practical power levels was selected. The initial cost plus cost of operation for 10 years was then calculated for each of the various power levels until a minimum cost design was found. The initial cost estimates did not have a high degree of accuracy; however, the estimated cost passed through a broad minimum. In this manner the power level was established at approximately 1000 kw.

Conductor Material

For practical reasons the only suitable conductor materials are copper and aluminum. A choice between these two materials becomes a matter of cost and reliability. To the first approximation, in magnets of the same power and ampere-turns, the ratio of the aluminum to copper weight is 0.5; this follows directly from the ratios of density and conductivity.

This rough approximation would require copper to cost half as much per ton as aluminum to be competitive. Of course, other factors were considered. The use of aluminum would require more yoke steel because of the larger coils. For a magnet the size of the ORIC (200 tons) this would amount to an increase of 10 tons or an approximate cost of $4400.00. Also, because of the greater volume of aluminum, the coil windings are displaced radially outward where they are magnetically less effective.

In making a choice of these conductor materials several studies were made of various coil and yoke configurations operating at different current densities and power levels. Complete magnets with both copper and aluminum were calculated for several cases of interest. At the market price for these metals at the time these studies were made, a substantial saving was indicated for aluminum.

A rating of reliability of the two conductor materials could only be estimated for particular designs. A possible difficulty with aluminum would result from corrosion or deposits in the cooling water passage. Difficulty with copper would be most likely to occur in connection with the several hundred brazed joints. These joints are necessitated by the limitation in copper extrusion technology needed to produce long length conductors at practical costs. In view of all these considerations aluminum was chosen for the conductor material.

Conductor Corrosion Test

Since an adequate degree of reliability of aluminum had been assumed, it was felt that a test for corrosion and deposit under operating conditions would be desirable.

Test sections of aluminum were obtained from Aluminium Limited Sales, Inc. The test was made in the water system used in cooling the r-f components of the ORNL 86-Inch Cyclotron. Two test pieces of Al conductor 24-in. long were separated from ground and from each other by 30-in. lengths of rubber hose. The unit was inserted in the circulating water system of the cyclotron in which the water is demineralized and filtered but not deaerated. The total capacity of the system is 15,000 gal, and the make-up is supplied by a central demineralization plant. Analysis of the water in the system showed a pH of 7, small amounts of carbonates, and approximately 4.2 mg of solids/liter of solution. The latter is in collodial suspension and gives the water a brown color. The total iron content was 3.3 ppm with 0.3 ppm of iron dissolved. The conductivity of the water was 6.5×10^{-6} mhos per cm^3. The piping in the system contains seamless mild steel pipe, admiralty brass tubes in the heat exchangers, copper tubing, and a small amount of aluminum in the cyclotron deflector. The average summer temperature of the water is 75°F; the average winter temperature is not available but can be presumed to be in the vicinity of 34-40°F. A conductivity of 9×10^{-6} mhos per cm^3 was obtained from the demineralizing plant on August 29, 1958.

A simulated operating potential was applied to the test sections, with one piece of aluminum conductor at 175 volts positive and the other piece at 175 volts negative to ground. Upon termination of the test after 6,900 hours, it was found that the specimen at negative potential had gained 5g (0.57%) and the positive 3g (0.34%). There was more deposit at the ends of the negative section; this was a relative loose material. There was very little pitting at the tips of the negative section; pitting at the tips of the positive section was heavier, averaging about 60 mils. As would be expected, the heaviest deposits and deepest corrosion occurred at the ends of the specimens facing one another where the effective potential was 350 volts. All significant changes in the aluminum test sections appeared within 0.5 in. of the ends; there was only a very thin layer of brown deposit beyond the ends.

The test was reassuring in that it indicated that no serious problems would be encountered in using aluminum conductors with a demineralized water system. A replaceable inspection section should be provided, however, at the entrance and exit of each strand of conductor.

Specifications for Aluminum Conductor

The specifications for the aluminum conductor were as follows:

> The material is to be EC (Electrical Conductivity) aluminum, ASTMB0236-56T, each strand (1170 ft) to be one continuous extrusion from one or more billets.
>
> The tensile strength is to be adequate to meet a hydraulic pressure test of 300 psi, the outside dimensions not to exceed the required tolerance of ±0.010 in. during the test.
>
> The cross section of the conductor to be 1.137 ± 0.010 in. square, with the radius of corners not to exceed 3/64 in., and with a center hole of 0.700 ± 0.010 in. diameter. The maximum allowable eccentricity to be 0.0218 in., with the wall no thinner than 0.186 in. at any point.
>
> A piece removed from each end of the conductor in the 1/4-hard maximum temper at shipment to be capable of being bent cold 90 deg around a 2.5-in. radius mandrel without cracking. Buckling, distortion, and the reduction in area of the 0.7-in. dia opening to be considered within tolerance if the buckling is undetectable by eye, if the bending decreases the outside edge by no more than 10%, and if the area of the 0.7-in. diameter opening is decreased by no more than 10%. (This test was made to determine the properties of the aluminum; the conductor would not be subjected to this extreme bending).

A chemical analysis was not requested; however, an analysis furnished with the conductor gave the following: Cu 0.007, Fe 0.29, Mn 0.003, Si 0.08, Ti 0.004, V 0.010, B 0.003, and Ga 0.017, all in percent. All specifications were satisfactorily within tolerances.

Magnet Coil Design

The main coils are designed with eight water and eight electric circuits each. Each circuit is a single conductor strand, 1170 ft long, wound as a double pancake so all connections are external to the coil. The double pancake coils were designed to have a resistance of 0.017 ohms at the terminals. These coil pancakes are appropriately connected across the magnetic gap to insure symmetrical currents on each side of the gap. The connections result in a total resistance of 0.07 ohms. This value was selected so that existing motor generators could be used if desired.

The coil insulation planned is 0.125-in. thick sheet stock axially and 0.0625-in. ribbon radially. This insulation and the water passage results in a form factor of 0.60. The pancake coils are securely mounted in a coil case and the entire assembly bolted to the yoke of the magnet.

Some of the characteristics of the coils are given below:

Total power	1034 kw
Ampere-turns	1.23×10^6
Total current	3838 amps
Current density	2113 amps/in^2
Total turns	640
Form factor	0.60
Turns, axial/coil	16
Turns, radial/coil	20
Total resistance	0.07 ohms
Coolant ΔP	166 lb/in^2
Inlet temp, max	100°F
Coolant, ΔT	60°F

Magnet Steel Specifications

Specification of a magnet yoke includes the steel composition, the yoke structure, and the fabrication procedure.

A most important and difficult specification to determine is the composition of the steel. Several types of high permeability alloy steels were considered. Most of the superior steel alloys do not maintain their superiority of relatively high permeability at magnetic fields above 20,000 gauss. The best alloys have objectionable components for a high neutron flux (e.g. cobalt) and give rather little gain in magnetic field at large costs. The choice made in this case was low carbon steel. The precise content of carbon and impurities was a compromise to permit feasibility of forging (see below); however the adverse effects due to the compromises are small. At high magnetic fields the effect of low impurities on the permeability of steel is small, and some investigations have found the level of carbon at low values to be completely negligible.

In the ORIC model magnet, with a permeability of approximately 90, it is estimated that a 1% decrease in permeability would result in a decrease of 0.21% in flux in the magnetic gap.

A steel known as Cyclotron Analysis Steel was chosen. It has the following composition:

	% Max
C	0.15
Mn	0.50
P	0.04
S	0.05
Si	0.20
Ni	0.08

A comparison was made of yoke structures fabricated of forgings and of laminations. To help make this comparison, the total magnetic and vacuum loads were calculated. The results indicated a magnetic load of 1,055,000 lb and a vacuum load of 60,000 lb could be expected. This range of forces made laminations unattractive, since in order to obtain a high moment of inertia for a laminated beam the yoke became either inefficient or costly.

The following fabrication procedure was specified:

> The material to be open hearth killed steel with both pole bases from a single heat and with the two ingots of the same size and shape and forged in the same manner.
>
> Sufficient discard to be made from each ingot to secure freedom from piping and undue segregation, and the forgings to be made from ingots having at least two times the cross sectional area. All sections to be ultrasonic tested.
>
> All mating surfaces to be machined to a finish of 125 micro-inches, and all other surfaces to 250 micro-inches.
>
> The mating surfaces of pole bases and yoke pieces to be planes within ±0.005 in. T.I.R. and parallel to within 0.005 in., as measured around the periphery.

The finished magnet forgings satisfactorily met these specifications. The chemical check analysis of the steel, well within our specifications, was:

	%
C	0.110
Mn	0.330
P	0.010
S	0.030
Si	0.015
Ni	0.060

Yoke Design

The magnet is of a conventional closed-yoke design with a 1/1 ratio of pole base cross section to yoke cross section. The finished magnet, less coils, weighs approximately 200 tons and is 180 in. high with base dimensions of 113 x 113 in. The four 20-in. thick yoke pieces are bolted together with through bolts.

Pole Tip Windings

The magnet will have three sets of coils other than the main coils, Fig. 42. They are the AVF valley coils, the pole-face circular trimming coils, and the harmonic coils. The valley coils will be water-cooled copper, enclosed in vacuum tight stainless steel cans and mounted in the valleys of the pole tips. (The choice of copper conductors for these coils was made because of space limitations). The valley coils will oppose the existing magnetic field in the valleys, thereby increasing the magnetic field ratio between hill and valley, thus increasing the axial focusing forces on the ions.

The pole-face circular trimming coils will be water-cooled copper windings mounted on the face of each pole. Each complete coil will consist of a set of 10 concentric helical coils one conductor thick. These coils will be used to obtain the isochronous field for various ions and to provide for some control over the magnetic median plane.

The harmonic coils will be small water-cooled coils placed in the valleys, on the gap side of the AVF valley coils. Three coils per valley will be used to compensate for any asymmetry of the ion center in the central region or near the exit radius.

UNCLASSIFIED
ORNL-LR-DWG 34925

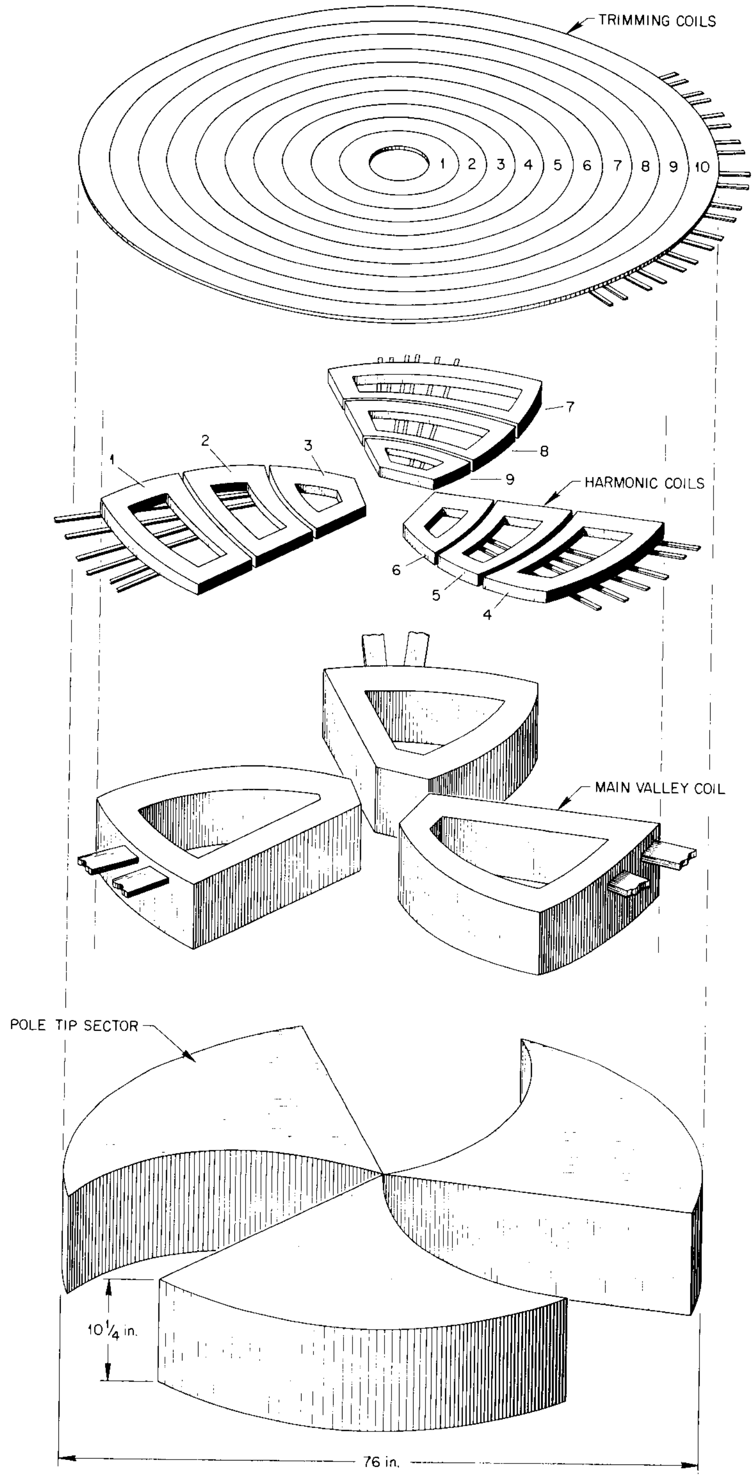

Fig. 42. Exploded View of a Pole Tip with Coils.

Resonant System

Only preliminary studies have been made concerning the mechanical design of the resonant system. Some consideration has been given, however, to the type of water-cooled surfaces. Tube-in-sheet type water cooled aluminum was considered, but r-f power losses ruled out aluminum. Tube-in-sheet copper was investigated; preliminary studies indicate that the difficulty of joining the tubes to headers and external circuits may offset the obvious advantages of this method. Further investigation is planned.

Vacuum System

The vacuum tank will be constructed of stainless steel with 76-in. dia, 4-in. thick magnetic steel inserts to maintain magnetic continuity of the pole bases. The total vacuum volume, including vacuum tank, dee stem house and diffusion pump manifold will be 700 ft^3.

The diffusion pumps will be mounted from the dee stem house since it comprises a large portion of the vacuum volume. The vacuum pumping system will probably include refrigerated cold traps, oil diffusion pumps with refrigerated baffles, and Rootes blowers backed with Kinney pumps.

The Ion Source

The ion source for the ORIC will be the hot cathode type now used for the ORNL 63-Inch Heavy Particle Cyclotron and the ORNL 86-Inch Cyclotron. Ion species higher than plus 4 (for nitrogen) have not yet been measured due to lack of resolving power. However, the ion currents obtained for N^{3+} and N^{4+}, 10 ma and 2.6 ma, respectively, lead one to expect satisfactory results for high order species. A new test system is planned to search for the higher ion states, although the basic cyclotron design does not depend on them. The proton currents obtained from the 86-Inch Cyclotron, 3 ma at 23 Mev, indicate fully adequate beam current for low-mass ions.

IX. EXPERIMENTAL FACILITIES

The design of the shielding and the experimental layout requires a reliable estimate of neutron yield. The shielding thickness determined by the fast neutron flux is more than adequate to reduce the thermal neutron and gamma ray flux to a safe level. The experimental data of Crandall and Milburn[1] indicate a yield of about one neutron for four 75-Mev protons hitting a thick target of high atomic number. Thus, a one-milliampere beam of 75-Mev protons would produce a point source of 10^{15} neutrons per second.

The most practical shield, in view of cost and general utility, is ordinary concrete. The thickness of such concrete to reduce fast fission spectrum neutrons to one tenth the intensity is 10.6 inches. If we assume that the effective neutron source is 20 ft from the shielding wall, the flux is 2.5×10^9 neutrons/cm^2-sec. A 7-ft thick concrete wall will reduce the flux to 25 neutrons/cm^2-sec; this is within the allowed level.

There are several assumptions made which in certain unfavorable cases could increase the radiation level. For example, the distribution of neutrons from a target will not be isotropic but peaked in the forward direction. Furthermore, the energy spectrum will certainly contain neutrons of higher energy than fission neutrons, and the effective source (where the cyclotron beam is stopped) may be closer to the wall than 20 feet. In these cases, it will be easier and more practical to place small quantities of additional shielding in the vicinity of the target. For local shielding it would be possible to use special shields of more complicated construction, such as layers of iron and concrete, for those cases where an unusually high yield of neutrons is involved. Since for many applications the beam power will be lower or the particles used will produce a much smaller neutron yield, the occasional need of assembling a one or two foot thick shield around the target will not be a serious disadvantage.

---

(1) UCRL-4931

It is clear that, with the very massive walls required to keep the radiation level safe and with the varied and complex type of experiments to be done with the ORIC, the experimental facilities must be carefully planned to provide for efficient use of the machine. Ever increasing demands are made on the experimental nuclear physicist which involve both higher precision and the measurement of more complicated phenomena. It is essential that one have enough time to set up and thoroughly test the apparatus before taking data. Since the equipment may include such items as 20-ton analyzing magnets, 6-ft dia scattering chambers, and complicated electronics, this testing must be done in the same room and position where the actual data will be taken. At least two separate rooms are needed so that while data is being taken in one room, the radiation level is low enough in the other room to permit the preparation of apparatus for the next experiment. The plan for the shielding structure, Fig. 43, provides for two experimental areas in addition to the cyclotron room.

The external beam of the cyclotron passes through a magnetic quadrupole lens for focusing and then through a beam switching magnet. The cyclotron operator can, by adjusting the field of the switching magnet, direct the beam to any one of several places in experimental Area II. It is desirable to keep the holes through the concrete wall small to minimize leakage of radiation from the cyclotron. A slot in the concrete to pass several 3-in. evacuated pipes will allow adjustment so that the beam can be directed to the several different experimental setups. The slot in the concrete can be filled with water or blocks. If the pipes do not point in the direction of a source of radiation, it should be safe to work in the room while experiments are being done in Area I. Area II is large enough that it can be partitioned into two rooms by adding a shielding wall at small cost, if the demand for experimental facilities requires it. The magnet for switching the beam will also have sufficient energy resolution for it to be used to determine the energy and the energy spread of the beam. Experiments which do not require high-energy resolution, such as statistical theories of nuclear behavior, production of transuranic and new isotopes, polarization scattering effects, and cross-section measurements can well be done in Area II.

UNCLASSIFIED
ORNL-LR-DWG 32527

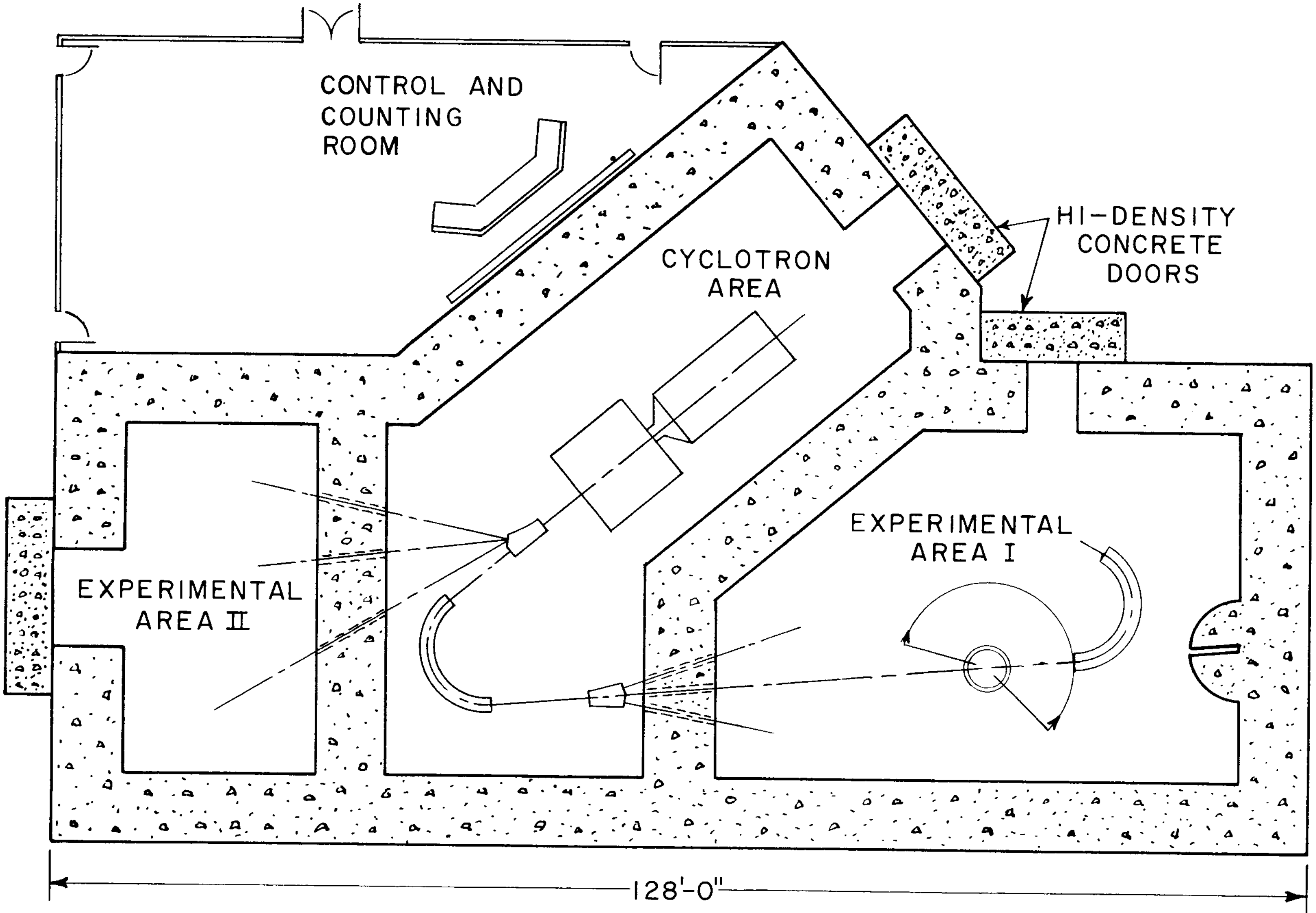

Fig. 43. Cyclotron Room and Shielded Experimental Areas.

For certain types of experiments a high energy resolution is necessary. The density of energy levels increases with excitation energy and atomic weight of the target. Furthermore, the number of nuclear reactions leading to different outgoing particles increases rapidly. One needs high energy resolution for two reasons. One is to be able to resolve discrete levels or, if the level density is too great, at least be able to examine fine structure in the spectrum. The second reason is that one can usually distinguish the outgoing particle, and quite often the mass of the recoil nucleus, by measuring the energy of the outgoing particle as a function of angle of scattering. The energy depends on the mass, and sufficient precision of measurement is then a valuable tool. In addition to precise magnetic analysis of the beam striking the target and of the outgoing charged particles from the target, an increasingly useful technique is time of flight. This requires a large room, both in order to have sufficient time intervals and to reduce background produced by radiation scattered from the walls. Experimental Area I is designed to meet these requirements.

Two large analyzing magnets have been designed with a dispersive power of 20 kev per millimeter for 75-Mev protons. To limit the physical size to a reasonable value they have nonuniform, double-focusing fields with $\frac{r}{B} \frac{dB}{dr} = 1/2$. The problem of shaping the magnetic field is small compared with the doubling in size required to obtain the same dispersive power with a uniform field magnet. By using slits one millimeter wide and a thin target, an energy resolution of 50 kev for 75-Mev protons becomes possible. Where less resolution is adequate, the slits can be increased, a thicker target used, and a larger solid angle of detection is possible, reducing by a major factor the time needed to get adequate statistics. One can thus adjust to optimum value the amount of beam, energy, and energy spread of the beam.

If a large amount of beam were to be stopped by slits placed in Area I, the background would be very high. Furthermore, one needs thick slits to stop 75-Mev protons. If the thickness of the slit is greater than the slit opening, an appreciable fraction of the beam will be scattered by the slit edges and strike the target if it is close to the slit. The slit is placed, therefore, inside the cyclotron enclosure, and a magnetic quadrupole lens is used to focus the desired beam through the slits onto a target placed in the center of Area I. A second magnetic analyzer similar to the previous one is used to analyze the outgoing charged particles from the target. This analyzer can be rotated about the target to cover an angular range of 160 deg in the laboratory system. To reduce background further, provision is made for a quadrupole lens to focus the beam which passes through the target into a shielded area in the wall. Area I is quite large to permit time-of-flight measurements and double-scattering experiments and to accomodate large and complex apparatus under conditions of minimum background and controlled energy conditions.

Appendix I: Articles Published - 86-Inch Cyclotron Programs

Physics Research

H. G. Blosser and T. H. Handley, "Survey of (p,n) Reactions at 12 Mev," Phys. Rev. 100, 1340-1344 (Dec. 1, 1955).

G. E. Boyd, "Technetium Activities at Mass 97," Phys. Rev. 95, 113-114 (July 1, 1954).

G. E. Boyd and R. A. Charpie, "Mass Assignment and Gamma-Radiations of the Seven-Hour Molybdenum Isomer," Phys. Rev. 88, 681-682 (November 1, 1952).

G. E. Boyd, J. R. Sites, Q. V. Larson, and C. R. Baldock, "Production and Identification of Long-Lived Technetium Isotopes at Masses 97, 98, and 99," Phys. Rev. 99, 1030-1031 (August 1, 1958).

B. L. Cohen, "Angular Distributions and Yields of Neutrons from (p,n) Reactions," Phys. Rev. 98, 49-55 (April 1, 1955).

B. L. Cohen, "Anomolous Inelastic Scattering of 23-Mev Protons by Heavy Elements," Phys. Rev. 105, 1549-1555 (March 1, 1957).

B. L. Cohen,"Coincidence Studies of the Ni^{58} (p, 2p) Reaction," Phys. Rev. 108, 768-773 (Nov. 1, 1957).

B. L. Cohen, "Gallium-64," Phys. Rev. 91, 74 (July 1, 1953).

B. L. Cohen, "(p, γ) Cross Sections," Phys. Rev. 100, 206-208 (Oct. 1, 1955).

B. L. Cohen, "The Statistical Theory of Nuclear Reactions," Phys. Rev. 92, 1245 (Dec. 1, 1953).

B. L. Cohen, "Theory of the Fixed Frequency Cyclotron," Rev. Sci. Instr. 24, 589 (Aug. 1953).

B. L. Cohen, B. L. Ferrell Bryan, D. J. Coombe, and M. K. Hullings, "Angular Distribution of Fission Fragments from 22-Mev Proton-Induced Fission of U^{235}, U^{233}, Th^{232}, and Th^{230}," Phys. Rev. 98, 685 (May 1, 1955).

B. L. Cohen, R. A. Charpie, T. H. Handley, and E. Olson, "Manganese-57," Phys. Rev. 94, 953 (May 15, 1954).

B. L. Cohen and T. H. Handley, "An Experimental Search for a Stable Dineutron," Phys. Rev. 92, 101 (Oct. 1, 1953).

B. L. Cohen and T. H. Handley, "Experimental Studies of (p,t) Reactions," Phys. Rev. 93, 514 (Feb. 1, 1954).

B. L. Cohn, W. H. Jones, G. H. McCormick, and B. L. Ferrell, "Angular Distributions of Fission Fragments from 22-Mev Proton-Induced Thorium Fission," Phys. Rev. 94, 625 (May 1, 1954).

B. L. Cohen and S. W. Mosko, "Inelastic Proton Scattering and (p,d) Reactions in Heavy Elements," Phys. Rev. 106, 995-1000, (June 1, 1957).

B. L. Cohen and R. V. Neidigh, "Angular Distribution of 22-Mev Protons Elastically Scattered by Various Elements," Phys. Rev. 93, 282 (Jan. 15, 1954).

B. L. Cohen and R. V. Neidigh, "Measurement of Angular Distributions of Nuclear Reaction Products with an Internal Cyclotron Beam," Rev. Sci. Instr. 25, 255 (March 1954).

B. L. Cohen and E. Newman, "(p,pn) and (p,2n) Cross Sections in Medium Weight Elements," Phys. Rev. 99, 718-723 (August 1, 1955).

B. L. Cohen, E. Newman, R. A. Charpie, and T. H. Handley, "(p,pn) and (p,αn) Excitation Functions," Phys. Rev. 94, 620 (May 1, 1954).

B. L. Cohen, E. Newman, and T. H. Handley, "(p,pn) + (p,2n) and (p,2p) Cross Sections in Medium Weight Elements," Phys. Rev. 99, 723-727 (August 1, 1955).

B. L. Cohen, E. Newman, T. H. Handley, and A. Timnick, "Angular Distribution of Deuterons from $Be^9(p,d)Be^8$", Phys. Rev. 90, 323 (April 15, 1953).

B. L. Cohen, H. L. Reynolds, and A. Zucker, "A Comparison of Nitrogen-and Proton-Induced Nuclear Reactions," Phys. Rev. 96, 1617 (Dec. 15, 1954).

B. L. Cohen and A. G. Rubin, "Further Studies of Anomalous Inelastic Proton Scattering," Phys. Rev. 111, 1568-1577 (Sept. 15, 1958).

J. L. Fowler, W. H. Jones, and J. H. Paehler, "Fission Asymmetry as a Function of Excitation Energy of the Compound Nucleus," Phys. Rev. 88, 71-72 (October 1, 1952).

T. H. Handley, "Neutron-Deficient Activities of Holmium," Phys. Rev. 94, 945 (May 15, 1954).

T. H. Handley and W. S. Lyon, "Neutron-Deficient Activities of Terbium," Phys. Rev. 99, 1415-1417 (Sept. 1, 1955).

T. H. Handley, W. S. Lyon, and E. L. Olson, "Holmium-167," Phys. Rev. 98, 688 (May 1, 1955).

T. H. Handley and E. L. Olson, "Dysprosium-157," Phys. Rev. 90, 500 (May 1, 1953).

T. H. Handley and E. L. Olson, "Erbium-163 and Thulium-165," Phys. Rev. 92, 1260 (Dec. 1, 1953).

T. H. Handley and E. L. Olson, "Neutron-Deficient Activities of Praseodymium," Phys. Rev. 96, 1003 (Nov. 15, 1954).

T. H. Handley and E. L. Olson, "New Radioactive Nuclides of the Rare Earths," Phys. Rev. 93, 524 (Feb. 1, 1954).

T. H. Handley and E. L. Olson, "Ytterbium-167," Phys. Rev. 94, 968 (May 15, 1954).

W. H. Jones, A. Timnick, J. H. Paehler, and T. H. Handley, "Bombardment Energy and Fission-Product Yield Patter for Protons on Natural Uranium and U^{235}," Phys. Rev. 99, 184-187 (July 1, 1955).

R. S. Livingston, "The Oak Ridge 86-Inch Cyclotron," Nature 170, 221 (Aug. 9, 1952).

G. H. McCormick, H. G. Blosser, B. L. Cohen, and E. Newman, "(p,He^3) and (p,t) Cross Section Measurements," Jr. of Nuc. and Inorganic Chem. 2, 269-270 (1956).

G. H. McCormick and B. L. Cohen, "Fission and Total Reaction Cross Sections for 22-Mev Protons on Th^{232}, U^{235}, and U^{238}," Phys. Rev. 96, 722 (Nov. 1, 1954).

J. W. Mihelich and B. Harmatz, "Some New Isomeric Transitions in Rare Earth Nuclei," Phys. Rev. 106, 1232-1235 (June 15, 1957).

J. W. Mihelich, B. Harmatz, and T. H. Handley, "Nuclear Spectroscopy of Neutron-Deficient Rare Earths (Tb through Hf)," Phys. Rev. 108, 989-999 (Nov. 15, 1957).

Articles Submitted for Publication

B. L. Cohen and A. G. Rubin, "Inelastic Proton Scattering in Medium Weight Nuclei," Phys. Rev.

C. B. Fulmer and B. L. Cohen, "23-Mev Proton-Induced (p,α) Reactions," Phys. Rev.

Biology Research

W. K. Baker and E. von Halle, "The Production of Dominant Lethals in Drosophila by Fast Neutrons from Cyclotron Irradiation and Nuclear Detonations," Science 119, 46-49 (January 1, 1954).

C. W. Edington, "The Induction of Recessive Lethals in Drosophila Melanogaster by Radiations of Different Ion Density," Genetics 41, 814-821 (November 1956).

G. S. Hurst, W. A. Mills, F. P. Conte, and A. C. Upton, "Principles and Techniques of Mixed Radiation Dosimetry Application to Acute Lethality Studies of Mice with the Cyclotron," Radiation Research 4, 49-64 (January 1956).

J. S. Kirby-Smith and C. P. Swanson, "The Relative Effectiveness of Various Ionizing Radiations on Chromosone Breakage on Tradescantia,"

G. H. Mickey, "Visible and Lethal Mutations in Drosophila," The American Naturalist 138, 241-255 (July-August 1954).

W. L. Russell, L. B. Russel, and A. W. Kimball, "The Relative Effectiveness of Neutrons from a Nuclear Detonation and from a Cyclotron in Inducing Dominant Lethals in the Mouse," The American Naturalist 138, 269-286 (July-August 1954).

C. W. Sheppard, M. Slater, E. B. Darden, Jr., A. W. Kimball, G. T. Atta, C. W. Edington, and W. K. Baker, "Biological Effects of Fast Neutrons from an Internal Target Cyclotron: Physical Methods and Dominant Lethals in Drosophila," Radiation Research 6, 173-187 (1957).

A. C. Upton, K. W. Christenberry, G. S. Melville, J. Furth, and G. S. Hurst, "The Relative Biological Effectiveness of Neutrons, X-Rays, and Gamma Rays for the Production of Lens Opacities: Observations on Mice, Rats, Guinea-Pigs, and Rabbits," Radiology 67, 686-696 (November 1956).

A. C. Upton, F. P. Conte, G. S. Hurst, and W. A. Mills, "The Relative Biological Effectiveness of Fast Neutrons, X-Rays, and γ-Rays for Acute Lethality in Mice," Radiation Research 4, 117-131 (February 1956).

A. C. Upton, G. S. Melville, Jr., M. Slater, F. P. Conte, and J. Furth, "Leukemia Induction in Mice by Fast Neutron Irradiation," Proceedings of the Society for Experimental Biology and Medicine, 1956, 436-438, Vol. 92.

Appendix II: Articles Published - Heavy Particle Physics Program

C. D. Goodman and J. L. Need, "Energy Distributions of Product Particles from Nitrogen-Induced Nuclear Reactions on Beryllium," Phys. Rev. 110, 676 (1958).

M. L. Halbert, "Fluorescent Response of CsI (Tl) to Energetic Nitrogen Ions," Phys. Rev. 107, 647-649 (Aug. 1, 1957).

M. L. Halbert, T. H. Handley, J. J. Pinajian, W. H. Webb, and A. Zucker, "Neutron-Transfer Reactions from the Nitrogen Bombardment of Be, C, O, Na, and $Mg^{24,25,26}$," Phys. Rev. 106, 251-256 (April 15, 1957).

M. L. Halbert, T. H. Handley, and A. Zucker, "Excitation Function for Two Nitrogen-Sodium Nuclear Reactions," Phys. Rev. 104, 115-117, (Oct. 1, 1956).

M. L. Halbert and A. Zucker, "Angular Distribution of N^{13} from N^{14} on Mg^{25}," Phys. Rev. 108, 336-341 (Oct. 15, 1957).

R. J. Jones and A. Zucker, "Two Ion Sources for the Production of Multiply Charged Nitrogen Ions," Rev. Sci. Instr. 25, 562 (June 1954).

H. L. Reynolds, D. W. Scott, and A. Zucker, "Nuclear Reactions Produced by Nitrogen on Boron and Oxygen," Phys. Rev. 102, 237-241 (April 1, 1956).

H. L. Reynolds, D. W. Scott, and A. Zucker, "Nuclear Reactions with Energetic Nitrogen Ions," Proc. Nat. Acad. 39, 975 (1953).

H. L. Reynolds, D. W. Scott, and A. Zucker, "Range and Charge of Energetic Nitrogen Ions in Nickel," Phys. Rev. 95, 671 (Aug. 1, 1954).

H. L. Reynolds, L. D. Wyly, and A. Zucker, "Equilibrium Charge Distribution of Energetic Nitrogen Ions," Phys. Rev. 98, 474-477, (April 15, 1955).

H. L. Reynolds and A. Zucker, "Cyclotron Ion Source for the Production of N^{3+}," Rev. Sci. Instr. 26, 894 (Sept. 1955).

H. L. Reynolds and A. Zucker, "Elastic Scattering of Nitrogen by Nitrogen," Phys. Rev. 102, 1378-1384 (June 1, 1956).

H. L. Reynolds and A. Zucker, "Equilibrium Charge Distribution of Stripped 26-Mev Nitrogen Ions," Phys. Rev. 95, 1353 (Sept. 1, 1954).

H. L. Reynolds and A. Zucker, "Excitation Functions for Nitrogen-Induced Nuclear Reactions in Carbon," Phys. Rev. 96, 1615 (Dec. 15, 1954).

H. L. Reynolds and A. Zucker, "Excitation Function for the Reaction $Be^9(N^{14}, \alpha n)F^{18}$," Phys. Rev. 101, 226-227 (Jan. 1, 1956).

H. L. Reynolds and A. Zucker, "Nuclear Reactions Produced by Nitrogen on Nitrogen," Phys. Rev. 101, 166-171 (Jan. 1, 1956).

H. L. Reynolds and A. Zucker, "Range of Nitrogen Ions in Emulsion," Phys. Rev. 96, 393 (Oct. 15, 1954).

W. H. Webb, H. L. Reynolds, and A. Zucker, "Nitrogen-Induced Nuclear Reactions in Aluminum," Phys. Rev. 102, 749-752 (May 1, 1956).

L. D. Wyly and A. Zucker, "Activities in Light Nuclei from Nitrogen Ion Bombardment," Phys. Rev. 89, 524 (Jan. 1953).

A. Zucker, "Protons and Alpha-Particles from the Nitrogen Bombardment of Aluminum," Nuclear Physics 6, 420 (1958).

Articles Submitted for Publication

D. E. Fisher, A. Zucker, and A. Gropp, "Nuclear Reactions Induced by the Nitrogen Bombardment of Sulfur," Phys. Rev.

M. L. Halbert and A. Zucker, "Light Particles from the Nitrogen Bombardment of Oxygen," Phys. Rev.

J. J. Pinajian and M. L. Halbert, "Nitrogen-Induced Nuclear Reactions in Potassium," Phys. Rev.

ORNL-2648
Particle Accelerators
and High-Voltage Machines
TID-4500 (14th ed.)

INTERNAL DISTRIBUTION

1. C. E. Center
2. Biology Library
3. Health Physics Library
4-5. Central Research Library
6. Reactor Experimental Engineering Library
7-126. Laboratory Records Department
127. Laboratory Records, ORNL R.C.
128. A. M. Weinberg
129. L. B. Emlet (K-25)
130. J. P. Murray (Y-12)
131. J. A. Swartout
132. E. H. Taylor
133. E. D. Shipley
134. S. C. Lind
135. M. L. Nelson
136. W. H. Jordan
137. R. R. Dickison
138. C. P. Keim
139. R. S. Livingston
140. F. L. Culler
141. A. H. Snell
142. A. Hollaender
143. M. T. Kelley
144. G. E. Boyd
145. T. A. Lincoln
146. K. Z. Morgan
147. A. S. Householder
148. C. S. Harrill
149. C. E. Winters
150. H. E. Seagren
151. D. Phillips
152. R. J. Jones
153. C. D. Goodman
154. F. T. Howard
155. J. A. Martin
156. A. Zucker
157. M. J. Skinner
158. R. A. Charpie
159. P. M. Reyling
160. R. F. Christy (consultant)
161. E. Creutz (consultant)
162. J. R. Richardson (consultant)
163. L. P. Smith (consultant)
164. M. S. Livingston (consultant)
165. ORNL - Y-12 Technical Library, Document Reference Section

EXTERNAL DISTRIBUTION

166. Division of Research and Development, AEC, ORO
167-694. Given distribution as shown in TID-4500 (14th ed.) under Particle Accelerators and High-Voltage Machines category (75 copies - OTS)